

REPORT DOCUMENTATION PAGE			Form Approved OMB No. 0704-0188	
Public reporting burden for this collection of information is estimated to average 1 hour per response, including the time for reviewing instructions, searching existing data sources, gathering and maintaining the data needed, and completing and reviewing the collection of information. Send comments regarding this burden estimate or any other aspect of this collection of information, including suggestions for reducing this burden to Washington Headquarters Services, Directorate for Information Operations and Reports, 1215 Jefferson Davis Highway, Suite 1204, Arlington, VA 22202-4302, and to the Office of Management and Budget, Paperwork Reduction Project (0704-0188), Washington, DC 20503.				
1. AGENCY USE ONLY (Leave blank)	2. REPORT DATE 11 October 1996	3. REPORT TYPE AND DATES COVERED Final Report		
4. TITLE AND SUBTITLE About the Control of the Underwater and Above Water Nuclear Explosions by Hydroacoustic Methods		5. FUNDING NUMBERS F6170895W0328		
6. AUTHOR(S) B. Khristoforov				
7. PERFORMING ORGANIZATION NAME(S) AND ADDRESS(ES) Russian Academy of Sciences Institute for Dynamics of Geospheres Leninsky Prospect, 38 Korpus 6 Moscow 117979, Russia		8. PERFORMING ORGANIZATION REPORT NUMBER SPC-95-4049		
9. SPONSORING/MONITORING AGENCY NAME(S) AND ADDRESS(ES) EOARD PSC 802 BOX 14 FPO 09499-0200		10. SPONSORING/MONITORING AGENCY REPORT NUMBER SPC-95-4049		
11. SUPPLEMENTARY NOTES				
12a. DISTRIBUTION/AVAILABILITY STATEMENT Unlimited		12b. DISTRIBUTION CODE		
13. ABSTRACT (Maximum 200 words) Since 1946, researchers from the Institute for Dynamics of the Geospheres (IDG) took an active participation in equipment design and observations of nuclear explosions and associated test (modelling) experiments by using chemical explosives. In this report, experimental data of hydrodynamic processes in water related to underwater, above water and coastal explosions are presented, analyzed and generalized. The principal goal of this work is improving existing hydroacoustic methods of monitoring and identifying underwater and above water nuclear explosions.				
14. SUBJECT TERMS			15. NUMBER OF PAGES 91	
			16. PRICE CODE	
17. SECURITY CLASSIFICATION OF REPORT UNCLASSIFIED	18. SECURITY CLASSIFICATION OF THIS PAGE UNCLASSIFIED	19. SECURITY CLASSIFICATION OF ABSTRACT UNCLASSIFIED	20. LIMITATION OF ABSTRACT UL	

**RUSSIAN ACADEMY OF SCIENCES
INSTITUTE FOR DYNAMICS OF GEOSPHERES**


Leninsky Prospect, 38 Korpus 6, Moscow 117979, Russia

**About the Control of the Underwater
and Above Water Nuclear Explosions
by Hydroacoustic Methods.**

Final Report for the Project SPC-95-4049

19961212 081

Principal investigator prof.


B. Khristoforov

11 October 1996.

CONTENS

1. INTRODUCTION. PRINCIPAL GOALS AND PROBLEMS OF THE PROJECT.....	4
2. UNDERWATER EXPLOSIONS.....	7
2.1 THREE UNDERWATER NUCLEAR EXPLOSIONS AT THE NZTS.....	9
2.1.1. <i>Test site A within the bay of Chernaya, procedures, equipment.....</i>	<i>11</i>
2.1.2. <i>Results of the underwater nuclear explosions.....</i>	<i>14</i>
2.2 CHEMICAL EXPLOSIONS IN DEEP WATER.....	18
2.2.1 <i>Explosion in infinite liquid.....</i>	<i>19</i>
2.2.2. <i>Underwater explosions of spherical charges in air-filled cavities.....</i>	<i>24</i>
2.2.3. <i>Influence of bulk energy concentration on underwater explosion effects.....</i>	<i>27</i>
2.2.4. <i>Free surface and bottom effects on an explosion in reservoir.....</i>	<i>29</i>
2.2.5. <i>Deep bomb blasts in the Sea of Okhotsk.....</i>	<i>37</i>
2.2.6. <i>Three tons detonating cord explosion in the Black Sea.....</i>	<i>41</i>
2.3. 100 KG SPHERICAL CAST CHARGE EXPLOSIONS IN SHALLOW RESERVOIRS WITH LOW-VELOCITY SANDY BOTTOM ($C_0 > C_3 > C_2$).	47
2.3.1. <i>Parameters of shock wave in water from explosions in shallow reservoir.....</i>	<i>49</i>
2.3.2. <i>Parameters of surface phenomena and air shock waves.....</i>	<i>50</i>
2.4. CONCLUSIONS.....	53
3.ABOVE WATER AND COASTAL EXPLOSIONS.....	55
3.1 THREE ABOVE WATER EXPLOSIONS AT THE NZTS.....	55
3.2 COASTAL ABOVE GROUND EXPLOSIONS.....	55
3.2.1. <i>Nuclear explosion as the coast of the bay of Chernaya.....</i>	<i>55</i>
3.2.2. <i>1000 ton TNT explosion at the coast of the Matochkin Shar strait.....</i>	<i>57</i>
3.3. MODEL CHEMICAL EXPLOSIONS ABOVE WATER AND GROUND.....	61

3.4. UNDERGROUND NUCLEAR EXPLOSIONS.	67
3.4.1. <i>Conditions of conduction</i>	67
3.4.2. <i>Near field measurements</i>	68
3.4.3. <i>Measurements at large distances</i>	70
3.5. CONCLUSIONS.....	73
4. MONITORING UNDERWATER AND ABOVE WATER NUCLEAR EXPLOSIONS.....	75
4.1. SPECIFIC FEATURES OF IDENTIFICATION UNDERWATER AND ABOVE WATER EXPLOSIONS BY SEISMIC AND INFRASOUND OBSERVATIONS.	76
4.2. HYDROACOUSTIC MONITORING UNDERWATER AND ABOVE WATER NUCLEAR EXPLOSIONS.....	81
4.3. CONCLUSIONS.....	85
5. GENERAL CONCLUSIONS.....	86
REFERENCES.	89

1. Introduction. Principal goals and problems of the project.

Since 1946 researchers from the Institute for dynamics of the geospheres (IDG) took an active participation in equipment design and observations of nuclear explosions and associated test (modelling) experiments by using chemical explosives. In this report, experimental data of hydrodynamic processes in water related to underwater, above water and coastal explosions are presented, analysed and generalised. The principal goal of this work is improving existing hydroacoustic methods of the monitoring and identification underwater and above water nuclear explosions.

The tasks of this investigation are as follows:

Task 1. Preliminary study of the experimental data available for nuclear and chemical explosions and associated with capabilities of the hydroacoustic monitoring. Preparation of a brief preliminary report with a description of the materials which would be analysed in the investigation: underwater and coastal nuclear explosions in the bay Chernaya (Black); underground nuclear explosions at a coast of the Matochkin Shar Strait and bay Chernaya.; large-scale chemical explosions within shallow reservoirs with various bottom conditions; deep mines blasts; laboratory studies with low-yield chemical charges detonated near the free surface, bottom and above water; underwater explosions inside gas-filled cavities.

Task 2. Analysis and generalisation of the experimental data obtained from underwater nuclear explosions and chemical explosions including the shallow reservoirs experiments with various bottom conditions, proving of the decoupling idea with chemical blast in spherical air-filled cavities, observations of hydroacoustic signals from deep mine blasts.

Task 3. Analysis and generalisation of the measurement results from coastal underground nuclear explosions in 1968, 1973 and 1974. Analysis and generalisation of the experimental data from surface (half-diven) and above water chemical explosions. Procedure for determination of wave-field in water from above water and shallow water explosions.

Task 4. Preparation of a final report with detailed description of the available data with principal results and conclusions.

Nuclear explosions used in the report are listed in Table 1.1 [1-4].

Table 1.1

№	Date	Yield, kt	Depth, m	Location
Underwater explosions in the bay Chernaya				
1	21.09.55	3.5	12	70.70N 54.67E
2	10.10.57	10	30	70.70N 54.67E
3	23.10.61	10	50	70.70N 54.67E
Above water explosions				
4	13.09.61	less 20		70.87N 53.33E
5	27.10.61	less 20		70.70N 54.67E
6	22.08.62	less 20		71.00N 53.50E
Coastal surface explosion				
7	07.09.57	30		70.69N 54.80E
Coastal underground explosions				
8	27.10.66	1300		73.40N 54.57E
9	12.09.73	4000		73.32N 54.97E
10	29.08.74	1500		73.41N 54.93E
11	02.11.74	2000		70.81N 53.91E

Hydroacoustic observations from underwater, above water and coastal chemical explosions are analysed. A list of these explosions includes:

- deep bombs blasts in the Sea of Okhotsk at depths from 10 to 300 m measured at distances to 300 km in the frequency band from 1 to 1000 Hz at ships, submarines and coastal points;
- detonating cord blast of 3 ton in the Black Sea with measurements of pressure peak and impulse in shock waves at close distances by mechanic gages;

- detonation of spherical TNT charges of 100 kg at various depths, including bottom and free surface, within artificial reservoirs with sandy bottom and 0.25 to 3 m deep;
- laboratory experiments with small chemical charges where various explosions were tested: near bottom, near surface, above surface, explosions with various specific energy of explosives, including explosions in air-filled cavities.

Investigations have shown that for an explosion in infinite liquid space only a half of energy is radiated with shock wave and a half of energy stays in a gas bubble with following radiation associated with the bubble pulsation. The energy remaining after dissipation of the shock wave and following gas bubble pulsation are propagated on large distances. If sonic wave guides are present, these disturbances may propagate at very large distances weakly attenuating. Also, there are some shadow zones, where the acoustic disturbances are weakened.

All the underwater nuclear explosions conducted by the Former Soviet Union were detonated in shallow water. In this conditions, large part of explosion energy were radiated into the atmosphere and solid Earth decreasing hydroacoustic part of the energy. Due to venting of gaseous products of detonation into the atmosphere motion of gas bubbles was considerably changed and radiated energy decreased. For above water explosions, hydroacoustic disturbances are induced by refracted from the atmosphere shock wave and water column fall. For coastal explosions near ground, hydroacoustic waves are generated by air shock and seismic waves, and for underground explosions - by refraction of seismic waves at the bottom.

The presented observational results for shock waves, gas bubble, as well as radiation and propagation of corresponding hydroacoustic disturbances depending on reservoir and source characteristics, conditions of conduction can be used for studying of possibilities of hidden conduction and identification at noise background. These and some other problems of underwater explosions and related questions are considered in the report.

2. Underwater explosions.

The Novaya Zemlya marine test site with the centre in the town at the coast of the bay Belushya has been constructed since 1954. Explosions were started in 1955. A scheme of the bay Chernaya, where 3 underwater explosions were conducted (table 1.1), and principal positions of technological sites at the test sites is presented on Fig. 2.1a,b [3-5]. Following notations are used:

- A - the region around the bay of Chernaya, the zone of conduction of a series of air (1957-1962), 3 underwater (1955-1961), 3 above water (1961-1962) and 6 underground (1972-1975) nuclear explosions in vertical drill-holes. The town of Belushya is of about 120 km from north-west of the bay of Chernaya.
- B - the region of the strait of Matochkin Shar, the zone of 36 underground nuclear explosions in horizontal mines (1964-1990).
- C - Sul'menov Bay, Matyushikh Bay - the zone of air nuclear explosions (1957-1960).

The first nuclear explosion - underwater - has been conducted within the bay of Chernaya 21.09.1955. The second nuclear explosion at the Novaya Zemlya test site has been conducted near ground on 7.09.1957 at the east coast of the bay of Chernaya at the top of a tower 15 m high. Then, after two air explosions, the second underwater explosion has been conducted. The Navy equipment was tested as well as parameters of explosion motion were measured. In 1961, one underwater explosion has been conducted and 2 above water. In 1962, the third above water explosion was fired. Characteristic snap-shots of underwater explosions in 1957 and 1961 are presented on Fig. 2.2a,b. There were conducted 3 underwater, 3 above water, 84 air and 42 underground nuclear explosions during 35 years.

All the underwater nuclear explosions were conducted within shallow water reservoirs. This condition has decreased considerably parameters of hydroacoustic waves at large distances. Because of this disadvantage some peculiarities of shallow and deep water explosions were studied and a comparison of those of generated hydroacoustic signals and energy at large distances was conducted on an example of modelling chemical explosions. It is necessary for the

efficiency analysis of the hydroacoustic monitoring underwater nuclear explosions.

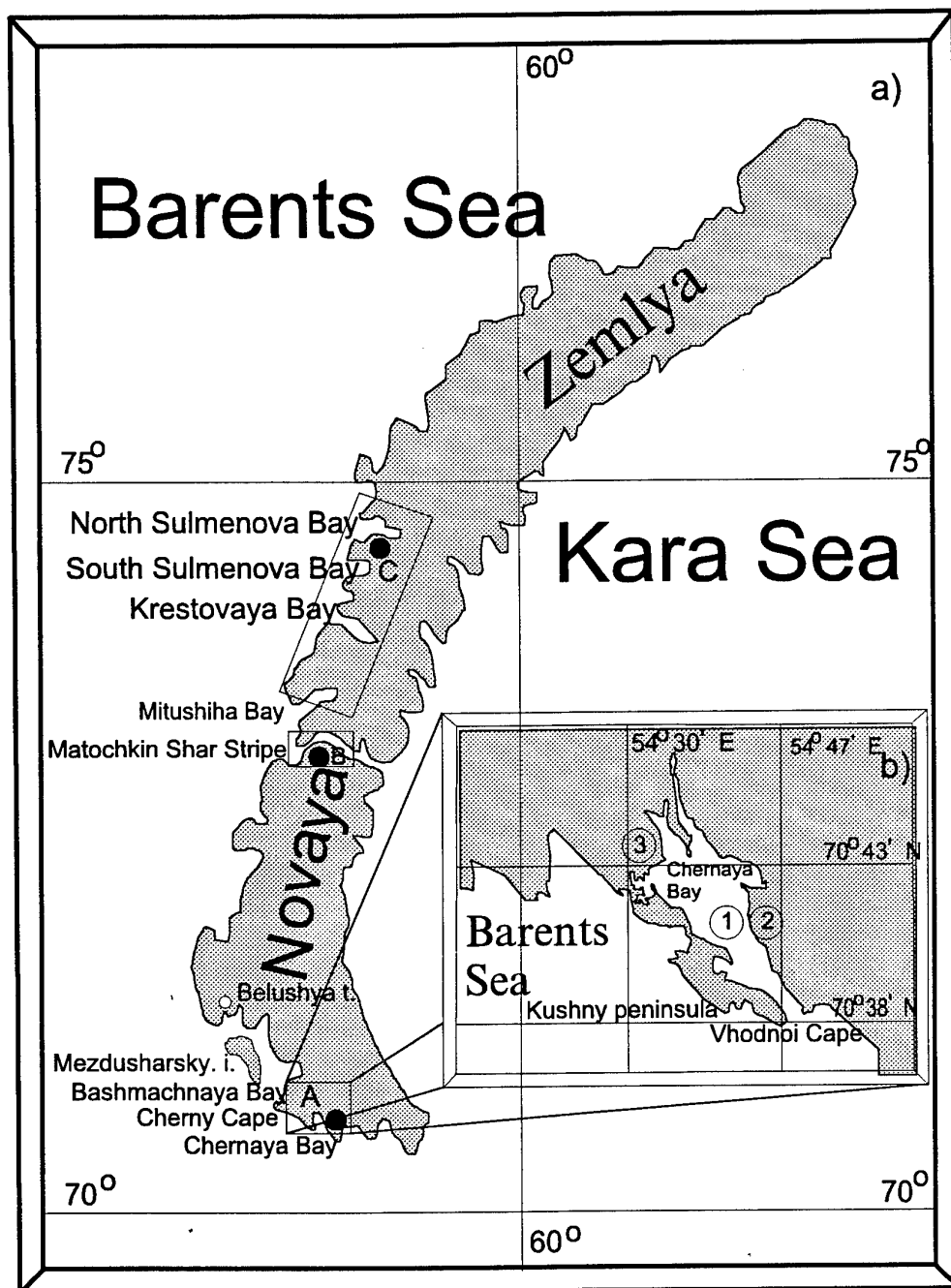


Fig. 2.1 a,b) Location of test sites at the Novaya Zemlya test site and a scheme of the bay of Chernaya.

A,B,C - zones of nuclear explosions.

1 - location of three underwater and one above water explosion.

2 - location of surface explosion.

3 - location of command centre.

2.1 Three underwater nuclear explosions at the NZTS.

The underwater nuclear explosions were conducted for testing of a torpedo with various versions of nuclear charge and for studying of that of effects on military equipment and armaments, including ships, submarines, coastal constructions, etc. Also, some peculiarities of underwater nuclear explosion evolution were studied, its parameters were measured and its effects on environment were determined.

A nuclear charge RDS-9 has been specially designed for a torpedo T-5 533 mm in diameter. The charge was of about 3 times lower diameter than that for an aviabomb. The charge has been tested in 1954 at the Semipalatinsk test site as an atmospheric explosion. It was the first time when a charge did not work. It had less initiation points and more complicated hydrodynamic characteristics miscalculated by theoretical modelling. Further, the torpedo was tested at the NZTS.

After assembly of the first device within a special building at the bay of Rogatchev coast it was delivered at a guard ship to the bay of Chernaya. A special steel frame was prepared for the device. The frame was attached to a tug-boat established at the place of detonation. On 21.09.1955 the device hung on steel wires at a depth of 12 m has been fired. The depth corresponds to a usual depth of torpedo motion.

Various techniques of yield estimation have given different results. Total TNT equivalent of the explosion estimated from shock wave parameters was of 3 to 3.5 kt, and from radiochemical measurements - from 5 to 5.5 kt. An announced yield - below 20 kt [2]. The recommended tactical-operative yield of 3 kt was accepted.

The State test of the T-5 has been conducted within the bay of Chernaya in 1957 and has included launching with and without the device. The second underwater nuclear explosion has been conducted on 10.10.1957 (Fig. 2.2a). A torpedo has been launched with a velocity of 40 knots from a submarine C-144 at a periscope depth. According to the Navy information the explosion depth was of 30 m. From measurements of shock wave, the explosion yield was larger than in 1955 due to some improvements of design.

In 1961, the third explosion has been conducted within the bay of Chernaya in the frame of the Navy training "Coral". A submarine of a 641 series with nuclear torpedoes on board took part in the training. Test shooting by model and two armed torpedoes with underwater (23.10.1961, Fig. 2.2b) and above water explosions were conducted.

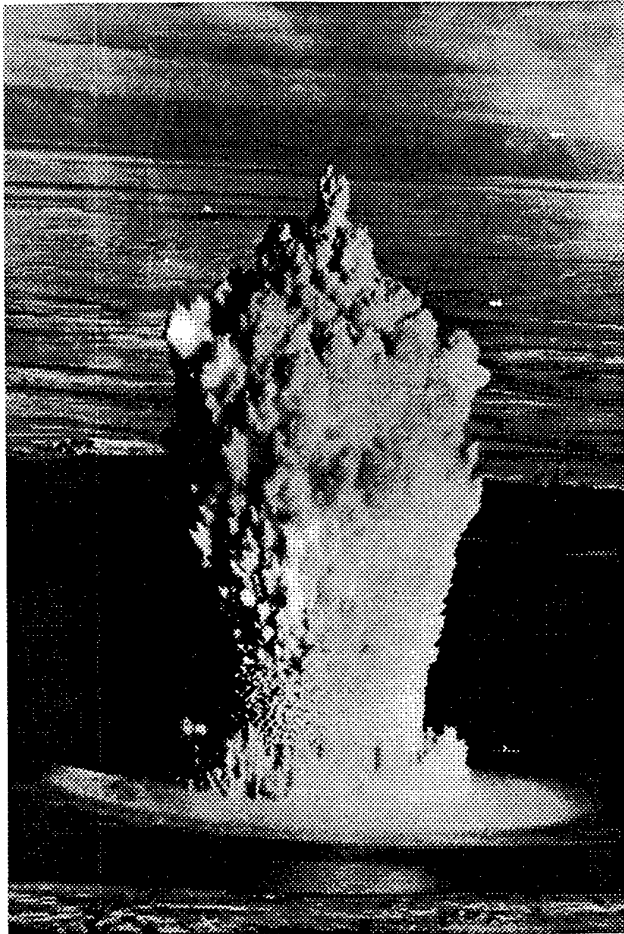


Fig. 2.2a. Snap-shot of underwater explosion within the bay of Chernaya in 1957.

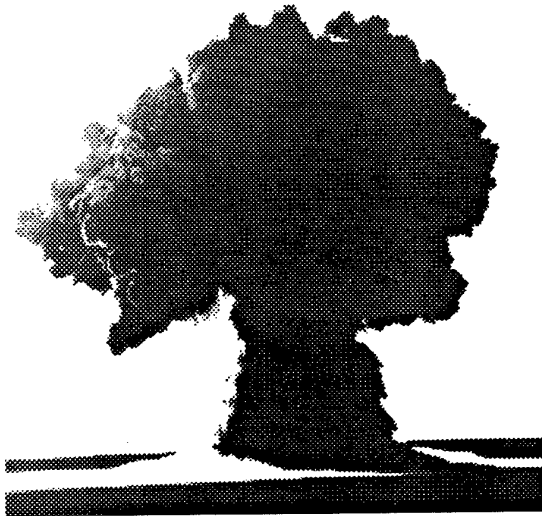


Fig. 2.2b. Snap-shot of underwater explosion within the bay of Chernaya in 1961.

2.1.1. Test site A within the bay of Chernaya, procedures, equipment.

The bay of Chernaya (Fig. 2.1) is one of numerous bays at the southern part of the Novaya Zemlya archipelago stretched in north-west direction and connected to the Barents Sea by a narrow strait. It is of 80 km². Characteristic depth of the bay is of 60 to 100 m. Tide height is of 1 m inside the bay. Along the narrow west spit, the bay coast is gently sloping, and along the east - surrounded by not high rocks.

The site of the underwater explosions was very advantageous since radioactive contamination of the Arctic ocean and Eurasia coast was very low due to low water exchange between the bay and the Barents Sea.

A test area has been prepared for the first explosion in the central part of the bay, and an observation and command site has been equipped at the north-west edge of the bay. Marine armaments, including 4 destroyers ("Gremyashii", "Reut", "Kuibyshev", "Karl Libkneht"), 2 demining ships (T-218 and T-219), 2 transports, and 4 submarines (two Soviet B-9 and C-19 and two German C-81 and C-84), were established at various distances from the shot point. At some ships armaments and animals were situated (about 100 dogs, 500 she-goats, and smaller animals) [5-8].

A part of the ships were specially re-equipped for the experiment. At the destroyer "Gremyashii", an armoured safety container was established within the first boiler section as well as an automatic system of fuel feed for boilers. In order to increase the ship vitality a steel shit has been attached along the side of the machine section, an armoured stand for high-speed recording cameras has been established at the half-back.

Along the coast, a concrete construction has been built at a distance of 1.3 km from the epicentre and wooden constructions at distances 1.3 and 1.8 km, anti-landing barrage at the same distances and various constructions.

In order to provide scientific programs for the test about 500 sets of equipment have been established on ships, floating 120 ton stands and coastal constructions. At the coast, 6 equipment and 5 optic point have been deployed as well as 8 stands for air and radioactive contaminant probing. Additionally, 11

airplanes and 4 helicopters have been used for this air probing, and 2 ships for water probing in the Barents Sea.

Similar set of equipment and procedures were used during the second test in 1957.

During the third test in 1961 number of tested ship was minimum (target-ship and several previously damaged ships) and the scientific programs were reduced.

In order to obtain scientific information special sets of measuring and recording equipment have been designed and systems of automatic control for them and nuclear device.

Shock wave parameters in water from all the underwater explosions were measured by mechanic gages MID-3 and piston impulsemeters IM-1 and IM-2. Also, piezoelectric gauges were used. Deformation of elastic membrane in MID-3 proportional to peak deformation in shock wave was recorded by residual deformation (crumpling) in a lead target. Pressure impulse was measured by gages IM-1 and IM-2 by deformation (crumpling) of a copper target by a piston accelerated by a shock wave. During the experiments the gages were being improved. The latest constructions allowed to measure shock wave and refracted in water seismic waves separately. Usage of composite bars allowed to avoid effects of cavitation and rarefaction waves. Accuracy of separate measurements was of 15 per cent.

Piezoelectric gages with sensing element made of tourmaline measured pressure in shock wave as a function of time. Two-ray oscilloscopes - piezoelectric meters of pressure with the highest pass frequency of 300 kHz - were used for recording. The oscilloscopes were equipped by control system from outer automatics, inner calibration, electrometric high-resistant preamplifier which inputs had been short-circuited before explosion and worked only after passing of EM impulse generated by the explosion. Recording was carried out onto a film in a cassette established in a drum for long recording with high resolution or by camera from the oscilloscope's screen.

Chiefly, parameters of shock waves were have been measured by mechanical equipment used in general. Hundreds of gages were hung on winch from boats at

various depths and ranges from supposed epicentres. Up to six similar gages were hung at given depths at each wire for more precise measurements of shock waves. TNT equivalent was estimated by peak pressure measurements from the closest gages not disturbed, by modelling, by the free surface and bottom. This equivalent was as large as 0.6 of the total explosion energy.

In order to start the oscilloscope, high-speed cameras and other waiting equipment an automatic system was used. This control system started and turned off equipment at given times before and after shot time.

A set of photographic equipment recorded surface effects from the explosions in two perpendicular directions by cameras AFA-33 with a rate of 1 shot in 2 sec onto a film 33 mm wide and automatic cameras AKS-1 and AKS-2 onto a film 36 mm wide. High-speed cameras SK-2 with recording rate of 2500 sps onto 10 cm film together with AKS and AFA-BAF were established at an aircraft IL-28 for recording the pattern from above.

Camera SK-2 was designed for recording of fire ball and brightness temperature behind red filter with an exposition time of 1 msec in the first experiment. However, its bright sensitivity was not enough.

Surface waves were measured by resistive sensors with recording onto tenso-stations, parameters of air waves - by pressure recorders SD-25 onto smoked paper on a drum with constant rotation rate. In order to measure γ -radiation and radioactive contamination by basic wave a set of special techniques and equipment was used. Total γ -radiation doses for 30-40 hours were measured by photographic indicators at various points of the experimental field and by automatic gamma-X-meters. In SGR instrument, the sensor was a flat ionisation chamber with electrodes made of aluminium foil glued on thin plates of organic glass. These instruments allowed recording doses rates from 100 R/sec to 0.001 R/sec with the lowermost accuracy of 20 per cent and time resolution of 0.005 sec if recorded onto oscilloscope and 1.5 onto potential meter. In DP instruments, the sensors were photographic multipliers FEU-S working in logarithmic regime with time resolution up to 20 msec. Range of doses rates was from 0.001 to 100 R/sec. The largest mistake was less than 20 per cent.

FDR instrument measured the total dose and gave estimates of its evolution by blackening of a film exposed which was driven behind a protecting screen by a given program. All X-meters were automatic started by outer signals. Various instruments showed consistent results.

Measurements of concentration of nuclear fission products in probes taken by a given time schedule from the basic wave and radioactive precipitation as well as from water at various depths and ranges have been conducted. The concentration of the nuclear fission products in probes collected after the explosions was determined as a sum of γ and β activity measured in standard conditions with preliminary laboratory calibration.

Parameters of seismic signals and infrasound were measured in near-field and far-field zones. Techniques of seismic and infrasound monitoring nuclear explosions were being developed. The closest seismic station was 120 km far in town of Belushya.

2.1.2. Results of the underwater nuclear explosions.

The first underwater nuclear explosion was fired on 21.09.1955 in 8 hours by Moscow time. Wind blew across the bay to the Kara Sea. The shot point was about 7 km of the west coast where command point and living area were situated. Shock wave at the surface was observed as an expanding light circle - distinct slick generated by cavitation in water induced by reflected shock wave. Then a dome appeared as a pillar of water jets, and above the dome - a condensed cloud of water and products of detonation. A plume has formed as a hollow water pillar with a mushroom-like cloud lifting from the top of the it. The pillar seemed to be white due to inner shining. Then the pillar began destroying and falling down. From the wind driven cloud dropped out precipitation as rain and hoarfrost. When the plume collapsed a series of gravitational waves and basic wave were arising propagating of the epicentre. The basic wave may be described as a whirlwind motion of a condensed cloud and water drops which contained radioactive products of the explosion and were lifted up during expansion. The basic wave detached from the water surface and merged with the cloud in three - four minutes.

The measured air shock waves were being generated as a superposition of a head wave, induced by the uplifting with supersonic speed plume, and water-air refracted wave. Processes of radioactive radiation were measured in three phases of the underwater explosions: from the uplifting plume, from the basic wave, and from the region of radioactive contamination by precipitation. A distinct intensity of radioactive radiation in the explosion region was observed when the gas bubble was reaching the free surface. The intensity increased with radioactive gas venting into the atmosphere reaching its peak value in 0.1 sec after the explosion. After the cloud uplift and nuclear fission products fall-out, the intensity dropped to low values. According to measurements, there was no shielding of radiation by the plume walls during the first explosion.

The basic wave's cloud trace passed through the damaged engineering constructions, anti-landing constructions, trenches and severely contaminated the site. A special plane measured the radioactive intensity flying through the cloud.

The boat with the attached nuclear device sank right after the explosion. Destroyer "Reut" at 300 m of the explosion was at the edge of the plume. It was thrown up, split into three parts and sank at once (its middle part was just a heap of metal, as further observations showed).

Some distinct damages were observed at the other three closest ships also. "Kuibyshev" (1200m) was severely damaged by did not sink. Its left-side covering was teared off and the inner parts was exposing. Radioactivity was high even after deactivation by water from the sea carried out by fire-ships. Destroyer "Gremyashii" (1200 m) with steam engine had similar damages. Both ships did not sink. A pre-existing leak in destroyer "Karl Libkneht" (1600 m) became much larger after the explosion and it was moved to a shallow. At the first trail-net ship (800 m) glass was broken, a fence around command point was damaged, hatches' lids were deformed, balance of a hydraulic clutch was disturbed, pipes were cracked in many places. At the second ship (1600 m), a section of rowing shafts was sunk, compasses were teared off. Other ships at larger distances were not damaged.

The closest to the epicentre submarine S-81 (500 m) was severely damaged and did not work at all. At 800 m, a submarine B-9 in underwater position at the

periscope depth was supported by ropes from a floating bridge. The submarine was in the same position after the explosion but sank in 30 hours due to leak through damaged insulation and hung on the ropes. At the same distance, another submarine S-84 in surface position was not damaged much. At the submarine S-19 a torpedo apparatus has had an opened head lid before the explosion. A cork was damaged and about 15 ton of water occurred in the torpedo section. Almost all the damages, except at S-81, were repaired in 2-3 days by special deactivation crews.

The concrete coastal construction at 1300 m from the explosion was severely destroyed. The wooden construction at 1800 m was completely destroyed and another one (2900 m) severely destroyed. The anti-landing constructions at the same distances were completely destroyed. Landing means near the coast sank and, at depths more than 15 m, were not damaged. The researchers' living area was not damaged. Shock wave was felt as a weak one. At the east coast, a strong radioactive contamination was observed, and the living area was clean for further staying.

The second underwater explosion on 10.10.1957 was a modified torpedo T-5 of larger yield. The torpedo was launched from a submarine S-155 of 613 series being at the periscope depth near the exit from the bay. An old ship 10 km far of the submarine was the target for the torpedo. The explosion was fired in 9 hours 55 minutes at a depth of 30 m.

Content and positions of tested armaments relative to the explosion was similar to those in 1955. To the survived after the first underwater explosion and following above ground explosion (September 1957) test ships were added 2 destroyers ("Groznyi" and "Raz'yarenniy"), 2 submarines (S-10, B-20), and a number of other ships and boats. The submarines were at the surface except one (S-19) which was at the bottom. Scientific and recording equipment as well as some animals were at the ships as in 1955. Due to some mistake in aiming the torpedo was fired behind the target, 120 m closer to the test ships than suggested. Announced yield is below 20 kt [1,2]. Measured yield is about 10 kt.

The explosion's pattern differed from that in 1955. A water dome arose above the surface. During the first explosion the plume did not shield radioactive

radiation and nuclear fission products vented into the atmosphere. During the second explosion the products did not break the water pillar and radiation intensity was relatively low.

The tested ships and submarines were damaged more severely than by the first explosion. Right after the second explosion destroyers "Groznyi" and "Raz'yarenyi" sank as well as all smaller ships, trail-net ships and submarines S-81, B-9 and B-20. Destroyer "Gremyashii" in critical state was floating despite severe damages and fire in many places. The destroyer was being moved to a shallow. These more severe damages occurred not only due to larger and deeper explosion, but also due to closer relative to suggested epicentre. This mistake destroyed the scientific program much. However, despite some loss of information on sunk ships, principal parameters of the explosion were measured by equipment on other ships and coastal observational points.

Parameters of radiation processes were measured in three phases: from the uplifting cloud, from the basic wave and from the region of radioactive contamination. A distinct intensity of radiation was marked when the gas bubble was reaching the surface. The radiation was increasing with venting the radioactive products into the atmosphere reaching its peak in about 0.1 sec after the explosion.

The basic wave in both explosions had about 10 per cent of radioactive products of nuclear fission. Radioactive fall-out was increasing radiation level considerably. The fall-out along with the basic wave created severe radioactive contamination of the ships and coast. The contamination was high for a long time. By data from X-ray meters, the radioactive contamination level was dropping as $t^{-1.2}$ with time. From the conducted investigations there were revealed principal relationships for radiation processes from underwater nuclear explosions. These radiation processes are of longer duration (up to 30 min), in comparison with an air explosion with many peaks of close amplitude.

During the third explosion conducted on 23.10.1961 in 13:30:48 (Moscow time) there were only a target-ship and floating stands with measuring equipment. There are also different data on yield and depth (below 20 kt and 20 m) [1-4] but, by our opinion, data in Table 1.1 more accurate.

Fig. 2.2c presents a seismogram obtained at town Belushya 120 km of the epicentre. The seismogram was recorded by broad-band equipment (0.2 to 30 sec). It is typical for underwater explosions at shallow water. Longitudinal (P), shear (S) and surface (L) seismic waves are presented by short wave-trains of several oscillations with periods from 0.8 to 2.5 sec. The latter, relatively long-period, oscillations associated with reflection at inner boundaries in the crust are modulated by short-period oscillations with periods of 0.1 to 0.3 sec which attenuate with distance below 200 to 300 km. A principal feature of underwater explosions is a distinct rarefaction impulse arrival, marked by a character i, with amplitude about 2 times larger than that of the first longitudinal wave P. At range beyond 200 to 300 km, this arrival transforms into a group of oscillations with periods of 0.2 to 0.6 sec. This impulse is associated with an impact when water at high speed fills the gas bubble.

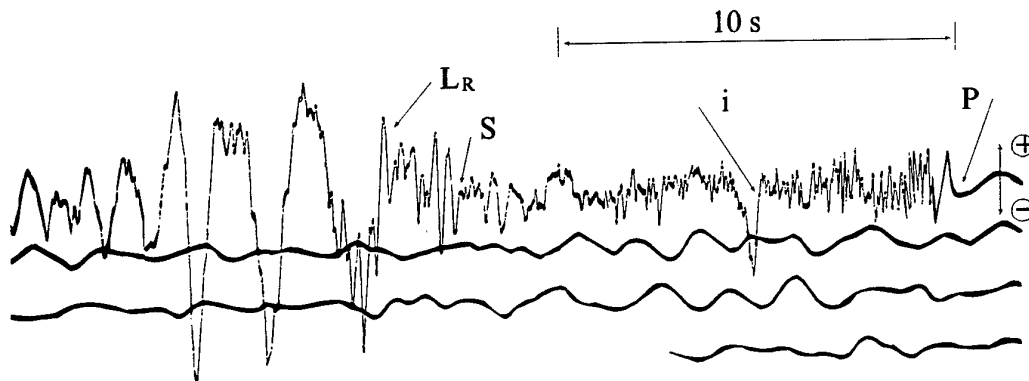


Fig. 2.2c. Seismogram from 1961 underwater explosion recorded at 120 km (Belushya).

2.2 Chemical explosions in deep water.

A reservoir is considered as deep if its depth is much larger than the peak gas bubble radius. Then no venting into atmosphere occurs. By this classification, all the nuclear explosions in the bay of Chernaya were conducted in shallow water. Conduction of nuclear explosions in deep water for hiding allows to prevent venting radioactive gas into the atmosphere. The latter complicates detection of the explosions. Below are described principal parameters of deep water chemical explosions which permit to estimate principal parameters for nuclear explosions by scaling laws.

2.2.1 Explosion in infinite liquid.

For a chemical explosion in infinite liquid [10] overpressure, P , in shock wave relative to hydrostatic pressure, P_0 , at the initial stage is given by relationships

$$P(t) = P_1 \exp(-t/\theta), 0 < t < \theta \quad (2.1)$$

$$P(t) = 0.368 P_1/(t/\theta), \theta < t < (5 \div 10)\theta \quad (2.1a)$$

where the parameters P_1 and θ depend of explosive's properties and distance to the charge, R . When analysing deep water explosions, relationship (2.1) is often used in a wider time interval $0 < t < t_1$, where t_1 is the time when pressure reaches the atmospheric value in the gas bubble. The peak overpressure P_1 and time constant θ in shock wave for blast of cast TNT (specific energy $Q=4.18$ MJ/kg, density $\rho=1600$ kg/m³) are described by following empirical relationships in scaled range $5 < R/M^{1/3} < 10$ m/kg^{1/3}

$$P_1 = 533 (M^{1/3} / R)^{1.13} \text{ kg/cm}^2, \quad (2.2)$$

$$\theta = 92 M^{0.26} R^{0.22} \mu\text{s},$$

where M is the mass in kg, R is the distance in meters. According to [11], relationships (2.2) are approximately valid to distances of $R_k/M^{1/3} \approx 2000$ m/kg^{1/3} and pressures $P_1 \approx 0.1$ kg/cm². At larger distance, θ is considered as constant, and $P_1 \approx A/(R(\lg R)^{1/2})$. For a deep bomb of 136 kg, R_k is about 10 km, and $\theta=2.6$ msec. Deviations of shock wave and gas bubble parameters from laws of energy similarity for various explosives are noted in [10,12].

After radiation of a shock wave, products of detonation expand to the hydrostatic value P_0 at $t=t_1$. Further dynamic expansion leads to negative pressure in the bubble reaching at time $t=t_2$ its lowermost value P^- , which can be as large as $-P_0$ at the explosion depth, if water does not lose its continuity due to cavitation. Then the bubble shrinks and pressure increases to peak value P_2^+ , and second pressure wave is being radiated. The wave is called the first pulsation and has a peak value for TNT

$$P_2 = 72,4 (M^{1/3}/R), \text{ kg/cm}^2 \quad (2.3)$$

During underwater explosion several such pulsation are radiated. Fig.2.3 shows a characteristic pressure recording at a depth of 150 m and distance of

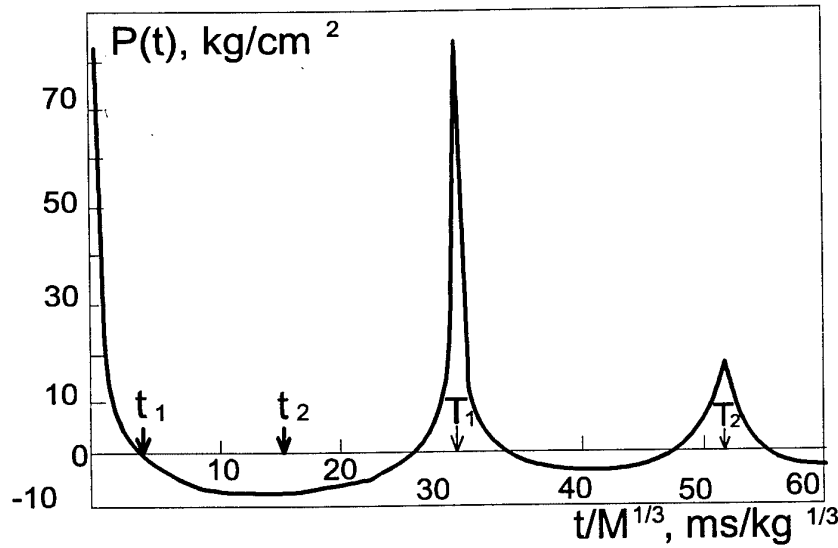


Fig.2.3. Time history of pressure at a depth of 150 m and distance of $R=1.1 M^{1/3} \text{ m/kg}^{1/3}$

$R=1.1 M^{1/3} \text{ m/kg}^{1/3}$. Periods of the first three oscillations T_i in seconds, peak bubble radius R_{lm} in meters from an explosions of mass M in kilograms at depth H in meters are determined by relationships:

$$\begin{aligned} T_1 &= 2.11 \cdot M^{1/3} / (H + 10.3)^{5/6}, \\ T_2 &= 0.72 \cdot T_1, \quad T_3 = 0.81 \cdot T_2, \\ R_{lm} &= 3.37 \cdot ((M/(H+10.3))^{1/3} \end{aligned} \quad (2.4)$$

Pressure dependence on time associated with gas bubble pulsation can be approximated either by a bell-like function, either by increasing and decreasing exponents. If $R < R_k$, ratio P_1/P_2 decreases with distance, and for $R > R_k$, the ratio is constant

$$\begin{aligned} P_1/P_2 &= 7.4 (M^{1/3}/R)^{0.13} & \text{for } R < R_k \\ P_1/P_2 &= 2.7 & \text{for } R > R_k \end{aligned} \quad (2.5)$$

Relationships for positive phase of impulse in shock wave I_1 , first I_2 and second I_3 pulsation in kg sec/m^2 for deep explosions are as follows [11]

$$\begin{aligned} I_1 &= 667 \cdot M^{1/3} (M^{1/3}/R)^{0.94} \\ I_2 &= 278 \cdot (M^{2/3}/R) \cdot (H+10.6)^{-1/6} \\ I_3 &= I_2/2.47 \end{aligned} \quad (2.6)$$

In [10] relationships for specific impulse I_1 in shock wave by time $t=6.7 \theta$ are given in a form $I_1 = AM^{1/3}(M^{1/3}/R)^b$, where, for TNT with $\rho=1520 \text{ kg/m}^3$ and pentolith with $\rho=1600 \text{ kg/m}^3$, $A=590$ and 926 , $b=0.89$ and 1.05 , respectively. In

[12] I_1 is determined at $t=5.5\theta$ for various explosive types. For PETN with density of 1600 and 400 kg/m³, $A=772$ and 1050, $b=0.92$.

According to [10,11], a shock wave takes about 45 per cent of total explosion energy of cast TNT. A large portion of the energy is dissipated in near-field zone. About 12 per cent of the total energy is radiated during the first pulsation and about 1.5 percent - during second. At the range $R=R_k$, only about 30 per cent remain in hydroacoustic disturbance after dissipation in near-field zone. For pressed and poured on PETN [12], shock wave takes 59 and 43 per cent of the total explosion energy respectively.

For nuclear explosions, shock wave parameters can be determined by relationships (2.2), where TNT equivalent by shock wave is used $M_s=k_s \cdot M$, where M is the total TNT equivalent equal to TNT charge mass which energy equal to the nuclear explosion energy. In the range from 0.1 to 100 kt k_s changes from 0.4 to 0.65. As a rule, k_s of about 0.6 is used. Parameters of the gas bubble are determined by relationships (2.4) with TNT equivalent $M_b=k_b \cdot M$, where k_b is of 0.8 to 0.9. Hence, nuclear explosions are characterised by weaker hydrodynamic disturbances than TNT explosions of the same energy and have 1.5 larger TNT equivalent by bubble pulsation than by shock wave.

Approximate relationship for shock wave spectrum can be obtained by Fourier transform of pressure function (2.1). For an exponent-like impulse of infinite duration, the spectrum has a shape shown on Fig. 2.4a in relative units (curve $t=\infty$). In complex variables

$$S(\omega) = P_1 \int_0^{\infty} \exp\left(-\left(\frac{1}{\theta} + j\omega\right)t\right) dt = \frac{P_1}{\frac{1}{\theta} + j\omega} \quad (2.7)$$

Converting to absolute values one can obtain the spectrum

$$\Phi(\omega) = \frac{P_1}{\left(\left(\frac{1}{\theta}\right)^2 + \omega^2\right)^{1/2}} \quad (2.8)$$

For a comparison, absolute frequency values for a TNT explosion of 10 kg ($\theta=200$ msec) are marked on the second X-axis.

For finite duration of exponent wave t_1 integral in (2.7) is calculated from 0 to t_1 , and, after decomposition by small values, one can obtain

$$P(t) = P_1 \exp(-t/\theta), \text{ for } t < t_1 \text{ and } P=0 \text{ for } t > t_1 \quad (2.9)$$

$$\Phi_1(\omega) = P_1 / [((1/\theta) + (2/t_1))^2 + \omega^2]^{1/2} \quad (2.10)$$

Approximate spectra for $t_1/\theta=3;2$ and 1 are shown on Fig. 2.4a. From (2.10) and curves on Fig. 2.4 it follows that the larger the charge mass the larger θ and low-frequency component of spectra is of relatively larger weight.

Spectrum of the first pulsation for the bell-like pressure function $P(t)=P_2 \exp(-b/t)^2$ has a form

$$\begin{aligned} \Phi_2(\omega) &= P_2 (\sqrt{\pi}/b) \exp(-\omega^2/4b^2) \quad \text{or} \\ \Phi_2(\omega) &= 0.825 P_2 \Delta t_1 \exp(-2.145 \Delta t_1^2 f^2) \end{aligned} \quad (2.11)$$

where Δt_1 is the effective pulse duration estimated for $P_2(t)=0.01P_1$. Then, $b=2.415/\Delta t_1$, $\omega=2\pi f$. This spectrum is shown on Fig. 2.4b by dashed line. For a comparison, a shock wave spectrum is also shown for the exponential form for duration of $t=\Delta t_1$, when $\theta=\Delta t_1/4.6$. It is seen that the shock wave spectrum is wider than that of pulsation. Assuming $\Delta t_1=0.22T_1$ [10] we have $\Delta t_1=50$ msec for a 136 kg TNT blast at a depth of 85 m. Distribution for this case on the second X-axis on Fig. 2.4b shows that secondary pressure waves contain, in general, low

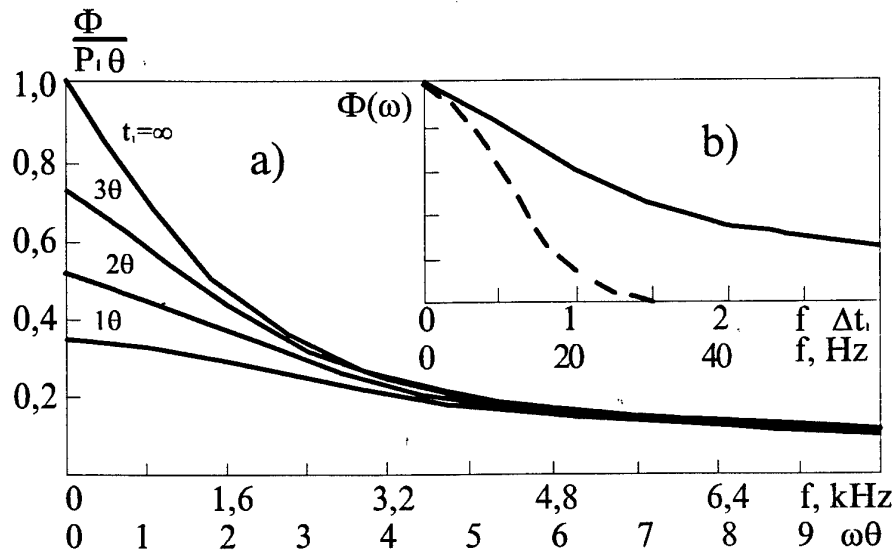


Fig.2.4. Approximate spectrum of shock wave (a) and comparison of spectrum of the first pulsation (dotted line) with shock wave spectrum (solid line) (b).

frequencies, and high frequency component is of lower amplitude.

An approximate analytic solution for total overpressure from an underground explosion can be represented in the form

$$P(t) = P_1 \exp\left(-\frac{t}{\theta}\right) + \sum_{i=1}^m P_i \exp\left(-\frac{t-t_i}{\theta_i}\right) + \sum_{i=1}^m A_i (t-t_i)(t-t_{i-1}),$$

$$A_i = 6 \frac{P_{i-1} \theta_{i-1} + P_i \theta_i}{T_i} \quad (2.12)$$

where the first term corresponds to the shock wave, the second - to the subsequent pulsation and the third - overpressure in the rarefaction phases. Parameter A_i is determined from the condition of equality of total overpressure impulse for one period of pulsation.

Fig. 2.5 presents amplitude spectra for total impulse from underwater explosions at various depths and various yields as calculated by (2.12). By using similarity law for energy[17] one can recalculate spectral curves obtained for 1 kg blast at a given depth to any mass multiplying overpressure and frequency by $M^{2/3}$ and $M^{1/3}$. An important feature of the spectra is two distinct peaks. The first peak frequency $f_{1\max} = 1/T_1$ corresponds to the frequency of the first gas bubble pulsation.

Fig. 2.6 displays curves for frequencies of spectral peaks $f_{1\max}$, $f_{2\max}$ and spectral minimum $f_{2\min}$ as a function of depth. The first peak frequency for 1 kg explosion increases from 6 to 60 Hz with depth increase from 10 to 300 m, and

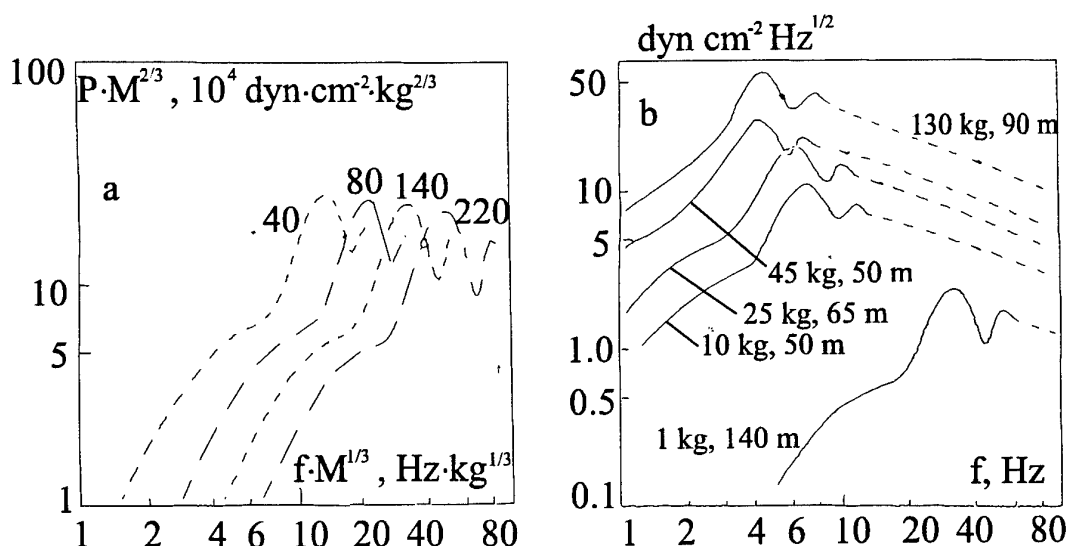


Fig. 2.5. Predicted amplitude spectra for total impulse from underwater explosions.

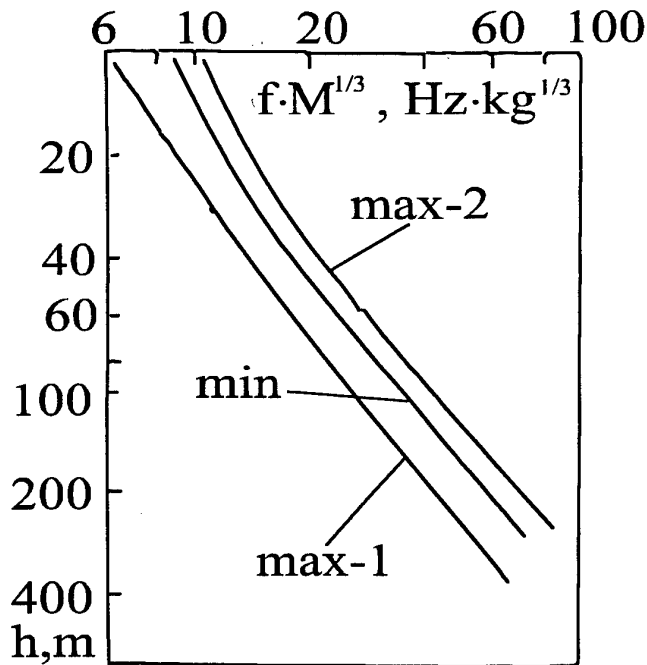


Fig.2.6 Frequency of spectral peaks as a function of depth.

in low-frequency band.

the second peak frequency increases from 11 to 100 Hz. (For 136 kg charge, the frequencies change from 1.17 to 11.7 Hz and from 2.15 to 19.5 Hz respectively.) Overpressure in the first and second peaks does not change much with depth increase. Analysis of the predicted spectra shows that the first gas bubble pulsation is an important factor influencing spectral content of hydroacoustic waves, especially

2.2.2. Underwater explosions of spherical charges in air-filled cavities.

In order to study effects of volume energy concentration of underwater explosions a series of PETN spherical charges explosions with density of 1600 kg/m³ and mass M from 0.4 to 2.5 g has been conducted. The charges were placed in the centres of spherical air-filled cavities with radius R_1 , where R_1/R_0 is from 1.79 to 12, $R_0 = 0.053 M^{1/3}$ is the charge radius in meters, M in kilograms. PETN specific energy is $Q = 5.85$ MJ/kg. Parameters of shock wave and gas bubble pulsation were measured by piezoelectric sensors and high-speed photographic equipment [13].

Fig. 2.7a displays characteristic overpressure time history as a wave train of decreasing amplitude arising from multiple reflections at boundaries and the shell centre. Fig 2.7b shows peak overpressure in shock wave, P_1 , as a function of scaled range, $R/M^{1/3}$. Dashed line shows measured initial pressure at the cavity wall. The pressure attenuates more rapidly with cavity growth than attenuates pressure in the water shock wave. Figs.2.7c,d present similar dependencies for scaled specific impulse $I/M^{1/3}$ and energy $\epsilon = E/MQ$ in the shock wave. These

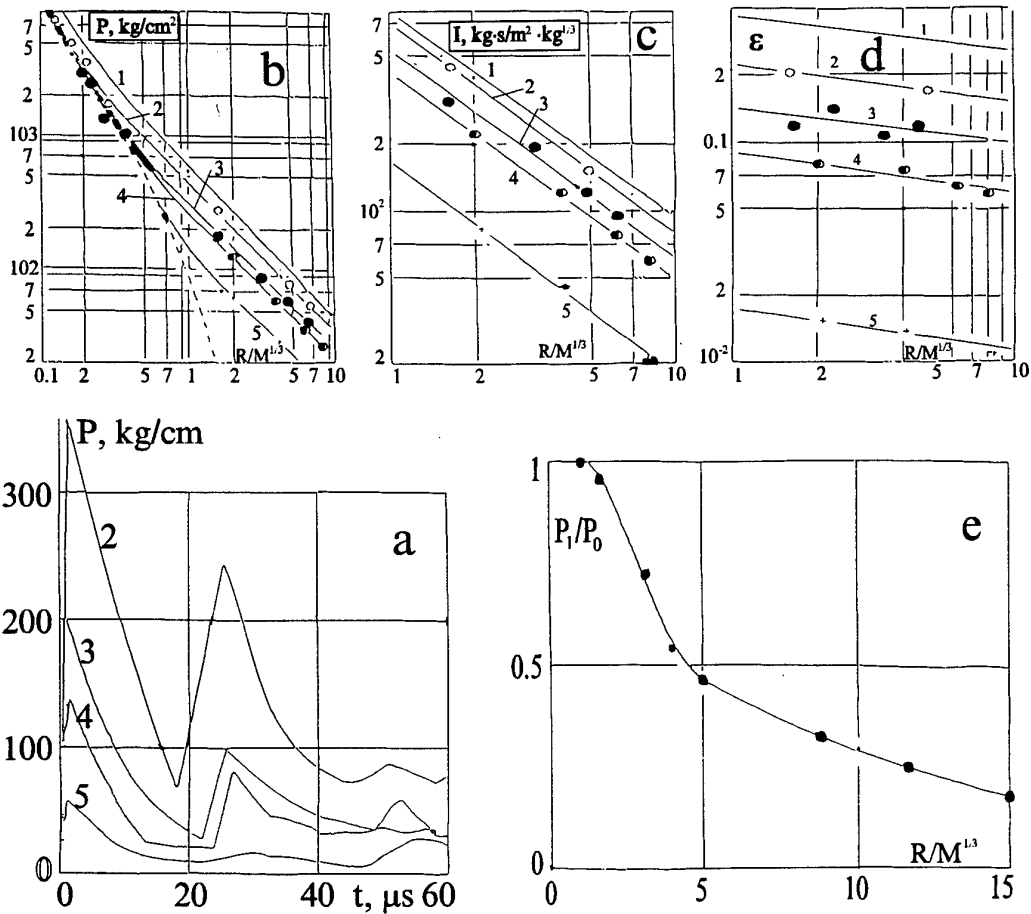


Fig. 2.7a,b,c,d,e Underwater explosion in a spherical air-filled cavity. 1-5 - $R_1/R_0=1, 2.64, 3.84, 5, 11.3$. (a) - shock wave oscillogram; (b,c,d) - peak overpressure P_1 , scaled specific impulse $I/M^{1/3}$ [kg sec/m²·kg²], and ratio of shock wave energy and explosion energy E/MQ as functions of scaled range $R/M^{1/3}$ [m/kg¹/³]. (e) - ratio of peak overpressure in shock wave at $R^*=5$ m/kg¹/³ from cavity and normal explosions as a function of scaled cavity radius R_1/R_0 .

values decrease in 5 and 10 times, respectively, with cavity radius increase to $R_1/R_0=11.3$ in comparison with normal explosion.

Energy balance of the explosions presented in Table 2.1 is determined from the measured parameters of the gas bubble and shock wave (R_m is the maximum bubble's radius, T_1 is the period of the first pulsation, $Y = \frac{P_0}{\frac{4}{3}\pi R_m^3}$ is the work done by the expanding bubble against hydrostatic pressure, E is the initial energy of the explosion, E_1 is the residual energy of the products of detonation, E_2 is the energy of the heated air in the bubble).

The parameters of the gas bubble are increased with scaled cavity radius in the range $1 < R_1/R_0 < 2.65$. For $R_1/R_0 = 2.65$, the peak radius and period of the

Table 2.1

№	R_1/R_0	R_m/R_0	T/R_0 , ms/cm	Y/MQ , %	E_1/MQ , %	E_0/MQ , %	E_2/MQ , %
1	1	32.6	51.7	38.2	6.1	59.4	0
2	2.65	38.1	62.5	59.8	5.65	31.5	3
3	2.86	36	56,4	51.2	5.7	32.5	10.6
4	3.84	33.6	56.1	41.2	6.1	17.5	35.2
5	5	33.6	60	41.2	5.95	11	41.8
6	9	33.4	-	40.4	6	3	50.6
7	11.3	30.9	-	32.6	6.35	2	59

first pulsation are about 20 per cent and the work against hydrostatic pressure in about 56 per cent larger than for the normal explosion. When $2.65 < R_1/R_0 < 11$, the parameters are decreased and a little lower than for the normal explosion. When the bubble expands to the peak radius, its energy is spent to do the work Y against ambient pressure. Residual energy $E = E_1 + E_2 = MQ - Y - E_0$, where E_1 and E_2 are inner energy of the detonation products and heated air, respectively. E_0 is the initial energy of the shock wave determined by extrapolation the curves on Fig.2.7d to the cavity boundary. The energy E_1 is determined by adiabatic curve for the detonation products, and E_2 from the energy balance which shows that the shock wave energy is decreased with the cavity growth, and the gas energy grows respectively.

When $R_1/R_0 = 11.3$, a portion of the shock wave energy, E_0/MQ , is of 2 per cent, and the residual energy in the cavity, when expanded to the peak radius, $E_1 + E_2 = 0.654MQ$. When the cavity is increased, the detonation products energy E_1 at peak cavity radius is being changed a little, and the heated air energy E_2 in the bubble is being highly increased, reaching 59 per cent for $R_1/R_0 = 11.3$. Since the heated air has the atmospheric pressure, it does not do any work. This leads to decrease of hydroacoustic energy at large distances. The study has shown that the cavity explosion can be used for evasion monitoring nuclear explosions. Further investigations with chemical explosions with mass to 1 ton in

underground air-filled cavities have confirmed the results from the underwater explosions.

2.2.3. Influence of bulk energy concentration on underwater explosion effects.

For underwater explosions energy similarity laws work only approximately and shock wave parameters depend not only on energy, but specific energy and density of charges. For illustration, Fig.2.8a,b present curves for peak overpressure and scaled specific impulse $I^*=I/(MQ)^{1/3}$ in shock wave as a function of scaled range $R^*=R/(MQ)^{1/3}$ for various explosion sources. In such coordinates, the shock wave parameters at equal scaled ranges R^* are decreased with decreasing bulk energy concentration ($MQ/V=\rho Q$ for chemical explosions).

The only dimensionless parameter $R^0=kA^\alpha R/R_0$, where $A=MQ/(V\rho C^2)$ is

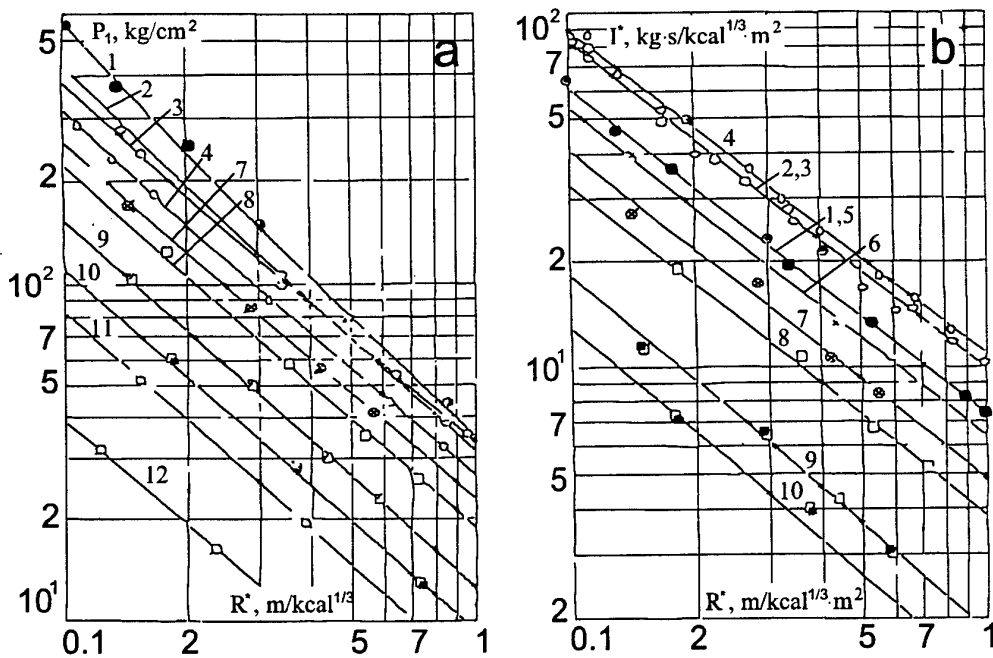


Fig.2.8. Dependencies on scaled range $R^*=R/(MQ)^{1/3}$ m/kcal^{1/3} for underwater explosion (a) - peak overpressure, P_1 , kg/cm² (b) - scaled specific impulse $I^* = I/(MQ)^{1/3}$ kg·sec/kcal^{1/3}·m²

1-4 - PETN explosions with $Q=1400$ kcal/kg, densities 1600 and 400 kg/m³; lead azide $Q=365$ kcal/kg and densities 1600 and 850 kg/m³, respectively.

5-8 - the same explosions in air.

9-17 - PETN explosions with 1600 kg/m³ density in the centre of spherical cavities of R_1 radius filled by air.

($R_1=1.25$ cm, $MQ=1.17$ kcal) - 9; ($R_1=1.85$ cm, $MQ=3.32$ kcal) -10;
 ($R_1=1.25$ cm, $MQ=3.5$ kcal) - 11; ($R_1=1.85$ cm, $MQ=1.18$ kcal) -12;
 ($R_1=1.85$ cm, $MQ=0.59$ kcal) -13; ($R_1=4.17$ cm; $MQ=1.12$ kcal) -14;
 ($R_1=4.37$ cm, $MQ=0.56$ kcal) -15; ($R_1=8$ cm, $MQ=1.12$ kcal) -16;
 ($R_1=12$ cm, $MQ=1.12$ cm, $MQ=1.12$ kcal) -17

the bulk energy density, k and α are constants, is determined by the dimension theory. The parameter determines shock wave impulse and pressure. Fig. 2.9a,b shows dimensionless peak overpressure and impulse as a function of dimensionless parameter R^0 for distances, where experimental data from Fig. 2.8 are described by unified relationships [12-14]. For the overpressure, the experimental data can be described by united relationship, where for $(0.015 < A < 4.5)$, $R^0 = A^{-1/2} R/R_0$,

$$P_1/\rho \cdot C^2 = 0.45/R^0{}^3 + 0.05/R^0{}^2 + 0.48/R^0 (\ln(R^0 + 1.75))^{1/2},$$

For shock wave energy, E , the obtained relationships against energy density, A , and range R/R_0 are of the form:

For chemical explosion in water: $E/MQ = 0.45(A^{-1/2}R/R_0)^{-0.11}$ ($0.6 < A < 4.5$)

For cavity explosion: $E/MQ = 0.99(A^{-5.2}R/R_0)^{-0.14}$

For the cavity explosion: $E/MQ = 0.99(A^{-5.2}R/R_0)^{-0.14}$.

Fig. 2.9c shows E/MQ as a function of A for $R/R_0 = 200$ as obtained from the presented experimental data and data from a nuclear explosion [15], which

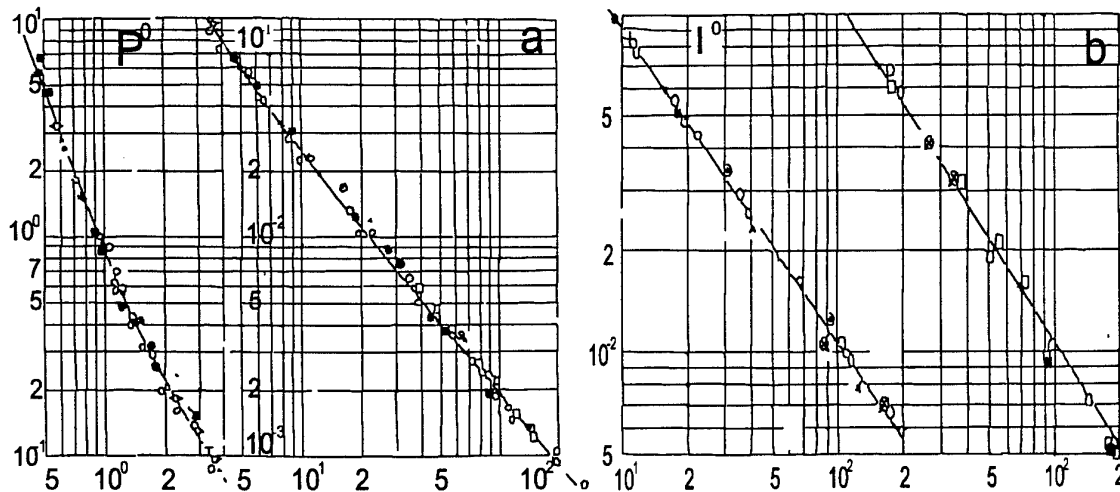


Fig. 2.9a,b Dependencies on scaled dimensionless range R^0 for underwater explosion (a) - dimensionless peak overpressure, $P^0 = P_1/C^2$, (b) - dimensionless specific impulse $I^0 = I/R_0 C_p$.

1-4 - PETN explosions with $Q=1400$ kcal/kg, densities 1600 and 400 kg/m³; lead azide $Q=365$ kcal/kg and densities 1600 and 850 kg/m³, respectively.

5-8 - the same explosions in air.

9-17 - PETN explosions with 1600 kg/m³ density in the centre of spherical cavities of R_1 radius filled by air.

($R_1 = 1.25$ cm, $MQ = 1.17$ kcal) - 9; ($R_1 = 1.85$ cm, $MQ = 3.32$ kcal) - 10;

($R_1 = 1.25$ cm, $MQ = 3.5$ kcal) - 11; ($R_1 = 1.85$ cm, $MQ = 1.18$ kcal) - 12;

($R_1 = 1.85$ cm, $MQ = 0.59$ kcal) - 13; ($R_1 = 4.17$ cm, $MQ = 1.12$ kcal) - 14;

($R_1 = 4.37$ cm, $MQ = 0.56$ kcal) - 15; ($R_1 = 8$ cm, $MQ = 1.12$ kcal) - 16;

($R_1 = 12$ cm, $MQ = 1.12$ cm, $MQ = 1.12$ kcal) - 17

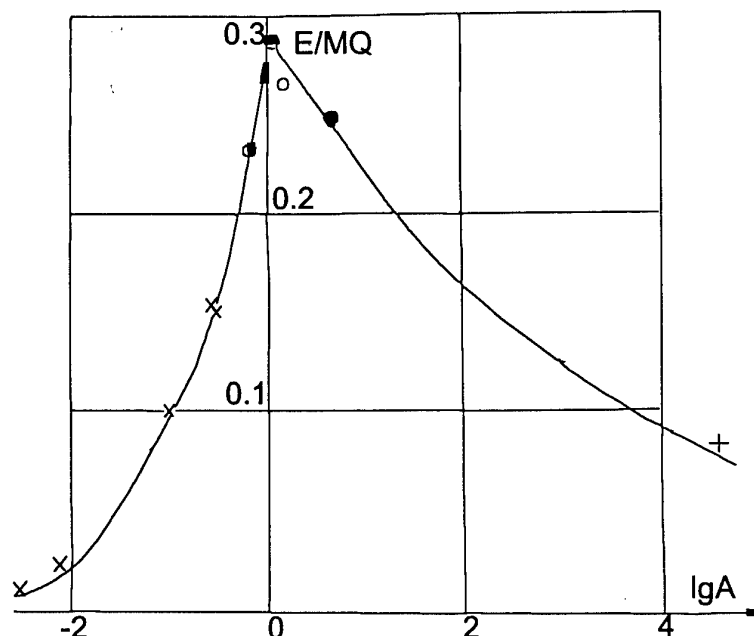


Fig. 2.9c. Scaled shock wave energy, E/MQ , as a function of bulk energy concentration in the source, A , at a relative distance $R/R_0 = 200$, - nuclear explosion [15]

has a peak at $A=1$. With A increasing in the range $\lg(A)<0$, the shock wave energy at large distances is increased due to increase of its initial value at the charge surface. When $\lg(A)>1$, the shock wave energy at large distances is decreased since dissipation losses are larger than increase of the initial shock wave energy associated with A increase. For nuclear explosions ($A \gg 1$), the shock wave energy at large distances is of about factor two lower than for TNT blasts ($A=1$).

2.2.4. Free surface and bottom effects on an explosion in reservoir.

For explosions in natural reservoirs overpressure is determined by a superposition of straight wave and waves reflected at the free surface and bottom. In this case, wave spectrum at some frequencies (depending on the explosion depth) is increased and at some frequencies is decreased due to interference.

A rarefaction wave from the free surface decreases overpressure usually to zero since water does not bear extension due to cavitation. This decreases duration, impulse and energy of the shock wave. Acoustic energy in spectrum of such a explosion is decreased due to attenuation of low-frequency component.

For an explosion near the free surface, period of the first pulsation is increased, and there may be no subsequent pulsation, if the bubble is being filled by water. In an acoustic approximation, where the sonic velocity C_0 and wave front velocity N are considered as constant and equal, relationships [17] are valid for peak overpressure P_1 , action time t , and specific impulse I of shock wave at distances R larger than 20 charge radii R_0 .

$$\text{For cast TNT, } P_1 = 14700/(R/R_0)^{1.13} \text{ kg/cm}^2, \quad (2.13)$$

$$t = 2Hh/RC_0, \quad I = \int_0^t P(t) dt$$

In hydroacoustic measurements, a system explosion/surface can be considered as a filter, whose frequency characteristic for an almost vertical incidence has the form:

$$\Phi_n(f, H) = \sin(2\pi H f / C_0),$$

Then, spectrum of the resulting wave is a product of the initial spectrum and the frequency characteristic of the explosion/surface system: $\Phi = \Phi_b \cdot \Phi_n$.

Fig. 2.10a presents some examples of the explosion/sea surface frequency characteristics for depths 40 and 140 m (solid and dashed lines, respectively). Explosion impulse is of about 3 periods long. The best conditions for wave propagation are occurred when $H = C_0 T / 4 = \lambda$. Fig. 2.10b shows optimal explosion depth and predominate frequency as functions of a TNT charge mass.

For a given charge mass the only optimal depth exists as well as the only

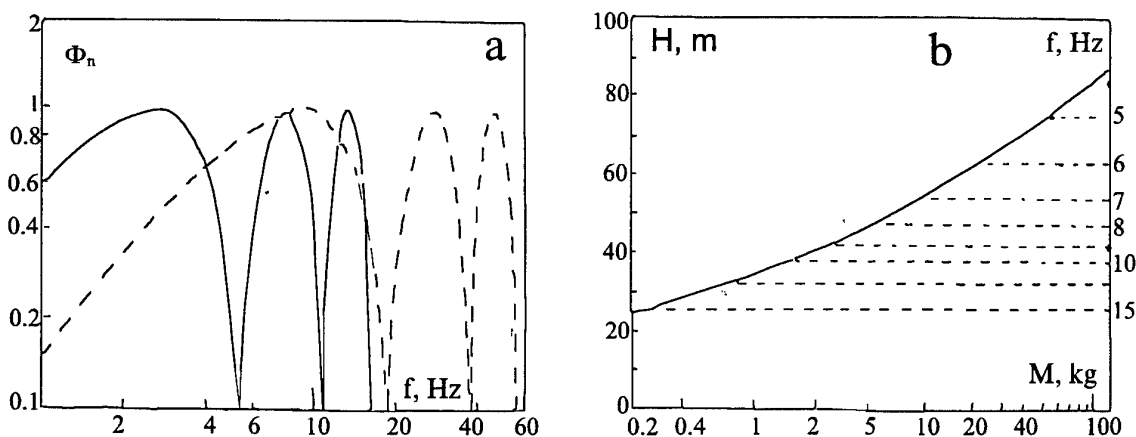


Fig. 2.10. Frequency characteristics for explosions near the free surface (a) and predicted relationships for optimal explosion depth and predominate frequency as functions of charge mass (b).

frequency at which recorded signals are of the highest amplitude and the signals spectra has the simplest form (except near-surface explosions without pulsation). The optimal frequency and depth for a 136 kg explosion are of 4 Hz and 95 m respectively. When explosions are not at the optimal depth, pulsation effects and surface reflections are not in the phase and spectra are being complicated.

For explosions at depth $H < (4-6)R_0$, the acoustic approximation is not valid for shock wave parameters at large distances. Due to nonregular reflection nonlinear effects become of importance. The effects lead to increased time action and decreased peak overpressure in comparison with predicted by (2.13). In a quasiacoustic approximation, which considers nonlinear effects, water isentropy curve is used as equation of state. Then, relationships for the front velocity, N , and sonic speed, C , are of the form:

$$N = C_0[1 + (n+1)P_1/4Bn]; C = C_0[1 + (n-1)P_1/2Bn]; u = C_0P_1/Bn$$

$$n = 7.15; B = 3045 \text{ atm}, Bn = \rho C_0^2 = 21800 \text{ atm} \quad (2.14)$$

If incident angle between the front normal and the free surface is low, then the horizontal component of the wave front velocity and rarefaction phase velocity, going from the free surface behind the shock wave, are as follows:

$$N/\cos\alpha = C_0[1 + (n+1)P_1/4Bn + \alpha^2/2] \quad (2.15)$$

$$C + u = C_0[1 + (n+1)P_1/2Bn]$$

When $C + u < N/\cos\alpha$, disturbances going from the free surface do not overtake the front and regular reflection occurs. for which the acoustic approximation is valid ($\alpha > \alpha^*$) [17]. The critical angle $\alpha^* = \{(n+1)P_1/Bn\}^{1/2}$ is determined from (2.15).

When $\alpha < \alpha^*$, nonregular reflection occurs. The shock wave front is curved due to interaction with overtaking rarefaction waves and overpressure is decreased to the free surface. Region of sharp overpressure changes for the nonregular reflection regime near the free surface is shown on Fig. 2.11a. The region is confined by a point b corresponding to intersection of the shock wave and rarefaction phase which propagates along a straight line passing through point O by an angle $\alpha^* - \alpha$ with the free surface and having depth $h_b = (\alpha^* - \alpha)R$.

Fig. 2.11b displays shadow photos from an underwater explosion near the free surface obtained by a high-speed camera SFR. The photos are consistent with the predicted pattern.

In a theoretical approximation used in [17,18] overpressure at the wavefront on the free surface P_1 is not equal to zero, but is determined by expression

$$P_1 = P_1(1 + \alpha/\alpha^*)^2/4 = P_1(1 + H/H^*)^2/4 \quad (2.16)$$

When $H = H^*$, $P_1 = P_1$, the latter is determined by relationships for an explosion in infinite liquid space (2.13). For nuclear explosions TNT equivalent by shock wave is used. Overpressure along the wavefront between point b and the free surface on Fig. 2.11a varies by a parabolic law [16]:

$$P_M = P_1[(1 + \alpha/\alpha^*)^2/4][1 + (\alpha^* - \alpha)(h/h_b)/(\alpha^* + \alpha)]^2 \quad (2.17)$$

For a low incident angle of a shock wave on the free surface, $\alpha \sim H/R$, $\alpha^* = H^*/R$. For $H^* < H$, the reflection is regular, and relationships (2.13) are valid. When $H^* > H$, the reflection is nonregular, and relationships (2.16, 2.17) are valid.

Shock wave parameters from cast TNT and pressed PETN (100 kg and 1 gram) blasts near the free surface were measured by piezoelectric sensors at

relative ranges $R/R_0 = 30, 60, 90, 120$.

The blasts were placed at depths H to $11 R_0$ and the sensors at depths h from 1 to $16 R_0$ [16].

Characteristic shock wave oscillogram from an explosion at a

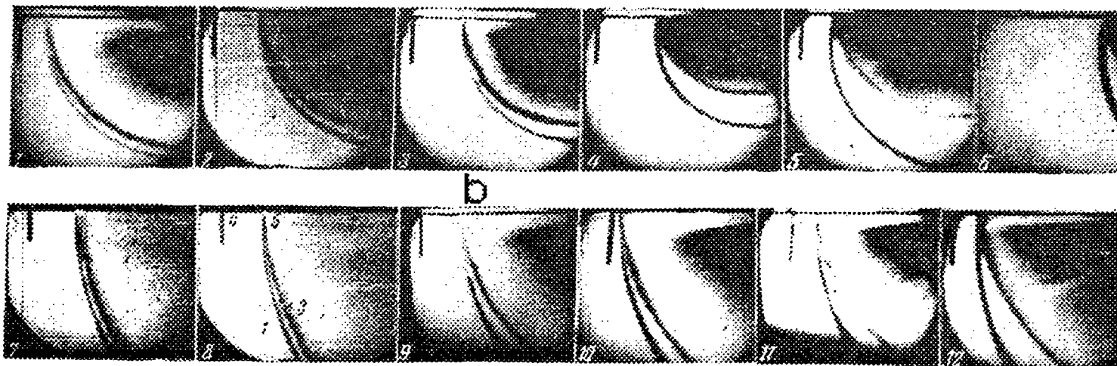
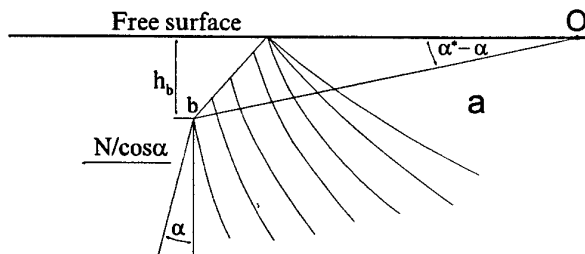


Fig.2.11. Nonregular shock wave reflection at the water free surface - (a). High-speed shock wave photos (b). 1 - direct shock wave, 2 - free surface, 3 - the first rarefaction wave, 4 - surface wave, 5 - second rarefaction wave. Blackened area near the free surface - cavitation zone.

depth $H=6R_0$ for a regime of regular reflection, when $P_M/P_1=1$, are shown on Fig. 2.12a. ($R=30R_0$, $h=4R_0$; $R=60R_0$, $h=30R_0$). $P(t)$ curves are exponent-like in the beginning, then transforming to a parabola. When $H<6R_0$, the wave has a shape of two parabolic sections, and nonregular reflection is occurred when $P_M/P_1<1$.

Fig. 2.12b,c,d show experimental dependencies for relative overpressure on shock wave front, action time, and specific impulse on depth of sensor, h , for various depths of blast H and distance R . For shock wave parameters experimental relationships are obtained in [16].

$$\text{Action time: } t = h[1.2(\alpha^* + \alpha) - (h/2R) + 2(h/2R)^2]/C$$

$$\text{Specific impulse } I = 0.5P_m t \text{ for } H=1 \cdot R_0; I = 0.6 \cdot P_m t \text{ for } 2 < H/R_0.$$

The reservoir's bottom, as well as the free surface, disturbs propagating hydroacoustic signals. If an explosion is far from the bottom, the later effects are only reflections and refractions. If an explosion is close to the bottom, initial shapes of the generated shock wave and bubble pulsations are disturbed

All possible bottom rocks can be separated into three types according to

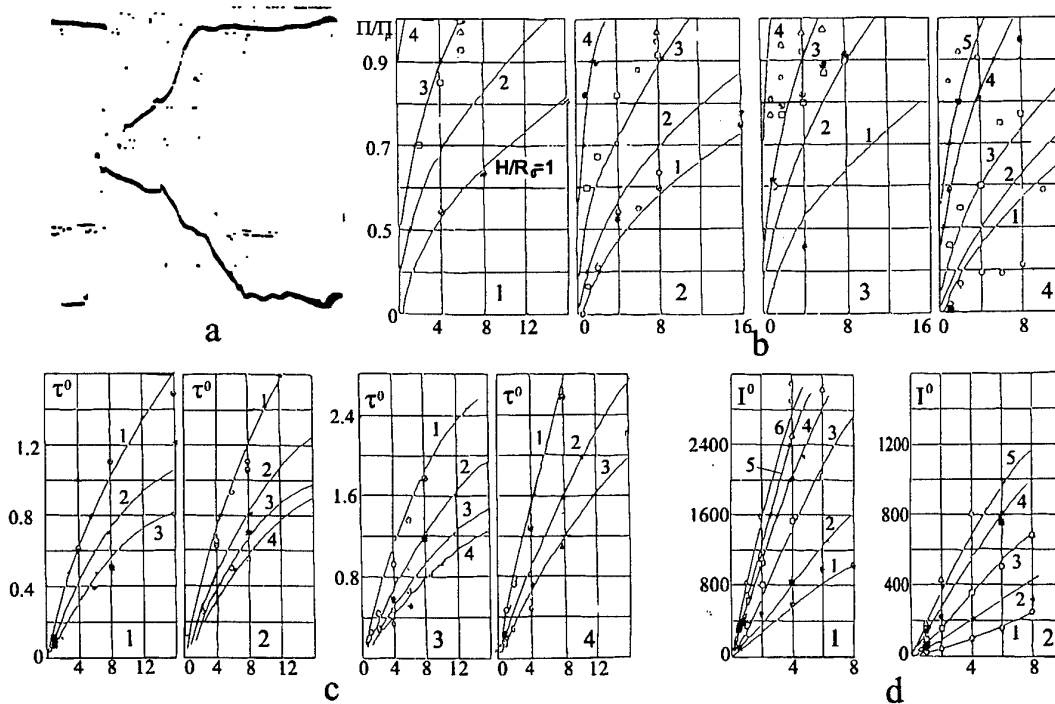


Fig. 2.12 Shock wave parameters for explosion near the free surface at various ranges R/R_0 . (a) - experimental recording ($h=4R_0$, $R=30R_0$ and $60R_0$) from spherical TNT charge blast at depth $H=6R_0$. (b,c,d) - relative overpressure at the front, action time in msec/m, and specific impulse in shock wave in kgsec/m^3 , against sensor depth, h , for various depths of blast, H , and ranges R/R_0 .

character of their interaction with shock waves in the near-field zone. The classes are determined by correlation between the water sonic speed C_0 , longitudinal C_3 and shear C_2 waves velocities in the ground.

For a low velocity bottom ($C_0 > C_3 > C_2$) elastic waves in the ground do not overtake the wavefront in water. The wavefield consists from direct wave, bottom wave, induced by Rayleigh surface wave propagating in the ground, and reflected wave. The latter may be a rarefaction wave (nonregular reflection), which may exist at large distance, as well as a compression wave (regular reflection).

For a high velocity bottom ($C_0 < C_2 < C_3$) or ($C_2 < C_0 < C_3$) head and side waves may arise in front of the water wave due to longitudinal and shear waves refraction from the ground into water. The head and side waves arise the direct wave incident angle α is below α_1 and α_2 , where

$$\alpha_1 = \arccos(C_0/C_3); \alpha_2 = \arccos(C_0/C_2)$$

Experiments near the low-velocity bottom ($C_0 > C_3 > C_2$) were carried out within a reservoir with a air-filled sandy bottom. Spherical TNT charges of 100 kg weight were being detonated. Density, sonic speed and bulk air concentration in the ground were 1950 kg/m^3 , $C_3 = 270 \text{ m/sec}$, ~ 0.001 [19]. Wavefield in water, as measured by tourmaline sensors, included direct wave, bottom wave and reflected wave. Principal shock wave parameters measured in water are presented on Fig. 2.13a,b,c. When $\alpha < \alpha^*$, nonregular reflection was observed with generation of a rarefaction reflected wave. In this case, a flow arises which is similar to the case of near-surface explosion. Overpressure and other parameters on the shock wave front are being decreased, when the charge and sensor approach the bottom.

Experiments with $C_2 < C_0 < C_3$ were carried out within a reservoir with an artificial bottom. The parameters were: $\rho = 1073 \text{ kg/m}^3$, $C_2 = 1130 \text{ m/sec}$, $C_3 = 2200 \text{ m/sec}$. PETN charges of about one gram weight and density of 1600 kg/m^3 were initiated in the centre. Tourmaline sensors were situated on the surface of a hemisphere 0.45 cm in radius and with the centre on the bottom just beneath the charges. The charges were placed at heights $H/R_0 = 1, 4, 8, 10, 12$ of the bottom. Such sensors' positions were convenient for observation wavefield's

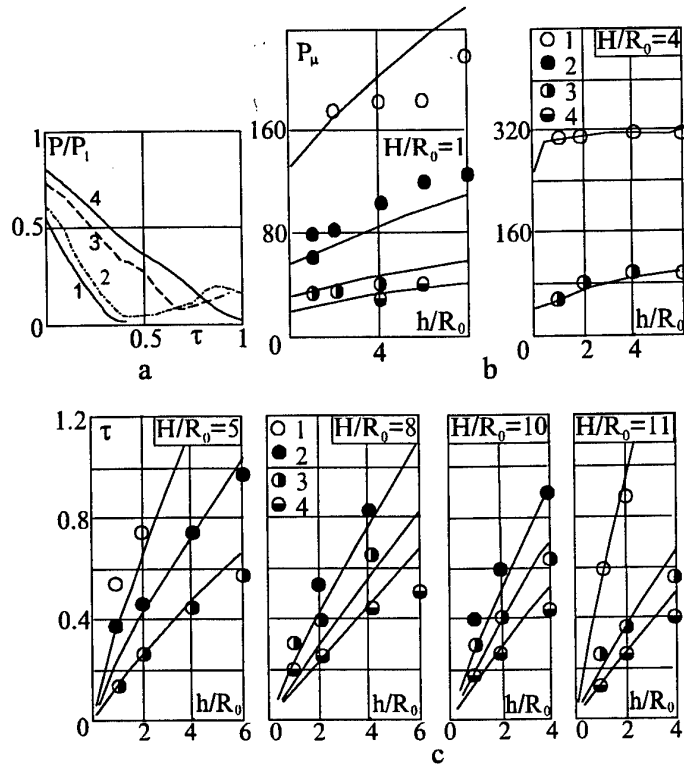


Fig.2.13a,b,c Shock wave parameters from 100 kg explosions at various charge, H , and sensor, h , heights above sandy bottom. (a) - relative overpressure P/P_1 as a function of scaled time τ (msec/m) for various h/R_0 ($R/R_0 = 60$, $H/R_0 = 1$). (b) - overpressure P_M as a function of sensor height h/R_0 . 1-4 - $R/R_0 = 30, 60, 90, 120$. (c) - action time τ (msec/m) as a function of sensor height above the bottom.

characteristic features at a surface close to wavefront [19]. Results of the measurements are presented on Fig. 2.14a,b,c.

Fig. 2.14a presents recordings revealing wavefield formation in water. On the recordings is shown incident angle, α , between the bottom and a ray passing from an imaginary source point beneath the charge to the observational point. Wave pattern measured by the sensors at angles $\alpha > \alpha_0$, where α_0 is determined by head wave and direct wave

intersection point, includes direct and reflected waves. For $H/R_0 = 1, 4, 8, 10$ and 12, α_0 is $38^\circ, 30.6^\circ, 26.3^\circ, 25.5^\circ$ and 24.5° , respectively. When $\alpha < 45^\circ$, reflection coefficient is becoming negative with a sensor approaching the bottom (this corresponds to decreasing α which is not the incident angle in this case), direct wave duration is decreasing due to arrival of rarefaction phase from the bottom, and also a bottom wave is arising from surface wave propagating in the ground. The bottom wave's intensity is increased with decreasing sensor and explosion heights. A rarefaction zone is observed between the direct and bottom waves.

For $\alpha < \alpha_0$, a head wave is observed before the direct wave. Its overpressure is increased with decreasing charge height above the bottom. For $H=1R_0$ the overpressure reaches 20 to 30 per cent of the peak overpressure in the direct wave. Due to superposition of the overpressures in the direct and head waves the peak overpressure may be of 40 per cent larger than that for the case of infinite

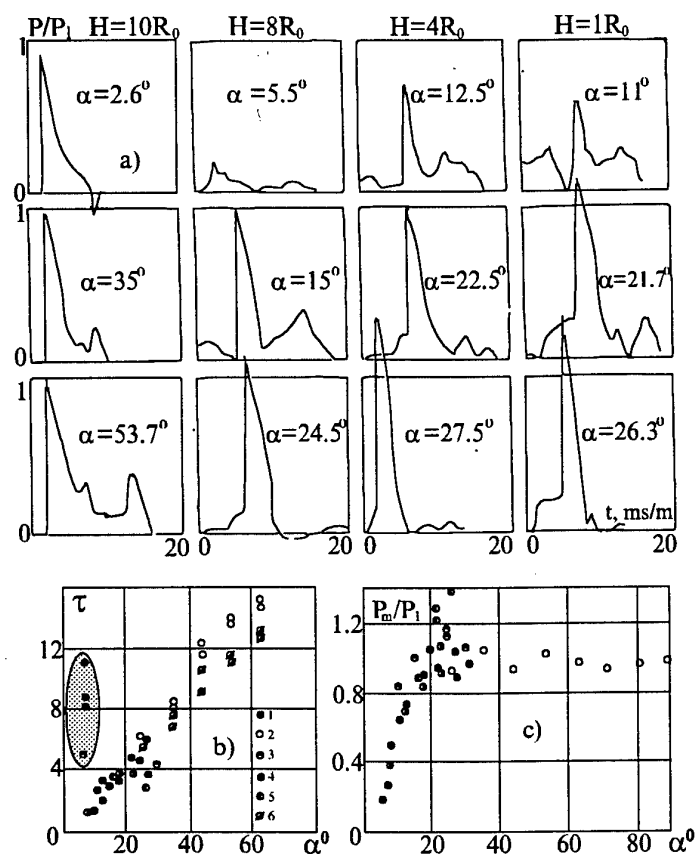


Fig. 2.14a,b,c Shock wave parameters from explosion near a solid bottom ($C_2 < C_0 < C_3$). (a) - relative overpressure P/P_1 as a function of scaled time $t_0 = t/R_0$ (msec/m), H/R_0 is the scaled explosion height: a - 12; b - 10; d - 4; e - 1. (b) - scaled action time t (msec/m) against angle α . H : 1-12 R_0 ; 2 - 10 R_0 , 3- 8 R_0 , 4 -4 R_0 , 5 -1 R_0 . (c) - relative overpressure in shock wave P_m/P_1 on angle α . Notations similar to the previous figure.

liquid space (Fig. 2.14a,d,e). Near the bottom, all the waves merge and are hardly to be separated. The peak overpressure in this zone is considerably lower than for the case of infinite liquid space.

Fig. 2.14b shows duration $\tau(\alpha)$ in the direct wave. For decreasing α , when the sensor is approaching the bottom, τ is decreased due to interaction between the direct and reflected at the bottom rarefaction wave. Near the bottom, total wavefield duration with consideration of the bottom wave is much longer than that of the direct wave (dashed area). Fig.

2.14c displays $P_m(\alpha)/P_1$. For $90^\circ > \alpha > \alpha_0$, the pressure at the front of the wave is constant and equal to P_1 which is characteristic for an explosion in the infinite liquid space. Near $\alpha = \alpha_0 \sim 20$ to 30° the peak pressure in the direct wave increases sharply due to interaction with the head wave and, on the curve $P_m(\alpha)$, a maximum is arose, with the amplitude increasing with the charge approaching to the bottom. When $\alpha < \alpha_0$, the pressure at the front of the direct wave is decreased due to nonlinear interaction with the rarefaction waves from the bottom.

Experiments with a high-velocity concrete bottom ($C_0 < C_2 < C_3$, $\rho = 2100$ kg/m³, $C_2 = 1620$ m/sec, $C_3 = 2800$ m/sec) were conducted with TNT charges of 0.2 kg weight. Wavefield from these explosions consisted of a direct wave,

reflected wave, bottom wave, head wave and a side wave. The latter began to overtake the direct wave when it had incident angle at the bottom of 57.5° and 22° , respectively. For low incident angles reflection coefficient became negative and rarefaction waves arising at the bottom decreased overpressure in the direct wave.

The experimental data analysis shows that, at large distances from the explosions, effect of any bottom type on shock wave parameters was similar to that of the free surface - a considerable peak pressure decrease.

2.2.5. Deep bomb blasts in the Sea of Okhotsk.

Hydroacoustic studies were carried out with deep bomb blasts of 136 kg. Hydrophones of various types with pass bands from 1 to 1000 Hz were used. The experiment was aimed at seismic sounding of seismically active regions in the Sea of Okhotsk with depth of 2.5 km and near the Kamchatka coast. Explosions conducted at depths from 10 to 300 m were measured on submarines at distance to 300 km. On moving ships, the measurements were conducted at distances of 250 to 500 m from explosions at depth from 60 to 180 m. Amplitude ratio of shock wave and following gas bubble pulsations, their periods, noise level, and propagation characteristics at large distances were determined. At a time, seismic measurements were carried out at Kamchatka at distances from 69 to 221 km.

For the measurements on submarines, hydrophones of three types were used: industrial hydrophones GICH with a sensitivity of $60 \mu\text{V}/\text{bar}$ and pass band to 5 Hz; standard ship's hydrophones with a sensitivity from 200 to $500 \mu\text{V}/\text{bar}$ to $500 \text{ mV}/\text{bar}$ and pass band beyond 1 Hz; designed in the Institute for physics of the Earth, USSR Academy of Sciences, piezoelectric hydrophones in artificial glass cases. The latter sensors were specially designed for measuring weak deep waves of low-frequency, in the range beyond 2 to 3 Hz, comparable at large distances with sea noise, and for nondisturbed measuring more intensive waves with frequency of 10 to 300 Hz at distances from 10 to 250 km. The sensors were placed outside on head, middle and back parts of the submarines. Cables were passed through the shells.

The lowermost noise was observed near the middle part, where the measurements, in general, were being conducted. The noise was considerably larger than the internal sea noise at large depth (0.2 bar). To suppress the noise during storms of 5 to 6 balls, the submarines were at depths at least 50 to 80 m. The optimal depth for reliable measurements at a given frequency f was determined from a well-known relationship $H=\lambda/4=C/4f$. For $C=1500$ m/sec and $f=3$ and 10 Hz, the optimal depth is $H=125$ and 37.5 m, respectively. The best for the noise suppression is a submarine to stay inside a density jump, when the submarine is being in the underlying layer and the noise is being much lower.

Measurements in deep sea were conducted at depths of 50 to 80 m, and, at depths of the bottom as large as 250 m, the submarines were just on the bottom. The lowermost noise level of 1 to 1.5 bar with signal to noise ratio of 5 to 9 was observed during a drift in the density jump layer in the open sea at distance from 100 to 130 km from the explosions. Near-bottom flows drove the submarine producing a high level noise.

On the above-water ships the noise was investigated in the bands from 1.5 to 7 Hz, from 2 to 12 Hz, and from 4 to 12 Hz. Amplitudes and visible periods were measured. The noise level was much larger than that measured on the submarines in similar frequency band. The ship-measured noise are concentrated in the frequency band from 1.5 to 17 Hz and amplitude range from 0.5 to 50 bar, the noise larger than 10 bar being very rarely observed. There were observed noise peaks near 1.5 to 3 Hz and around 10 Hz. The noise level decreased with frequency increase, but was unfavourable for recording weak deep waves at large distance, even in quite weather conditions. Thus, the waves were recorded on the submarines and stationary deep stations.

Fig. 2.15a shows characteristic hydroacoustic recordings from a deep bomb blast at a distance of 51 km as observed on a submarine near the bottom. The signals were produced by refracted into water seismic waves. Characteristic travel time of the signals is of 10.4 sec and its apparent velocity is of about 5 km/sec. The latter corresponds to longitudinal wave velocity in hard rocks.

From a moving ship in the sea from 1200 to 2500 m deep, low-frequency component of the signals from the explosions and gas bubble pulsations was

recorded. The first pulsation period T_1 and the ratio of shock wave and the first pulsation amplitudes $K_1 = \alpha_0 / \alpha_1$ were determined. Fig. 2.15b displays recordings from explosions at depths 70 and 180 m, and Fig. 2.16a,b - results of the measurements.

For a 100 m deep explosion, sound waves' intensity at a range 500 m and frequency 10 Hz was 50 kbars or 0.05 atm, i.e. about 2 orders of magnitude lower than a shock wave amplitude calculated by (2.2) for TNT [10].

When the explosion depth is increased from 60 to 120 m, T_1 is being decreased from 0.34 to 0.19 sec. These periods are consistent with those calculated by (2.4). The first wave train duration is being decreased due to mutual approaching of secondary impulses: the reflected on the free surface and the first

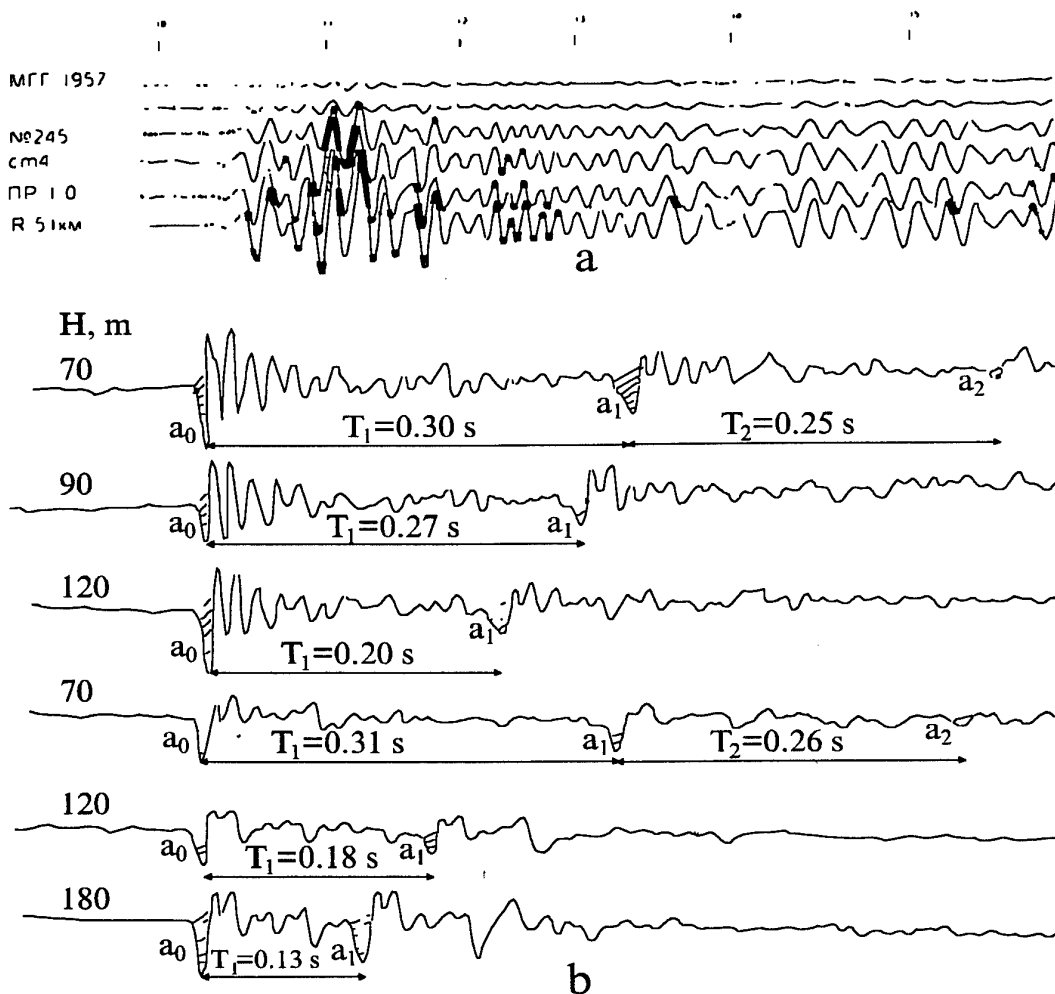


Fig. 2.15a,b Characteristic hydroacoustic recordings from a 136 kg deep bomb explosion. (a) - typical recordings on a submarine near the bottom 51 km far. (b) - recordings on a ship from explosions at various depths H m, T - pulsation period in sec.

pulsation. This effect decreases the total duration. K_1 values (Fig. 2.16a) were determined only with a little accuracy from measurements in the range from 350 to 600 m, where this parameter was changing from 3.7 to 1.7 due to high frequency attenuation in the shock wave.

Some recordings obtained at the coastal seismic station at ranges from 60 to

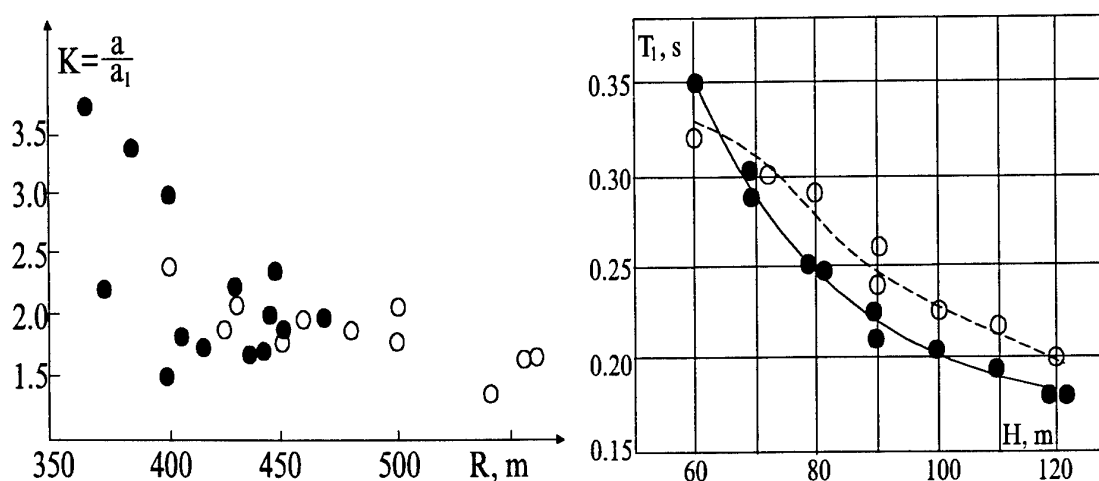


Fig. 2.16a,b Amplitude ratio K (shock wave/the first pulsation) as a function of distance from the gas bubble - (a) and the first pulsation period T_1 as a function of deep bomb explosion depth H - (b). \bullet , \circ - various explosion series.

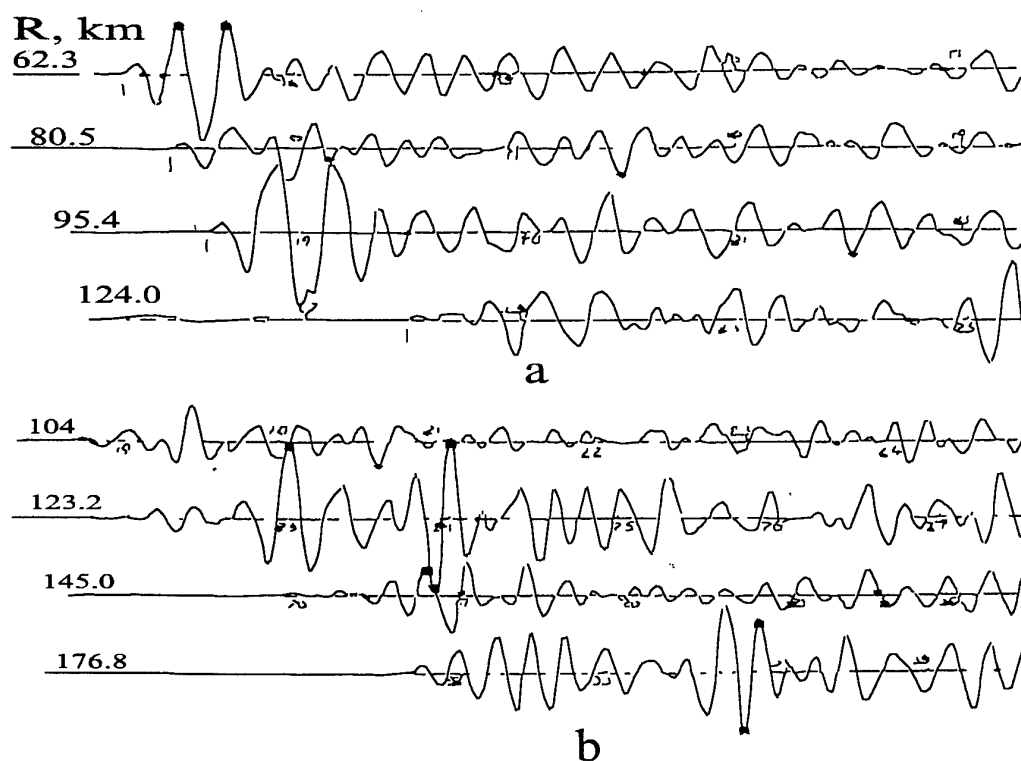


Fig. 2.17 (a) - typical recordings obtained at a station on a cap in the open ocean at various ranges from deep bomb blasts. (b) - At a station at the bay coast.

220 km and from explosions at a typical depth of 90 m are shown on Fig. 2.17. Characteristic period of the oscillations is consistent with the calculated by (2.4) value 0.237 sec for a 90 m deep explosion. The depth was determined by calculation from the measured time to the explosion. Possible variation of the depth may be induced by the different angle of motion of the bombs.

The conducted study shows that a larger portion of the energy from a deep underwater explosion is emitted with a shock wave, the first and the second pulsations. Nonlinear absorption effects in the shock wave from a 136 kg explosion are observed to 10 km. Ratio of the peak overpressure in the shock wave to that in the first pulsation decreases with distance and is of 1.7 to 2 beyond the nonlinear zone.

The shock wave is characterised by a relatively broad frequency spectrum, and the pulsations are of relatively low frequency. Spectrum of a summary wave has two distinct peaks in the low frequency band which positions are determined by the pulsation regime (frequency is equal to reverse period) and, hence, depend on the mass and depth of the explosion.

For explosions at depths of 100 to 200 m, the sea surface effects spectrum of radiated waves. Due to interference of the direct and the free surface reflected waves the spectrum is increased at some frequencies and is decreased at different frequencies. The best conditions for seismic waves generation and hydroacoustic disturbances propagation at large distances are created when the pulsation frequency is equal to the predominant wave frequency and, at a time, when the explosion depth and measurements are equal to $1/4$ of this wavelength. From near-surface explosions acoustic energy is considerably lower, chiefly, due to low-frequency components. In this case products of detonation vent in the atmosphere and no pulsations occur. The deep bomb explosions were distinctly recorded to 300 km. Usage of deep explosions permits to increase distance of their detection and to enrich low-frequency content.

2.2.6. Three tons detonating cord explosion in the Black Sea.

In February, 1957 an explosion of 3250 kg of detonating cord has been conducted at a depth of 1 m in the Black Sea near Sevastopol. The cord was of 3.65 cm in radius (R_0) and 500 m long. The explosion was recorded by a high-

speed camera. Shock wave parameters from the explosion were measured at distances $R=25, 50, 100$ and 200 m of the charge centre and at depths 1 and 10 m by mechanic pressure and impulse recorders MID-3 and IM, the same as used for nuclear explosions.

Table 2.2 lists mean measured values of peak overpressure P_e which are decreased with increasing depth due to free surface effect. At a distance of 200 m a sharp overpressure and impulse increase near the free surface is observed. This effect may be explained by some special features of sound propagation in inhomogeneity liquid with a waveguide. Peak overpressure in shock wave as a function of distance normal to the charge is determined in the range to $R/R_0 = 5840$ for an explosion in an infinite liquid space

$$P_1 = 17200 / (R/R_0)^{0.74}, \quad (2.18a)$$

where P_1 is measured in kg/cm^2 . When deriving this relationship, along with the experimental data corrected for the free surface effects, if necessary, an initial overpressure $P_1 = 252.6 \text{ kg/cm}^2$ at the maximum distance $R/R_0 = 300$ from Reah and Ginell [10] was used. Asymptotic formula peak overpressure at large distance from a cylindrical charge explosion in an infinite liquid space has the form [22]

$$P_1 = 18360 / (R/R_0)^{0.75} \quad (2.18b)$$

Table 2.2

R, m											
25			50			100			200		
h, m	P_m , kg/cm^2	P_e , kg/cm^2	h, m	P_m , kg/cm^2	P_e , kg/cm^2	h, m	P_m , kg/cm^2	P_e , kg/cm^2	h, m	P_m , kg/cm^2	P_e , kg/cm^2
3	137	130	1.5	40.4	42	1	18	20	1.5	10	34
4	137	136	2.5	50.3	50	2	21.2	22	2.5	11.2	23
6	137	140	4.5	73.2	74	4	28.4	30	4.5	13.8	15
8	137	143	6.5	82	83	8.6	49.1	51	6.5	16.6	17
10	137	140	8.5	82	80				8.5	19.7	19

In laboratory experiments [17] at distances to $R/R_0 = 221$ the following empirical formula is obtained

$$P_1 = 15482/(R/R_0)^{0.71} \quad (2.18 \text{ c})$$

For a comparison P_1 values calculated by all the equations (2.18) are presented in Table 2.3. Formula (b) with coefficients determined experimentally is consistent with the experimental formula (a). Divergence of values predicted by (a) and (c) is increased with increasing range since the latter is determined only to $R/R_0=220$.

The features of a weak shock wave propagation near the free surface have been treated already in (2.14-2.17). For a cylindrical charge the formulas may be applied for quantitative estimates at large distance, when the shock wave front is close to a plane. Incident angle of the shock wave decreases with distance since $\alpha \sim H/R$. Assuming $P_1 = 17200/(R/R_0)^{0.74}$ for an explosion in an infinite liquid space one can obtain a critical incident angle $\alpha^* = [(n+1)P_1/2Bn]^{1/2} = 1.8/(R/R_0)^{0.37}$.

Table 2.3

R, m	25	50	100	200
R/R_0	685	1370	2740	5480
$P_1, \text{kg/cm}^2(\text{a})$	137	82	49.1	29.4
$P_1, \text{kg/cm}^2(\text{b})$	137.1	81.5	48.4	28.8
$P_1, \text{kg/cm}^2(\text{c})$	150	91.8	56.1	34.3
H^*/R_0	110.1	170.4	264	408
H^*, m	4.02	6.22	9.62	14.9
α^*	0.16	0.124	0.0962	0.0745
α	0.04	0.02	0.01	0.005
h_b, m	3	5.2	8.62	13.9
$P^1, \text{kg/cm}^2$	53.4	27.7	15	8.37

Since $\alpha^* = H^*/R = 1.8/(R/R_0)^{0.37}$,

$H^*/R_0 = 1.8(R/R_0)^{0.63}$ and $H^* = 0.0657(R/R_0)^{0.63}$ m.

When $H^* < H$, reflection at the free surface is regular and pressure on the front is the same in a liquid space. When $H^* > H$, reflection is nonregular and the pressure is decreased with decreasing depth of explosion. Table 2.3 presents predicted values for H^*/R_0 , H^* , h_b , α^* , α , P_1 which determine a character of the shock wave interaction with the free surface. Table 2.2 presents predicted peak pressure values in shock waves P_m corrected on the free surface effect and their comparison with mean experimental values P_e .

The predicted and measured values are consistent at any distance except $R=200$ m, where the predicted overpressure value is of a factor 2 to 3 larger than averaged by 5 measurements by sensors at small depths, and impulse if of a factor 1.7 larger. This discrepancy may be associated with sound wave propagation in an inhomogeneous liquid with an underlying layer having a sound speed gradient. Characteristic distribution with depth of salt concentration, temperature t , and sound speed C is presented in Table 2.4 for winter time.

$$C = 1410 + 4.21t - 0.037 t^2 + 1.14 S + 0.018 h$$

Fig. 2.18 presents sound propagation in a waveguide having characteristics listed in Table 2.4. Sound speed distribution with depth is given by the relationship [23]

$$C = C_0 [1 + h d(C/C_0)/dh] = C_0 ((1 + k(h-11)));$$

$$k = d(C/C_0)/dh = 0 \text{ for } h < 11 \text{ m}; \quad k = 41 \cdot 10^{-4} \text{ m}^{-1} \text{ for } h > 11 \text{ m}.$$

Table 2.4

h, m	S, ‰	t, °C	C, m/c	h, m	S, ‰	t °C	C, m/c
1	8	0	1419	14	18	1.5	1437
2	8	0	1419	16	24	2.5	1448
10	8	0	1419	18	30	3.5	1460
11	8	0	1419	20			1471
12	12	0.5	1426	22			1483

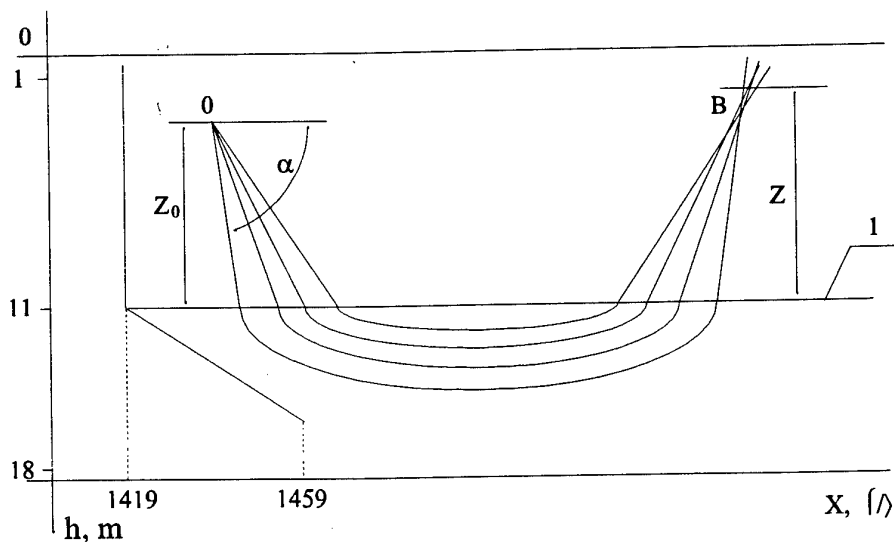


Fig. 2.18. Sound propagation in a waveguide from an explosion in a point O. Z_0 and Z are the distances from the explosion and the sensor to the interface (1) - the layer with sound speed gradient at a depth of $h_0=11$ m, α is the ray emergence angle from the explosion, incidence angle upon the interface and emergence angle from the interface.

Let an explosion be in a point O in the layer with a constant sound speed (where $k=0$) at a height Z_0 above the interface (1) with the region with the speed gradient. In a geometric acoustics approximation, which is valid for short-length waves from an explosion near the free surface, it is assumed that the explosion generated signals may propagate to a point B at a height Z above the interface (1) by various paths, as shown in Fig. 2.18. In the upper water layer, where $k=0$, the sound rays are straight and incident angles α upon the interface from both sides are equal. In the lower water layer, where $k \neq 0$, the rays are curved to the interface (1) by the Snellius law:

$$\cos \alpha / \cos \alpha_0 = C(h) / C_0; n \cos \alpha = \cos \alpha_0; n = C_0 / C$$

An analysis conducted in [23] shows that the rays radiated from the source at an angle $\alpha_0 = \alpha = \arccos[1/(1+kh_0)]$, return back to the horizontal plane, where the explosion is conducted, and are focused at a distance $R = 2(\operatorname{tg} \alpha_0 + p/\operatorname{tg} \alpha_0)/k$, the focusing factor f_1 being equal to $(\cos 2\alpha_0)(\operatorname{tg} 2\alpha_0 + p)/(\operatorname{tg} 2\alpha_0 - p)$, where $p = k(Z+Z_0)/2 = 0.041$, h_0 is the thickness of the gradient layer. If h_0 is large enough, when $\alpha_k = 90^\circ$ and all the incident rays are back to the upper layer at various ranges R .

In table 2.4 $h_0=11$ m, $k=41 \cdot 10^{-4} \text{ m}^{-1}$, $\alpha_k=16.9^\circ$ and only the rays with radiation angles $\alpha_k < 16.9^\circ$ can return through the interface (1). When $\alpha_0 = \arctg(p)^{1/2} = 11.5^\circ$, f_1 is infinite. For such angles the rays are concentrated near a caustic surface, where the geometric approximation does not work and potentials should be used [23].

Table 2.5 presents parameters calculated by the above formulas. The parameters characterise focusing conditions for $Z=Z_0=10$ m, $p=41 \cdot 10^{-3}$, $k=41 \cdot 10^{-4} \text{ m}^{-1}$ in the permissible range of angles $11.5^\circ < \alpha_0 < 16.9^\circ$. Mean values $R \sim 200$ m, $f \sim 4$ are consistent with the experimental data from Table 2.2.

Section of the caustic surface by a horizontal plane, which is a circle with a radius R_k , focusing factor f_2 and width of a zone Δr , where intensity drops by 3 to 5 times, determined by potential technique have the form: $R_k = 4(p)^{1/2}/k = 198$ m; $f_2 = 1.257(k_0 r p)^{1/3} = 8$; $\Delta r = 0.287(\lambda^2 r / p^{2/3})^{1/3} = 4$ m [23].

In the caustic zone, amplitude of a wave is of the maximum value and drops rapidly of this zone. The conducted analysis and results of the measurements show a possibility of a considerable sound impulse increase in the water with an underlying layer characterised by positive sound speed gradient comparable with charge length. There are also shadow zones, where sound intensity many times lower than in homogeneous water. Optimal conditions for long distance propagation of hydroacoustic signals generated by explosions are created in underwater waveguide with a minimum sound speed along the waveguide. Attenuation in the waveguide is large only above 1 kHz [23]. Inside the global sound channel (SOFAR), situated within the southern and central parts of the world ocean at a depth of about 1 km, attenuation of standard explosion

Table 2.5.

α_0°	12	13	14	15	16	17
$\text{tg} \alpha_0$	0.2126	0.231	0.249	0.268	0.2862	0.3057
R, m	198	199	201.8	205.4	204.5	214.5
f_1	19.6	7.27	4.58	3.42	2.76	2.34

generated frequencies below 100 Hz is negligible. Thus, the detection by hydroacoustic methods is possible to distances of 10,000 km.

2.3. 100 kg spherical cast charge explosions in shallow reservoirs with low-velocity sandy bottom ($C_0 > C_3 > C_2$).

Experiment was conducted in a man-made reservoir 87 m long, 20 m wide in the even part, and with a depth of $H^*=3$ m. The reservoir had an air-saturated sandy bottom. Water level was changed from 0.25 to 3 m ($H^*/R_0 = 1, 2, 4, 12$). Density, sound speed and bulk air concentration were 1950 kg/m^3 , $C_3 = 270 \text{ m/sec}$, and ~ 0.001 , respectively.

Shock wave parameters in the water and atmosphere were measured by piezoelectric sensors. Surface effects were measured by strain gauges and photographed by high-speed cameras. Horizontal and vertical components of particle velocity in seismic waves were measured at ranges to 45 m and depths to 2 m. Fig. 2.19 shows schemes of the experiment and the piezosensors positions in water. Fig. 2.20 presents some photographs of the explosions at depths 3 and 1 m in the central part of the reservoir. The used equipment set allowed to measure principal motion parameters in various media from the underwater explosions and to determine efficiency of energy radiation into water, air and ground.

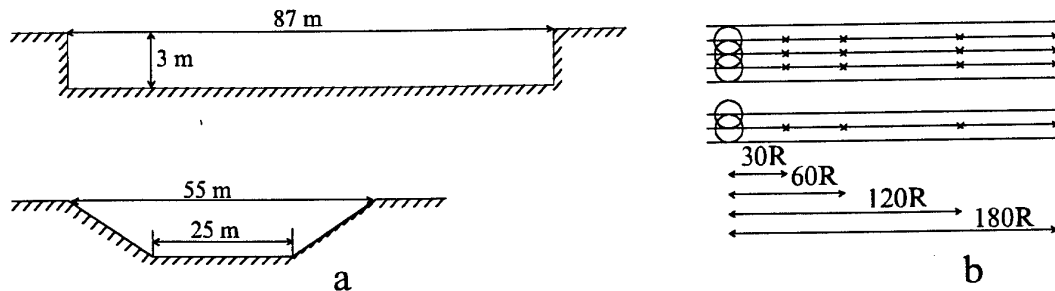


Fig. 2.19. Experiment scheme for 100 kg spherical cast TNT charges in a man-made reservoir with a sandy bottom. (a) - the reservoir cross section. (b) - positions of the charges and sensors.

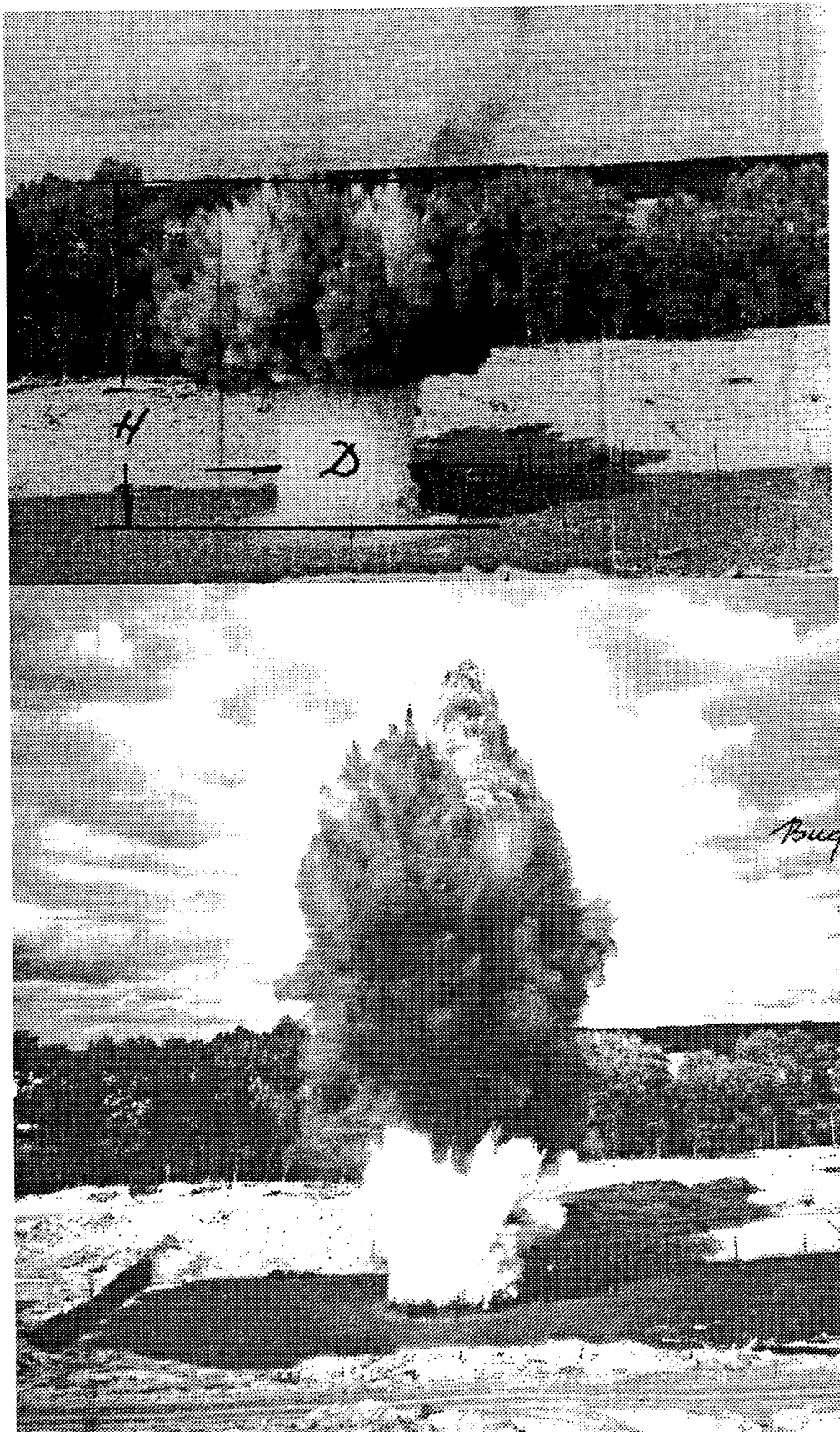


Fig. 2.20 Photography of explosions in the centre of the reservoir at depths 3 m (upper) and 1 m (lower).

2.3.1. Parameters of shock wave in water from explosions in shallow reservoir.

Shock waves were measured at relative ranges $R/R_0=30, 60, 90$ and 120 from explosions at various depths H by gauges located at various depths h .

Fig. 2.21 shows some experimental recordings. Fig. 2.22a presents peak overpressure P_m , duration τ , and specific impulse I in shock waves as functions of gauge depth h for various depths of the explosions H and water depth of $H^*=4R_0$. Peak overpressure in shock waves as a function of range for the explosions in the centre of the reservoir with water depth $H^*=2R_0, 4R_0, 12R_0$ is shown in Fig. 2.22b. Also, in the figure is shown similar relationship for a nuclear explosion of 1 kt TNT equivalent in the centre of a reservoir 20 m deep [15,17].

In the reservoir $12R_0$ deep, regular and nonregular reflection on the free surface and bottom were observed depending of explosion/receiver relative positions.

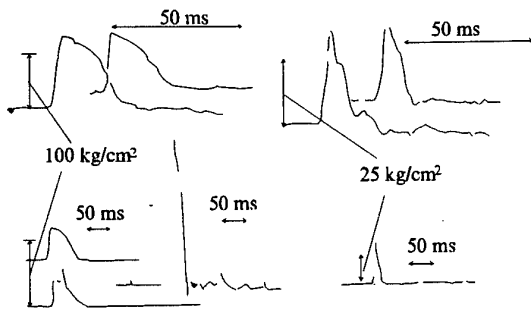


Fig. 2.21 Experimental recordings.

positions. For the reservoir depth $4R_0$ and lower, only nonregular reflection was observed on the both surfaces in the studied distance range. In such conditions shock wave parameters are maximum in the reservoir centre independent on the explosion depth, since rarefaction

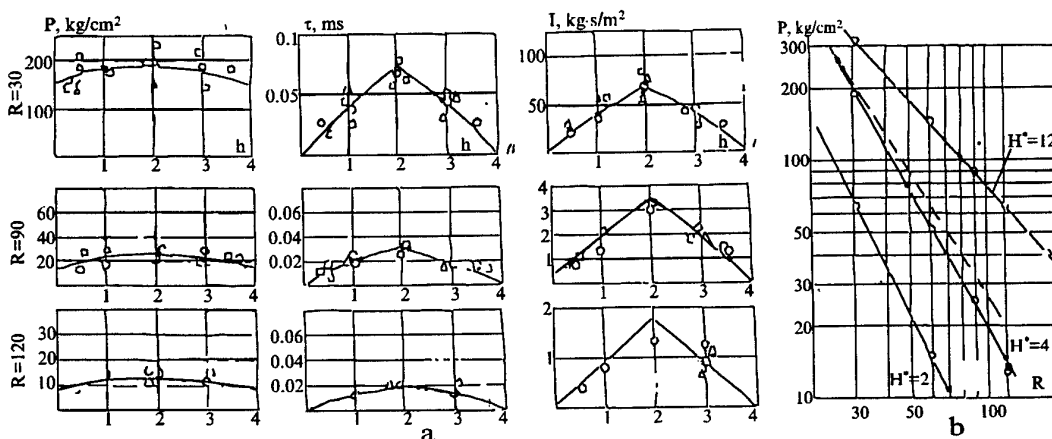


Fig. 2.22 Distributions of shock wave parameters as a function of depth in the reservoir with the sandy bottom $H^*=4R_0$ deep - (a). Peak overpressure in shock wave as a function of range for the explosions in the centre of the reservoir with water depth $H^*=2R_0, 4R_0, 12R_0$. Depth and ranges are expressed in the charge radii.

waves are reflected on the surfaces.

At large distances from the explosions a critical regime is arose due to multiply reflections. In such a regime overpressure depends only little on charge and gauge positions and is determined by effects of the reservoir surfaces. Asymptotic values are $P_m \sim A(H^*/R)^2$, $t \sim 1/R$ [17,20]. In [24] similar relationships have been obtained for spherical and cylindrical explosions at the rigid bottom of a shallow reservoir. Since the air-saturated bottom effects as the free surface, the problem of an explosion in the centre of a reservoir is equivalent to the problem of a half-yield explosion at the rigid bottom of a half as deep reservoir. Hydroacoustic wave energy is decreased with decreasing depth due to a sharp increase of energy radiated into air and ground.

2.3.2. Parameters of surface phenomena and air shock waves.

Fig. 2.23 presents some photographs illustrating a 100 kg explosion evolution in the shallow reservoir with the sandy bottom. The plume shape in various conditions is determined by water motion in shock wave, following gas bubble expansion and gas venting into the atmosphere. Initial surface uplift velocity is equal to double particle velocity in the shock wave near the free surface. Following gas bubble expansion leads to water motion and plume creation. Through the central part of the plume gaseous products of detonation are vented producing an almost cylindrical water column with narrowing with height walls. Gas ejection through the walls produces a mushroom-like plume. The larger the reservoir depth the later the ejection occurs and the resulting plume shape changes to a conical one with an expanding upper part.

Experimental relationships for scaled plume height H_k/R_0 as a function of scaled time t/R_0 for various explosion depths H in a 3 m deep reservoir are shown in Fig. 2.24a. Fig. 2.24b displays initial surface velocity V_0 in the plume centre and the plume peak height H_m as a function of explosion depth H/R_0 .

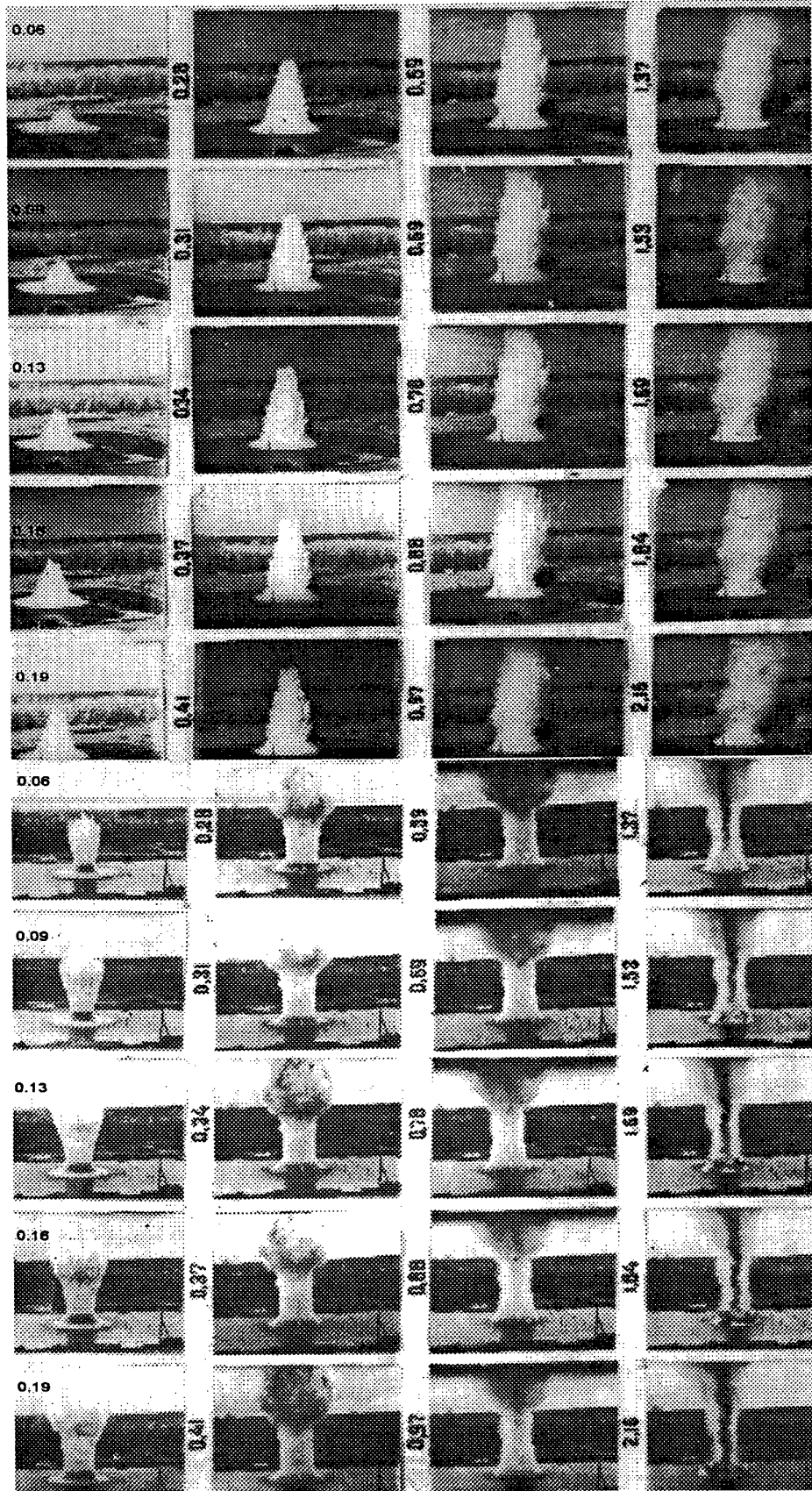


Fig. 2.23 Plume evolution in a reservoir 3 m deep from a 100 kg TNT explosions at 1.5 m (upper) and 1 m (lower) depth.

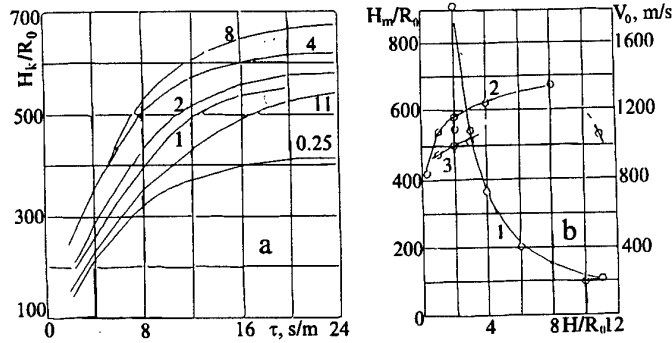


Fig. 2.24a,b Scaled plume height H_k/R_0 as a function of scaled time t/R_0 sec/m for a 3 m deep reservoir. Digits indicate scaled explosion depth - (a). Initial plume uplift velocity (1) and its peak height (2,3) as a function of explosion depth. Curves 2 and 3 are for the reservoir depths of $12R_0$ and $4R_0$ respectively - (b).

energy similarity laws. This allows to estimate explosion energy if the explosion conditions are known. Fig. 2.25 shows experimental relationships for the plume neck peak diameter D/R_0 as a function of scaled depth H/R_0 for charges of 100 and 0.00025 kg mass (open and solid circles, respectively).

Air shock wave from shallow underwater explosions includes 3 shock waves produced by piston-like plume motion, gas ejection from the gas bubble, and refracted into the atmosphere water shock wave. For explosions at depths $0 < H/R_0 < 4$ the first two waves are of the largest amplitude. For $H/R_0 > 4$ all the three waves are comparable by amplitude. The refracted shock wave front has a conical shape. For explosion depth $H > 30R_0$ the refracted wave is of the highest amplitude.

In shallow reservoirs explosion generated air shock waves are of cylindrical symmetry and are produced by piston-like motion of supersonic plume expansion. For $H^* = 4R_0$, such a zone is of $150R_0$ in diameter. Fig. 2.26 presents peak overpressure in air shock wave as a function of distance as calculated for a 1 kt TNT equivalent explosion, modelling nuclear explosion "Baker", and for

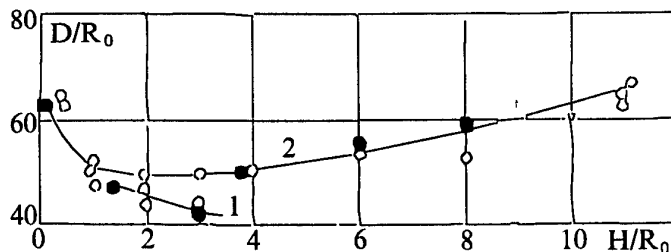


Fig. 2.25 Neck peak diameter D/R_0 against scaled depth H/R_0 : 1 - $H^* = 4R_0$; 2 - $H^* = 12R_0$.

The cylindrical water column has a distinct narrow part near its base called plume neck. The neck radius increases at first to its peak value, and then begins to decrease. At that time the plume collapses. The base and neck diameters for various yields follow geometric or

100 kg explosions at depths $H/R_0 = 0, 1, 2, 3$ [15,17,25,26].

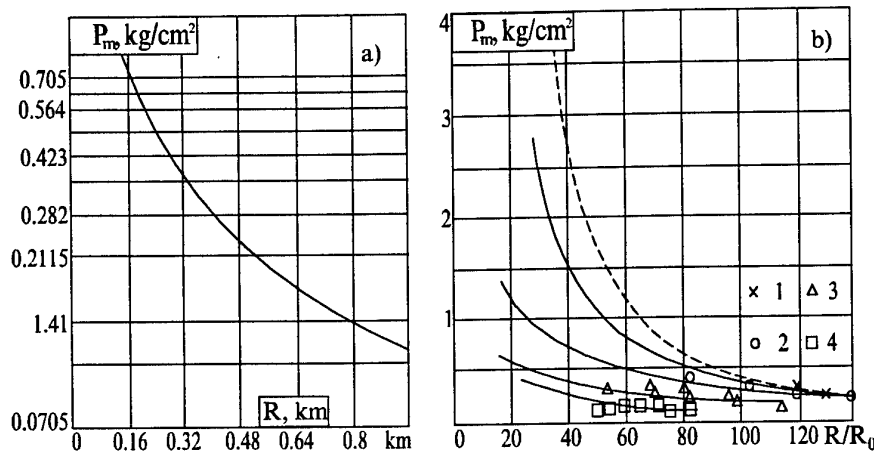


Fig. 2.26 Peak overpressure at the water surface as a function of distance from a 1 kt explosion, modelling nuclear explosion "Baker" - (a), and (b) - 100 kg explosions, 1-4 - explosion depth $H/R_0=0, 1, 2, 3$, respectively. Dashed line - predicted by (3.1) for a surface explosion.

2.4. Conclusions.

In this section we have analysed and generalised available experimental data on effects from underwater nuclear and chemical explosions. The data may be useful for improvement the hydroacoustic methods designed for the International monitoring system (IMS).

1. Data for 3 underwater nuclear explosions at the Novaya Zemlya test site with the bay of Chernaya are described including conditions, methods, equipment, and some results of the explosions effects measurements in near-field and far-field zones. The results concern the problem under investigation. Results of hydroacoustic, infrasound, seismic and radioisotope measurements in a wide range and their analysis show that at large distances only the last two methods provide reliable results. Hydroacoustic equipment recorded refracted into water seismic waves. This effect is associated with some specific features of nuclear explosions in closed shallow basins, where a larger portion of explosion energy is radiated into the atmosphere and ground. Hydroacoustic energy is small and its propagation into the open ocean is complicated by the bottom relief. In such a situation only complex methods can provide an effective monitoring.

2. Results from underwater chemical explosions in various basins are presented, including deep bomb blasts in the Sea of Okhotsk, 3 ton detonating cord blast in the Black Sea, explosions of 100 kg spherical cast TNT charges in a man-made reservoir with a sandy bottom, model small charge explosions in deep and shallow reservoirs with various bottom conditions. Effects of bottom and free surface as well as depth of basin on parameters and spectra of hydroacoustic signals in near-field zone are studied.
3. Effect of energy concentration of chemical underwater explosion on radiated hydroacoustic energy is studied. Explosions in air-filled cavities as well as explosions with various specific energy were used. Optimal concentration corresponds to TNT explosions. For nuclear explosions and air-filled cavity explosions hydroacoustic energy generation is less effective. Usage of large cavities promotes evasion the monitoring nuclear explosions, but hard to be carried out.
4. Experimental results of hydroacoustic noise measurements in the Sea of Okhotsk conducted from submarines and ships are presented. The noise level is decreased with frequency and at 50 Hz is of 0.1 to 0.01 dyne/cm² within quiet regions and at large depth. It is shown that artificial noise from submarines and ships can be several order of magnitude larger than natural noise in quiet regions. So, we can not recommend to use them for monitoring purposes.
5. Hydroacoustic wave propagation in inhomogeneous liquid is considered on an example of a 3 ton detonation cord explosion within a basin with a positive velocity gradient near the bottom. Focusing effect was observed near the bottom where a sharp amplitude increase is possible. There may be shadow zones, however. Optimal conditions for hydroacoustic waves propagation at large distances are created in the global sound waveguide (SOFAR), situated in the southern and middle parts of the world ocean. Attenuation in the waveguide is very low at frequencies below 100 Hz - the range which is characteristic for underwater explosions. Thus, such explosions can be detected at distances as large as 10,000 km by hydroacoustic methods.

3. Above water and coastal explosions.

3.1 Three above water explosions at the NZTS.

The first above water nuclear explosion has been conducted on 13.09.1961. There was no published information on this explosion below 20 kt [5]. As some participants recollect [6,7] the explosion was conducted for testing self-aiming wing rocket. A test field filled by armaments has been prepared near the cape of Chernyi, north-west of the bay of Chernaya (70.78N, 53.33E, Fig. 2.1).

The second above water nuclear explosion has been conducted within the bay of Chernaya on 27.10.1961 in 11:30:26 (Moscow time). Announced yield was below 20kt [5]. A torpedo was launched from the same submarine B-130 as for the underwater explosion of 23.10.1961. From seismological observations, the explosion yield was of 12 kt. The torpedo passed about 11 km at depth 12 m and emerged above the surface in the predicted point. Characteristic pattern of the explosion, water column uplift and cloud shape differed from those from an underwater explosion which had been conducted four days before almost in the same point of the bay of Chernaya.

The third above water explosion with yield below 20 has been conducted on 22.08.1962 in 12:00:00 (MSK) [7]. An aviation wing rocket with a nuclear charge was tested. The rocket had been designed on the basis of MiG fighter for destroying large ships. An aircraft Tu-16 carried the rocket. A test area has been prepared on the outer road stead of the bay of Bashmachnaya, about 70 km north-west of the bay of Chernaya. An artillery shield with a reflector was used as a target. Equipment stands and two optical points have been established for measurements.

3.2 Coastal above ground explosions.

3.2.1. Nuclear explosion as the coast of the bay of Chernaya.

An above ground explosion of about 30 kt has been conducted on 07.09.1957 in 11:00:01 MSK. A nuclear device has been established at the top of a tower 15 m high at the eastern coast of the bay of Chernaya and about 100 m far from the coast line. Relief of the site was hilly with ground covered by moss, peat

and loamy soil with pebble. Armaments were established on the coast and ships within the bay.

A crater 80 m in diameter and 15 m deep was created by the explosion. Some ships were severely damaged. At the destroyer "Gremyashii" sides and superstructures were deformed and burnt, doors and hatches were damaged, almost all animals on board were killed.

Acoustic recordings have been obtained at a number of acoustic station within the FSU, with infrasound being recorded not only by microbarographs but by vertical seismographs also. (There were no acoustic waves recorded from underwater explosions at these stations.) The most distinct and intensive recordings have been obtained at stations to east of the Novaya Zemlya. Fig. 3.1 shows a recording measured by a microbarograph of EDMB-1 type on the most remote station "Gamburtsevo" located at the Far East at a distance of 4430 km in 15:04:10 MSK.

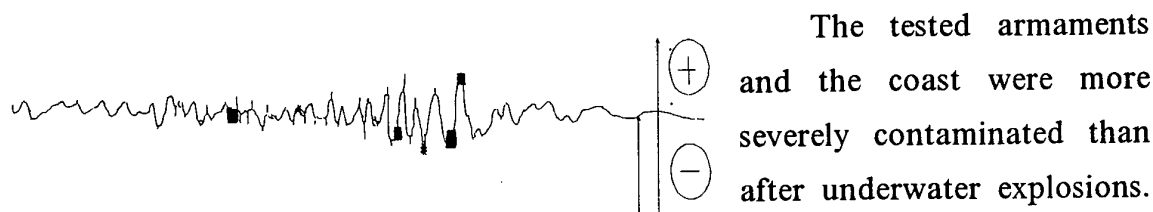


Fig. 3.1 Infrasound recording 4430 km of the above ground explosion near the bay of Chernaya on 07.09.1957.

The tested armaments and the coast were more severely contaminated than after underwater explosions.

A radioactive cloud from the explosion propagated to east

into the Kara Sea and further to the Yamal, Gydan and Taimyr peninsulas. By aerogammasounding methods a radioactive trace of 1500 km long has been observed after the explosion. In 7 year (in 1965) the trace has been observed with a peak level at the test site of 0.3 mR/h. Study of the territory near the resulting crater in 1991 and 1992 has shown that to 400 m from the crater radioactivity level (RL) (dose power) has varied from 1 to 15 mR/h. At the northern outer slope of the crater RL has reached 1 mR/h, at the western - 0.4 mR/h. At distance of 100 m RL has decreased to 0.14-0.16 mR/h.

Radiochemical analysis of samples extracted from the ground during many years after the explosion showed that there were fusion and induced radionuclides as well as residual plutonium. The soil activity around the crater was induced by particles of high-active silicate slag which was variously

dispersed. The total specific activity of the slag was of 80 kBq/kg. Cs^{137} was the principal gamma-radiating radionuclide around the crater. Its surface activity varied from 30 to 0.25 Ku/km². Sr^{90} surface activity varied from 15 to 0.04 Ku/km². Surface activity of plutonium varied in a range of two orders of magnitude. At 30 km of the crater Cs^{137} activity varied from 0.6 to 0.07 Ku/km². Sr^{90} contamination at 30 km was of 0.07 Ku/km².

3.2.2. 1000 ton TNT explosion at the coast of the Matochkin Shar strait.

Fig. 3.2. shows a picture of an explosion conducted on 25.08.1987 in 18:00:00 MSK at the southern coast of the Matochkin Shar strait, about 100 m of the coast line (73.38N, 54.78E).

A charge of 24,000 sacks filled by scaled TNT had a mass of 974 ton. The charge was of a cylindrical shape 17.8 m in diameter and 4.8 m high with a truncated conical top 1.6 m high and the base diameter of 3.8 m. In the central part a firing pin consisted of 880 boxes filled by cast TNT and total mass of 22 ton have been placed. In the upper part of the charge 165 boxes filled by cast TNT and total mass of 4 ton have been placed. The charge has been placed on planks. The charge has been initiated in the lower central part.

The explosion has been conducted over a small but relatively plane section of the coast 300 to 400 m wide. The site had a slope of 3 to 12 degrees from south to north. Permafrost layer beneath the site was of about 300 m deep. In summer time, the upper layers of soil filled by pebble and gravel were melted to depth of 3.8 to 4.6 m. Sand and sandyclay layers filled by pebble and gravel were observed to a depth of 20 m.

A crater created by the explosion was 26.7 m in diameter and 16.5 m deep. The crater bottom and sides were formed by damaged materials of the frozen soil. The upslope side of the crater was more steep, and downward side - more gently sloping. A cloud from the explosion has lifted to 3.5 km. Some shock wave recordings at various distances are presented in Fig. 3.3. Peak overpressure, action time and positive phase impulse as functions of distance over the surface are presented in Fig. 3.4. Dashed-dotted lines present predicted by Sadovskii's

relationship values for a TNT explosion over a rigid surface, which is valid in the range $R_0 > R/M^{1/3} > 0.8 \text{ m/kg}^{1/3}$ [33,35]

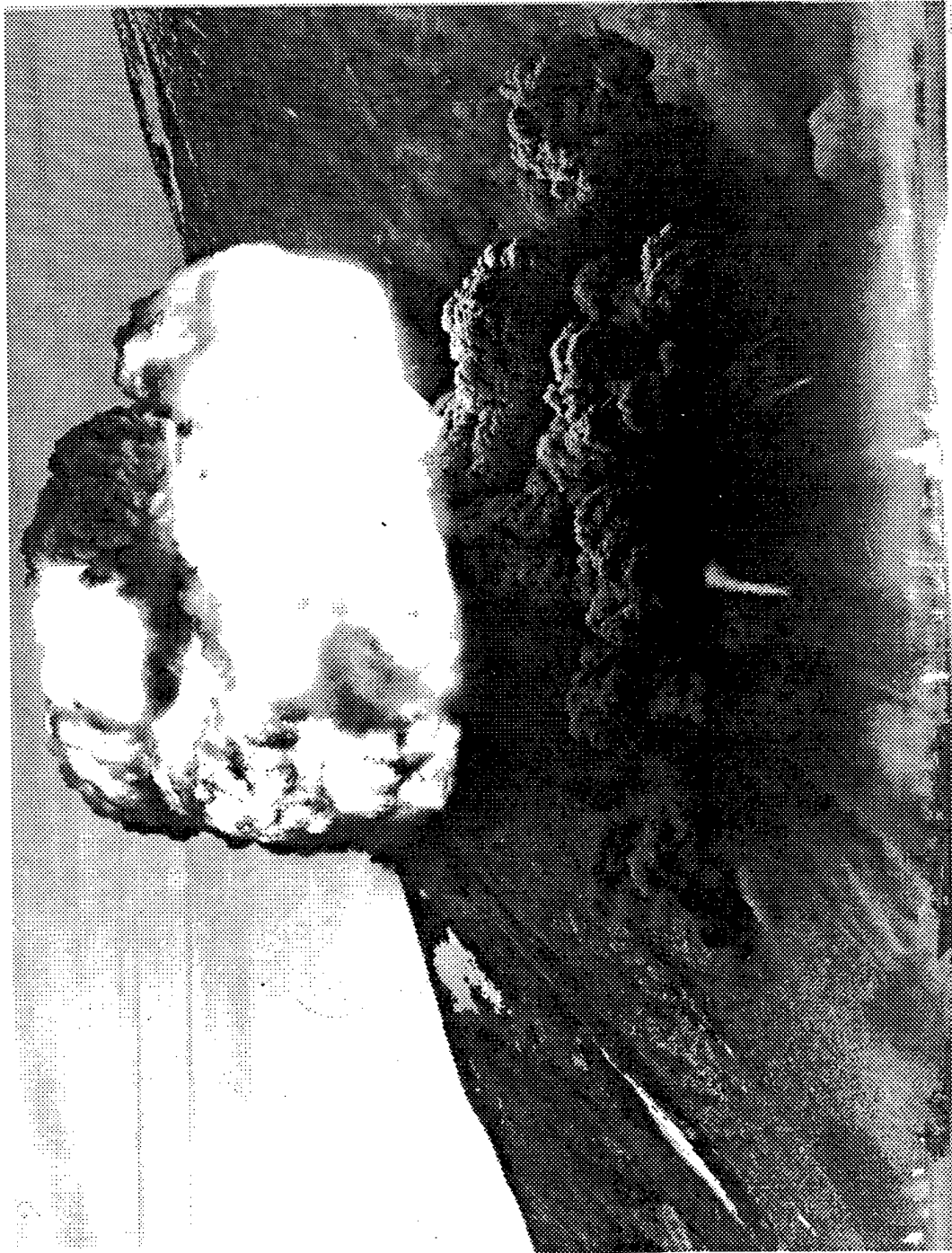


Fig.3.2. Picture of 1000 ton TNT explosion at the coast of the Matochkin Shar strait on 25.08.1987.

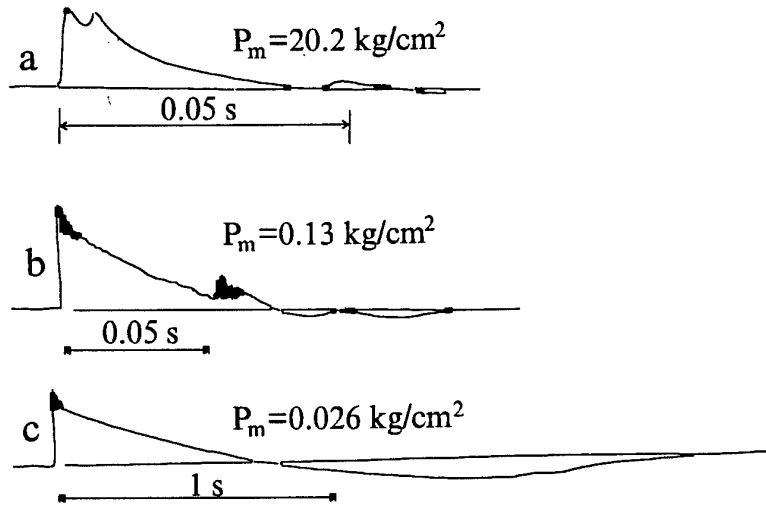


Fig. 3.3. Shock wave recordings from the chemical explosion conducted on 25.08.1987 at distances 70 m (a), 997 m (b), 4184 m (c).

$$\begin{aligned}\Delta P &= 1.06/(R^0) + 4.3/(R^0)^2 + 13.9/(R^0)^3 \\ t_+ &= 1.35M^{1/6}R^{1/2} \\ I &= 35M^{2/3}/R\end{aligned}\tag{3.1}$$

where ΔP is measured in kg/cm^2 , $R_0 = R/M^{1/3}$ is in $\text{m/kg}^{1/3}$, t_+ is in msec, I is in kg sec/m^2 . For an air explosion in infinite space the above relationships have the following form

$$\begin{aligned}\Delta P &= 0.83/(R^0) + 2.7/(R^0)^2 + 7/(R^0)^3 \\ t_+ &= 1.2 \cdot M^{1/6}R^{1/2} \\ I &= 19 \cdot M^{2/3}/R\end{aligned}\tag{3.2}$$

A distinct overpressure deviation at small distances from relationship (3.1) is due to soil softness. Similar effect may be expected for above water explosions.

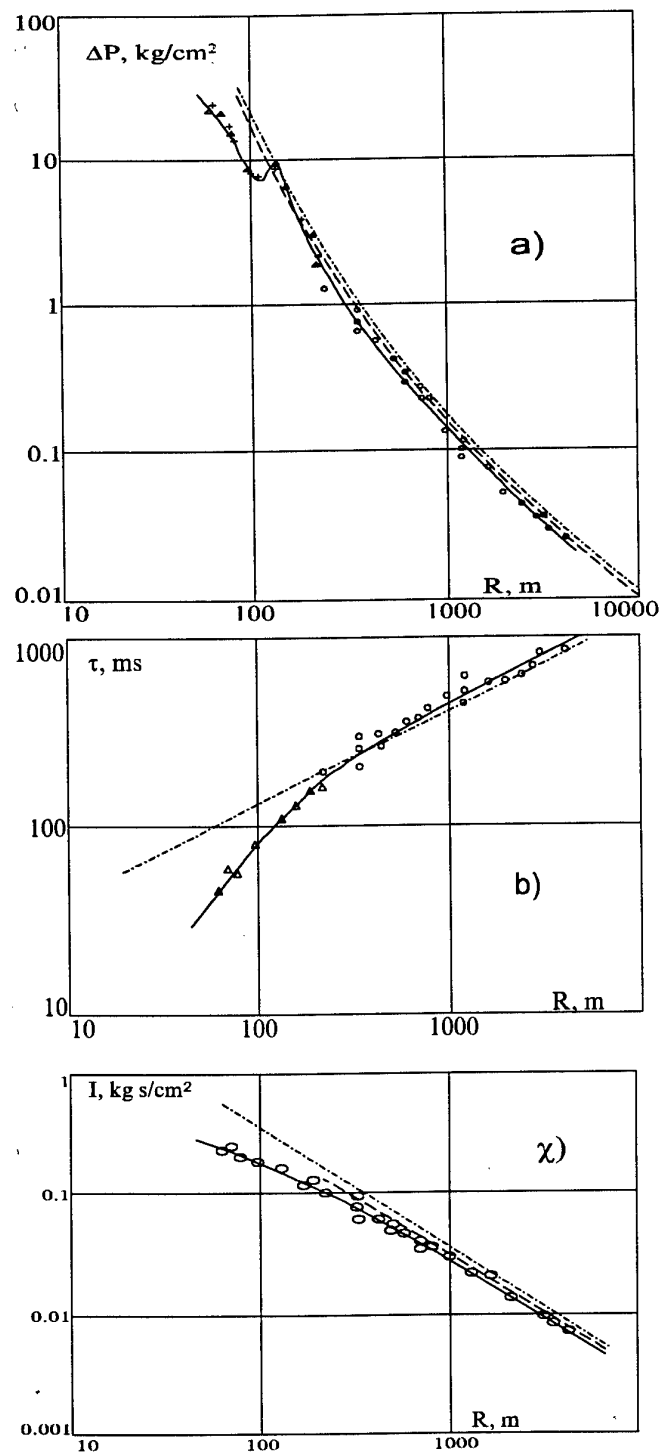


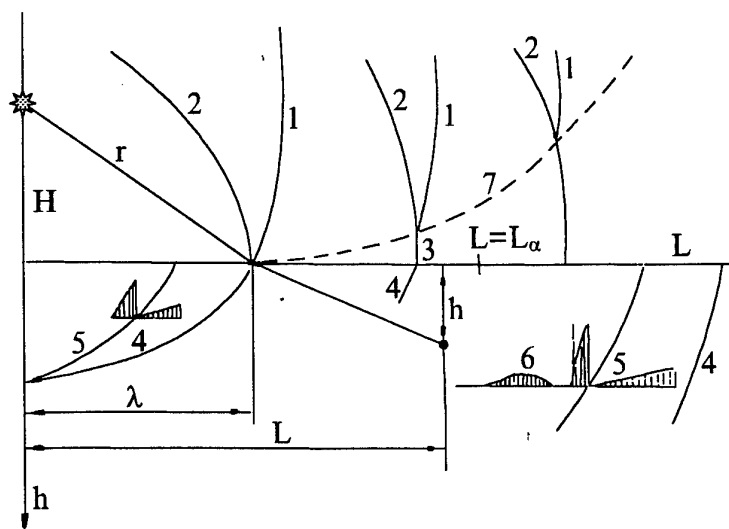
Fig. 3.4. Peak overpressure (a), action time (b), impulse (c) in the compression phase of the shock wave from the chemical explosion conducted on 25.08.1987. Solid lines - approximated experimental data; dashed-dotted lines - predicted by Sadovskii's relationships.

3.3. Model chemical explosions above water and ground.

Parameters of shock waves from explosions near the surface of water and ground are similar in many aspects and experimental data from such explosions are supplementary.

A complex wavepattern similar to shown in Fig. 3.5 for an above water explosion has been observed from above water explosions of 100 kg TNT charges and 2.5 g of PETN explosions in water and air. A refracted wave, epicentral wave induced in water by a shock of detonating gas, and compression wave induced by air wave at distances $R > 18R_0$, when the wave lags behind the refracted one, are generated in water. When $H_0 < 0.1 \text{ m/kg}^{1/3}$, the first two waves are of largest importance. Empirical relationships are obtained for all the wavefield components in water. The relationships can be scaled by TNT equivalent to any yield [17,27,28]. Pressure in the gas bubble during its expansion does not drop below the atmospheric one. Back motion and following pulsations are absent due to gas venting into the atmosphere.

Fig. 3.6 presents characteristic features of a flow and its parameters in the near-by zone of a half-immersed TNT charge of 1 kt recalculated from model experiments with smaller charges for tree time moments, when shock wave in the air has larger velocity than in the water. Only one pulsation of gas bubble with



vertical radius of 170 m and period of 190 sec occurs after this explosion. These values are much larger than for an explosion in the infinite liquid space with atmospheric pressure - $r_m = 157 \text{ m}$, $T_1 = 24 \text{ sec}$, respectively.

Fig.3.5. Wave pattern at above water explosion. 1,2,3 - direct, reflected and Mach waves in air. 4,5,6 - refracted, epicentre and pressured waves in water.

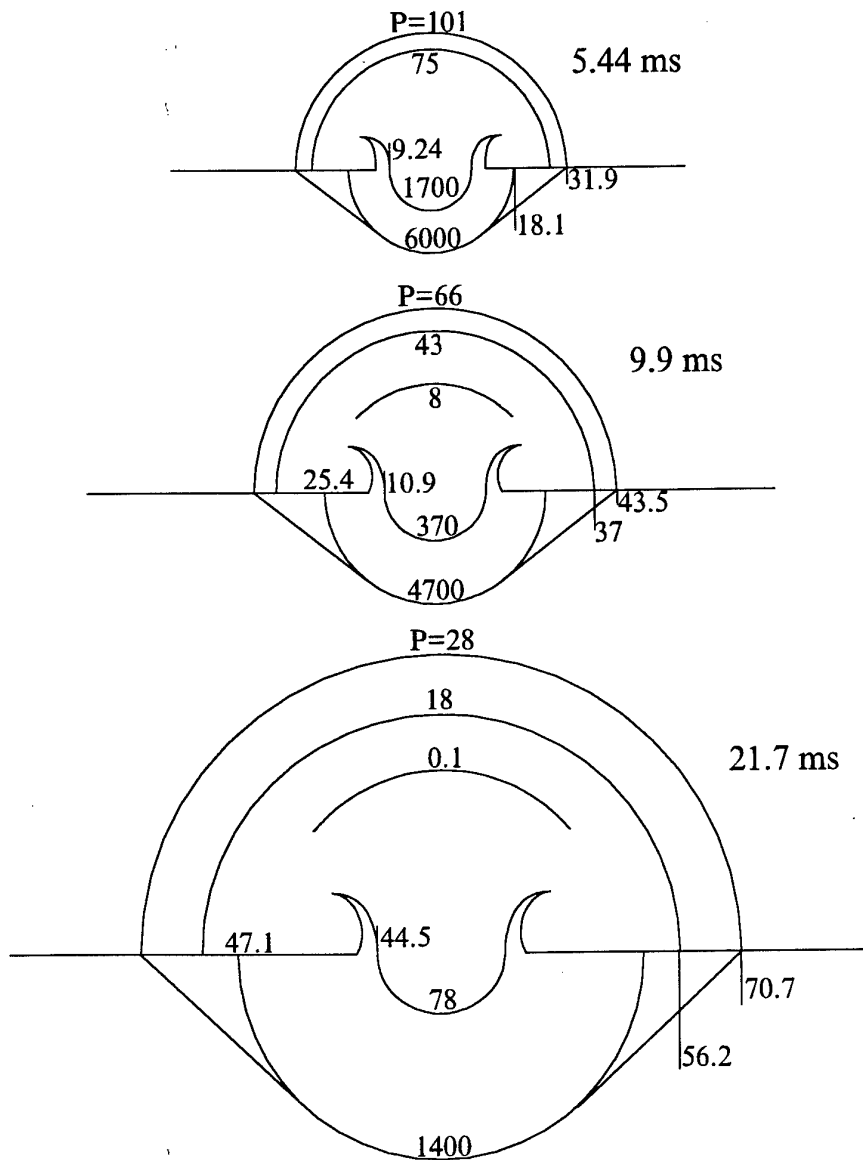


Fig. 3.6. Characteristic features of a flow in the nearby zone of a half-immersed 1 kt TNT explosion. Pressure, given in atmospheres, is indicated along the vertical axis, range in meters - along the horizontal axis.

Fig. 3.7 presents parameters in shock waves measured in a 3 m deep basin from a half-immersed spherical charge cast TNT explosion of 100 kg, with shock wave velocity in the air larger than in the water. Scaling of these parameters to 1 kt gives for $R/R_0=60$ ($R=318$ m) following peak values: $P_m=72$ atm, $t_m=3.45$ msec, $I_m=1400$ kgsec/m², and for $R/R_0=120$ ($R=638$ m) - $P_m=27$ atm, $t_m=2.6$ msec, $I_m=320$ kgsec/m² [17,28].

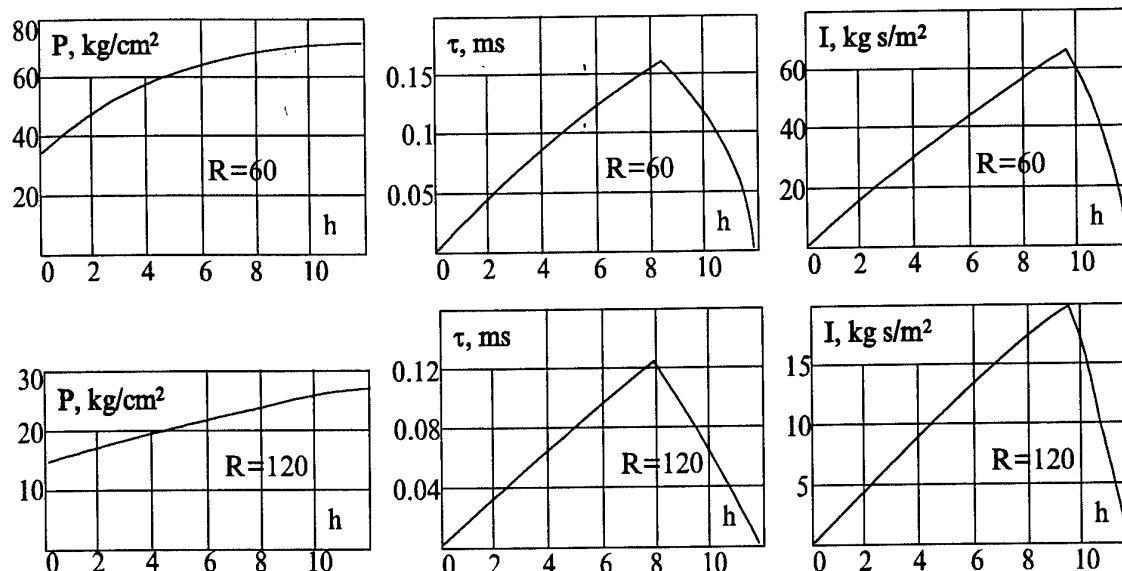


Fig. 3.7. Measured peak overpressure, duration and specific impulse in water shock wave as functions of sensor depth during a half-immersed spherical 100 kg cast TNT explosion in a 3 m deep basin with a sandy bottom. R , H , h are the distance, depth of explosion, depth of sensor in the charge radii $R_0 = 0.246$ m.

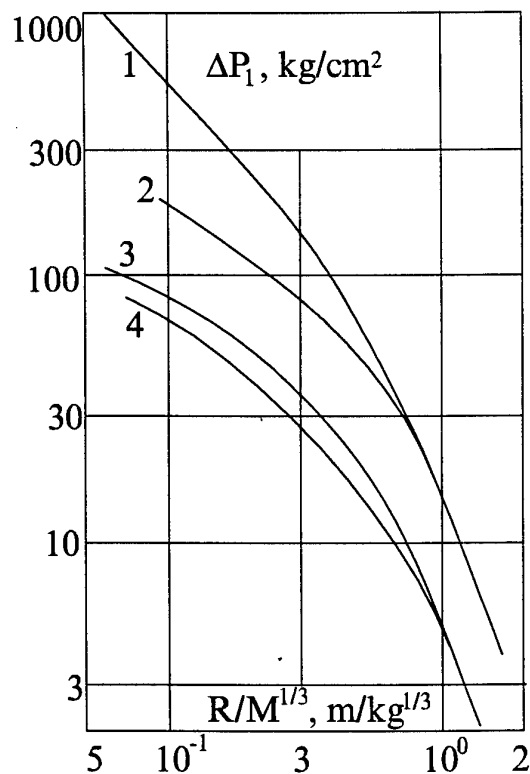


Fig. 3.8. Peak overpressure ΔP_1 in shock wave against scaled distance $R/M^{1/3}$ from air explosions of spherical charges of PETN with density of 1600 and 400 kg/m^3 and lead azide with density of 1600 and 850 kg/m^3 (curves 1-4 respectively).

Fig. 3.8 displays peak overpressure ΔP_1 in shock wave against scaled distance $R/M^{1/3}$ from air explosions of spherical charges of PETN and lead azide of various energy density, with their specific energy $Q=1400$ and 365 kcal/kg almost not dependent on density. For $R/M^{1/3} > 0.8$ $\text{m/kg}^{1/3}$, overpressure and other shock wave parameters are described by Sadvoskii's relationships (3.2) with taking into account TNT equivalent according to similarity laws (scaling) and not dependent on density. For $R/M^{1/3} < 0.8$ $\text{m/kg}^{1/3}$ [14], the larger the energy concentration of an explosion Q_p the larger overpressure at a given distance for any explosive [29,33,34].

Figure 3.9 presents overpressure in

the reflected wave ΔP_2 as a function of the explosion height $H/M_e^{1/3}$ above surface for spherical pressed PETN charges of 2.5 g as obtained from optical and piezoelectric measurements in water (curve 1). For a comparison, curve 2 predicted by Izmailov's relationship is displayed for a wave reflected on solid surface without taking into account pressure of products of detonation [35]:

$$\Delta P_2 = 2\Delta P_1 \{ (3\gamma - 1)/2(\gamma - 1) + [(2\gamma/(\gamma - 1))P_0/\Delta P_1] / [1 + (2\gamma \cdot P_0/\Delta P_1)/(\gamma - 1)] \},$$

where γ is the heat capacities ratio for air. For $H/M_e^{1/3} > 0.25 \text{ m/kg}^{1/3}$ the measured and predicted overpressures in the reflected waves are consistent. At closer distances, the measured overpressure is larger than the predicted due to additional products of detonation pressure. The products of detonation, as observed by optical methods, follow just after the air shock wave at these distances. Fig. 3.10 presents overpressure in the reflected on a solid surface wave, ΔP_2 , in the range $0.06 < H/M_e^{1/3} < 4 \text{ m/kg}^{1/3}$ and its comparison with the predicted by Izmailov's relationship. M_e is the TNT equivalent charge mass. For $H/M_e^{1/3} > 0.8 \text{ m/kg}^{1/3}$ all chemical explosives are described by a common curve. In the nearby zone, increase of energy concentration leads to increase of the reflected

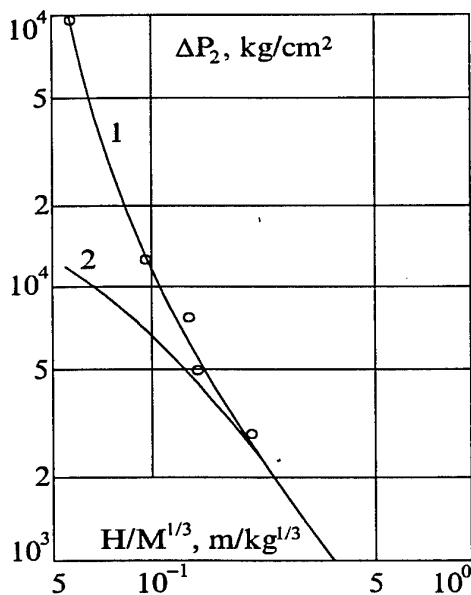


Fig.3.9. Peak overpressure ΔP_2 in reflected shock wave against scaled height $H/M_e^{1/3}$ from above water explosions of spherical charges of PETN. 1-experiment, 2-calculated reflected pressure from hard wall.

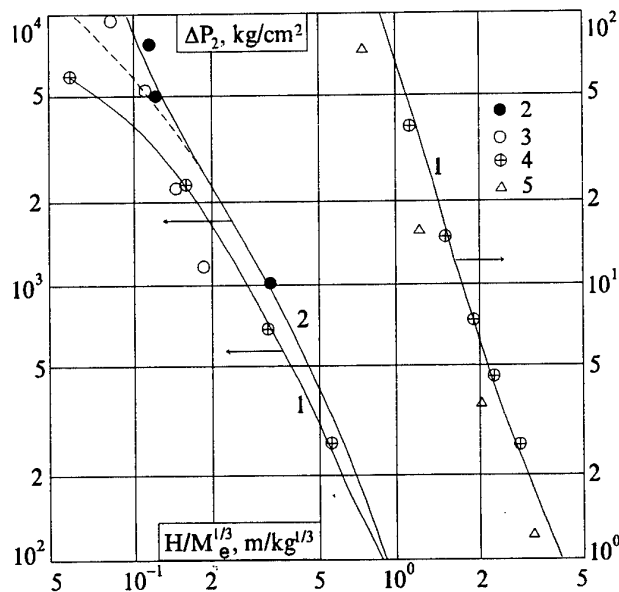


Fig.3.10. Peak overpressure ΔP_2 in reflected from hard wall shock wave against scaled height $H/M_e^{1/3}$ from explosions of different HE. 1-experiment, 2-calculated reflected pressure from hard wall. M_e -TNT equivalent. 1-casting TNT, 2-PETN with 1600 kg/m³ density, 3-TNT/RDX - 50%/50%, 4-calculations by Izmailov's relationship for TNT, 5-Nuclear explosion.

wave amplitude [13]. For nuclear explosion, ΔP_2 (triangles) is much lower than from chemical explosions. Thus, the water shock wave also is lower, especially, in the nearby zone.

The largest overpressures ΔP_{1mw} at the reflected into water wave front are arose in the epicentre $R=0$.

For $5R_0 < H < 7.6R_0$, $\Delta P_{1mw} / \Delta P_2 = 1(1 + 0.14h/H^{1/3})$.

For $7.6R_0 < H < 38R_0$, $\Delta P_{1mw} / \Delta P_2 = 1(1 + 0.07h)$, where H and h are the heights of the charge and sensor, scaled by the charge radius $R_0 = 0.053 M^{1/3} m$, respectively.

Overpressure P_{mw} in the compression wave generated by explosions at any height, when shock wave in water leaves behind air shock wave, $P_{mw} = \Delta P_2 / (1 + 0.16h)$.

Hydroacoustic signal from an above water nuclear explosion may have a high frequency precursor induced by light pressure effects on the water surface. Modelling of above water explosions by high-speed plasma jets has been conducted. There have been no distinct precursors induced by powerful UF radiation. In order to determine TNT equivalent for these sources of high energy concentration, which is similar to that from nuclear explosions, the results of shock wave and gas bubble measurements were compared with those obtained from underwater and surface chemical explosions. Scaled cavity volume as a function of scaled time for underwater (1), half-immersed (2) and for plasma jet (3) is given in Fig. 3.11. For a jet impact the volume is much lower than for the explosions. This may be due intensive dissipation at the initial stage of the jet impact. This is also characteristic for nuclear explosions.

The conducted study has shown that the larger the above water explosion height the lower hydroacoustic energy and the larger acoustic energy radiated by the explosion. However, as distance is increased correlation between sound energy in the water and atmosphere may increase if the former propagates in a sound channel.

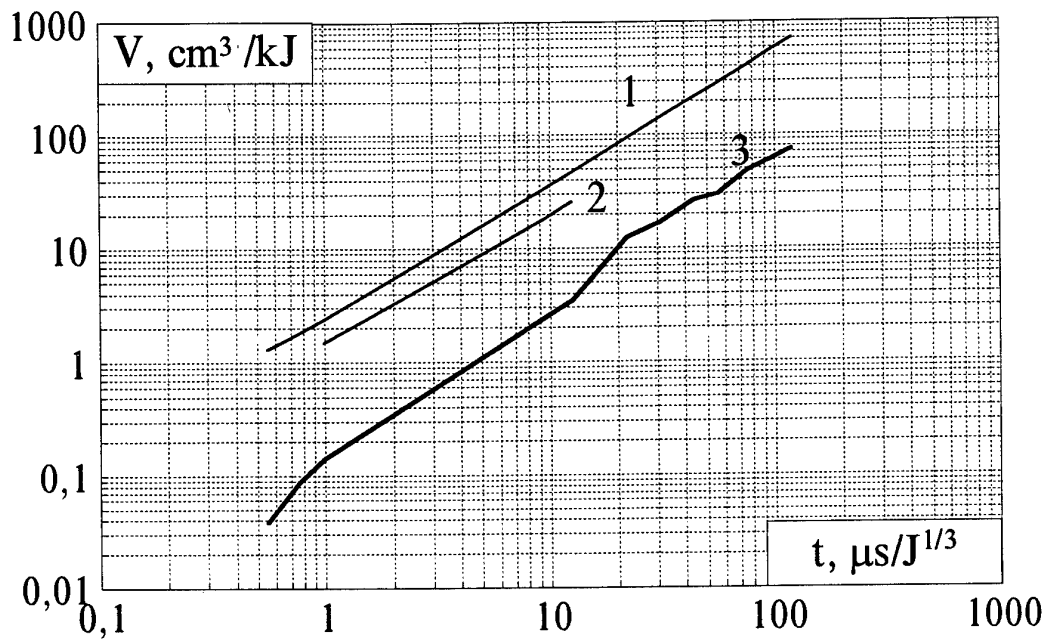


Fig. 3.11 Specific cavity volume as a function of scaled time for underwater (1), above water (2) chemical explosions and plasma jet shock (3).

3.4. Underground nuclear explosions.

3.4.1. Conditions of conduction.

The nuclear explosions listed in Table 1.1 have been conducted at two different sites of the Novaya Zemlya test site: the explosions 8-10 - in mines of the southern coast of the Matochkin Shar strait, the explosion 11 - in a drillhole north-west of the bay of Chernaya (in Fig. 2.1, zones A and B, respectively). Yields and coordinates in the table are obtained from seismological data [11,12], as well as origin times. Data from various seismological stations are quite different sometimes. For example in [10], yields for the explosions 8-10 are, apparently, 2 to 2.5 times lower than actual. The explosion parameters presented in the report should be also corrected.

The explosion №8 (27.10.1966, 08:58:00 MSK) has been conducted inside two nearby mines A-1 and A-2 with a time delay of several milliseconds. Complete yield of the explosion was 1300 kt. In about 15 minutes after the explosion venting of radioactive inert gases into the atmosphere was observed with total quantity of $3.7 \cdot 10^{17}$ Bq. Radionuclides of xenon and krypton were identified. A cloud from the explosion propagated to east along the strait and then to south-east, to the Kara Sea, with general trend to south-east. Within the test area, power of the exposure dose of γ -radiation (MED) reached 7 R/hour sometimes [12,13].

The explosion №9 (12.09.1973, 09:59:54.6 MSK) has been conducted in a mine B-1 which had an additional vertical shaft 500 deep. The explosion scaled depth was $95 \text{ m/kt}^{1/3}$. Radioactive gas venting into the atmosphere was observed in 10 to 12 m after the explosion. Total quantity of fallen out secondary caesium around the test site was of $5.6 \cdot 10^{11}$ Bq. The products were carried out to the Kara Sea in 5 hours at a height of 1 km with following motion to south-east. At heights below 1 km, the cloud of inert gases propagated over the Novaya Zemlya to south.

The explosion №10 (29.08.1974, 12:59:55.8, MSK) has been conducted in a mine A-11. Leaking of inert gases into the atmosphere was observed in 10 to 15 m after the explosion. Three days later they were observed out off the test site in the

direction to the Yamal peninsula with following turning to north-east. Total quantity of the gases was $1.8 \cdot 10^{14}$ Bq. Near the mine mouth MED was not above 3 R/hour. No radioactive fall out were observed.

The explosion №11 (02.11.74, 07:59:56.7) has been conducted at the southern edge of the test site in a mine Yu-5N practically without any gas leaking into the atmosphere. At a station SP-22 in the Arctic Ocean refracted into water seismic waves were measured at various depths and in various frequency bands.

3.4.2. Near field measurements.

During the explosions №№8-10, at the coast of the Matochkin Shar strait, in 1966, 1973, 1974, the peak overpressure in shock waves was measured by membrane gauges MID at 6 points within the strait and the Barents Sea. The points are presented in Fig. 3.12a at scaled distances $R^0 = R/M^{1/3} = 1000 \div 3000$ m/kt^{1/3}.

Deformation of a membrane in MID sensor proportional to overpressure was measured by a lead target deformation. Air pressure in the sensors was equal to hydrostatic one.

Fig. 3.12b shows a characteristic dependence of peak overpressure ΔP in shock wave on sensor depth h as recorded from the explosion №10 at a point №5 at a scaled distance of $R^0 = 1350$ m/kt^{1/3}. The peak overpressure ΔP increases from 0.18 to 1.3 atm with h increase from 10 to 60 m (the basin was 70 m deep).

The dependence obtained is characteristic for wavefield in water, which is determined by a superposition of the refracted from the ground seismic compression wave with increasing with time overpressure and the reflected at the free surface rarefaction wave. The data of the mechanical measurements have allowed to estimate time characteristics of water sound impulse and its energy.

Vertical component of particle velocity in seismic waves in the near-field zone, where attenuation depends only little on frequency, is determined by the following expression

$$V_z = 12000/(R^0)^{1.6} \text{ m/sec.}$$

From this expression one can obtain overpressure in the refracted wave in the form

$$\Delta P = V_z \rho C = 180000 / (R^0)^{1.6} \text{ kg/cm}^2,$$

where R^0 is measured in $\text{m/kt}^{1/3}$, ρ is the water density and C is the sound speed in the water.

Solid line in Fig. 3.12c shows a predicted curve $\Delta P(R^0)$ for the refracted wave. The curve is consistent in the range $R^0 = 1000 \div 3000 \text{ m/kt}^{1/3}$ with experimental data near the bottom of the basin where the measurements were conducted.

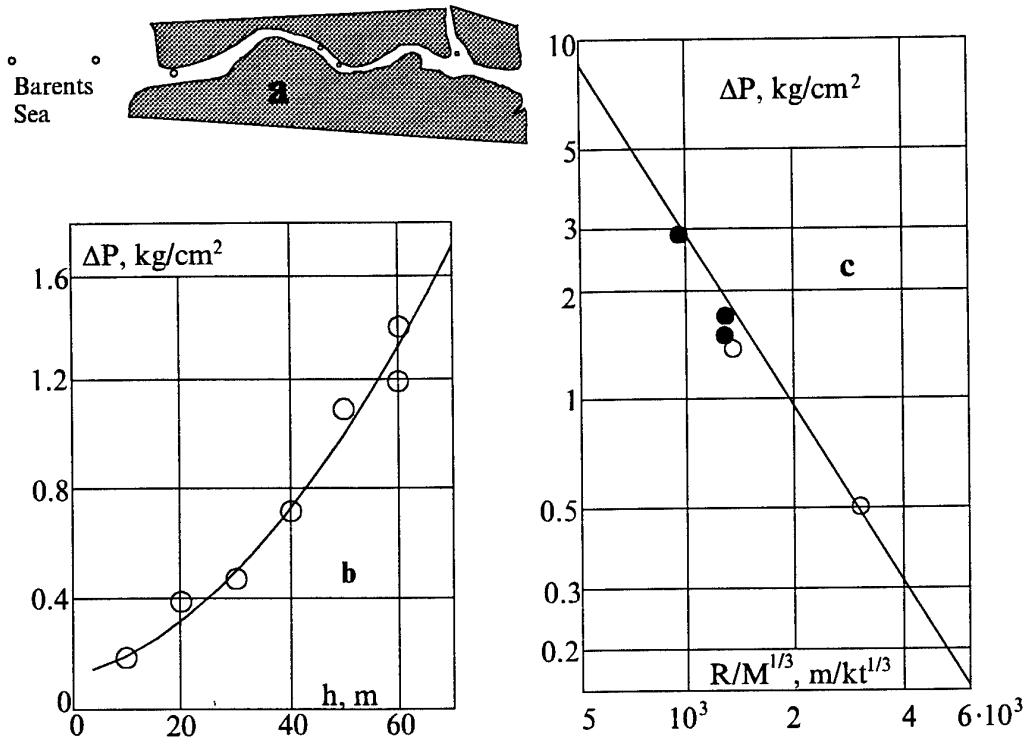


Fig.3.12a,b,c Scheme of observational points locations in the Barents Sea and Matochkin Shar strait during underground explosions - (a). Peak overpressure ($\Delta P \text{ kg/cm}^{1/2}$) in shock wave as a function of sensor depth h for the explosion #10 at a scaled distance $R^0 = 1350 \text{ m/kt}^{1/3}$ - (b). ΔP as a function of $R/M^{1/3} \text{ m/kt}^{1/3}$ - (c).

3.4.3. Measurements at large distances.

During the explosion №11 (02.11.1974) of 2 Mt yield measurements were conducted at a station SP-22 with coordinates $82^{\circ}13.8'N$, $185^{\circ}27.7'$ situated at an ice-floe 2 by 5 km and 26 to 28 m thick which drifted in the Arctic Ocean 2700 to 3000 m deep. The station was 1500 km and 3000 km far from the continent and epicentre, respectively. Refracted into water seismic signals were measured by hydrophones and seismometers. Preliminary noise measurements had been conducted in the period from 15 October to 1 November, 1974.

The vertical component of the ice motion was measured by LDF seismometer with natural period of 1 sec and by borehole seismometer SD-1F put at a depth of 6 m into a borehole. Overpressure in the water was measured by hydrophones of three types with piezoelectric sensors. Hydrophones "Oceanolog-3 and 4", PDS-21 and "Sphere" were placed at depths 470 m, 70 m, 190 m, and 270 m, respectively. The latter had a spherical piezosensor 7.5 cm in diameter with 0.6 cm thick shell. Its sensitivity was to $130 \mu V/\text{dyne}/\text{cm}^2$ and it had a high inner capacity, which allowed to improve its sensitivity at low frequencies and provided a flat amplitude-frequency characteristic. Parallel piezoelements were used in the "Oceanolog-3,4" in order to increase pass band.

Such hydrophones allowed measuring overpressures from $40000 \text{ dyne}/\text{cm}^2$ to $0.3\text{-}0.4 \text{ dyne}/\text{cm}^2$ with frequency band from 0.1 to 4 Hz and inner noise level of $30 \mu V$. Since signal to the inner noise ratio should be more than 2-3 times, only signals over $1 \text{ dyne}/\text{cm}^2$ could be measured. The frequency band for the refracted seismic signal was optimal. Frequencies above 2 Hz were of low amplitude due to higher attenuation in the Earth and were not measured at large distances. Characteristic pressure noise levels beneath ice-floe and in the ocean from published data are presented in fig. 3.13. At 4 Hz, noise is below $0.01 \text{ dyne}/\text{cm}^2$ at depths from 100 to 500 m beneath drifting ice-floe.

An active drift with mean velocity increase from 1.2 to 6.5 miles per day had begun before the explosion. This had increased noise level beneath the ice-floe. During the passive drift phase, noise level at 1.2 to 1.6 Hz at depth 470 m was of 1.4 to $1.7 \text{ dyne}/\text{cm}^2$. During the active drift phase, noise level at 1.5 Hz was 35 to 200 times larger and reached 50 to $350 \text{ dyne}/\text{cm}^2$.

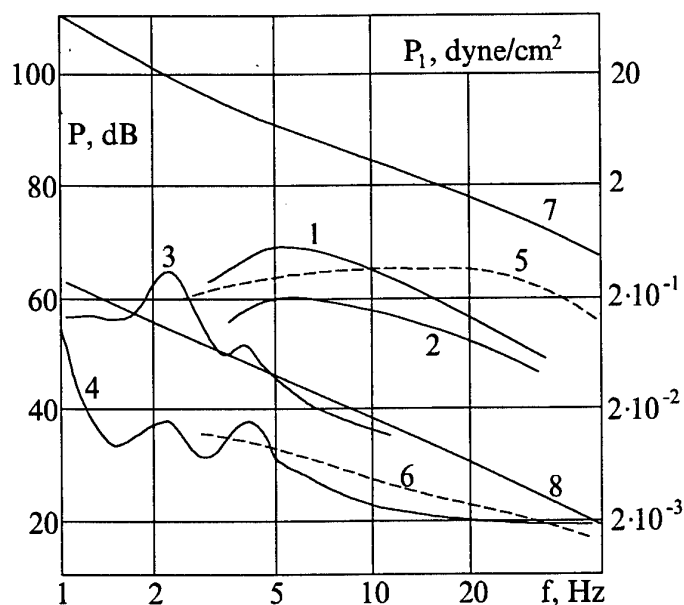


Fig.3.13 Characteristic noise overpressure beneath ice and in the open ocean by literature data.

Fig. 3.14a,b presents experimental recordings obtained by seismographs and hydrophones. Overpressure from the nuclear explosion, as averaged by 4 channels, is of 225 dyne/cm² and below noise level. Vertical displacement measured by seismometers is of 3 μ m. Spectral analysis has shown different frequency content of the signal and noise allowing the signal detection by filtering.

Analysis of P wave signals measured by seismometers established at the surface and at a depth of 6 m was conducted for the initial 2 to 4 sec. Zero phase spectral analysis has revealed direct P and reflected PP waves.

Scaled distance to the station was $R^0 = R/M^{1/3} = 318 \text{ km/kt}^{1/3}$. At this distance, the predicted overpressure in the refracted into water seismic wave $P = 330 \text{ dyne/cm}^2$ is larger than the measured overpressure. At this relatively large distance the signal level was close to that of noise. The conducted measurements allowed to measure infrasound amplitudes beneath ice and in the open ocean, to elaborate a technique and to conduct measurements of refracted into water seismic waves from underground nuclear explosions at floating objects.

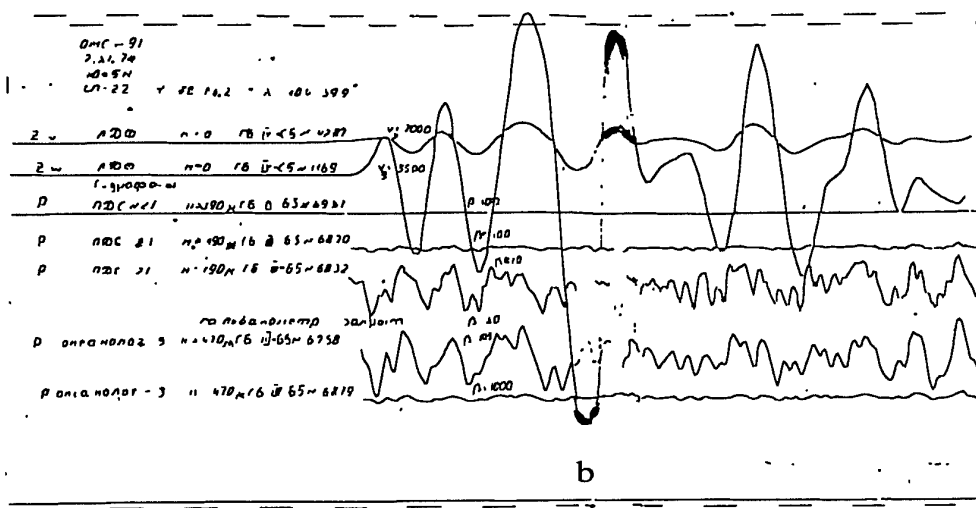
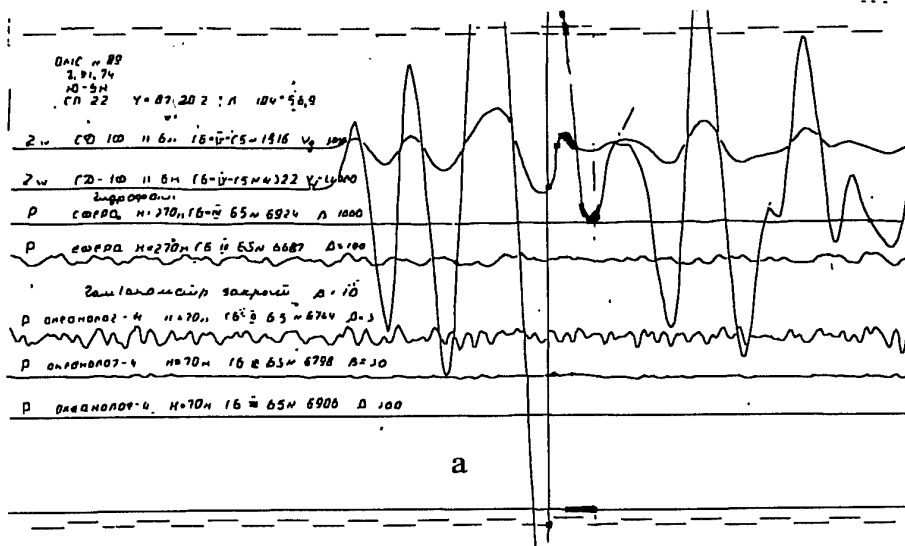


Fig. 3.14a,b Signals from underground nuclear explosion recorded at SP-22.

3.5. Conclusions.

This section presents, analyses and generalises the available experimental data on processes during above water and coastal nuclear explosions and chemical explosions conducted in Russia. The data may be useful for improving elaborated hydroacoustic methods for the International Monitoring System (IMS).

1. Data from nuclear explosions at the Novaya Zemlya test site including 3 above water explosions as well as coastal explosions: 1 surface, 4 underground, and 1 surface chemical explosion of 1000 ton. Conditions for the explosions are described as well as techniques and equipment used for study explosions effect associated with the problem under investigation.
2. Results of measurements up to 100 kg above water chemical explosions in various condition in an artificial basin are presented. Evolution pattern and capabilities of the explosions detection by hydroacoustic methods are analysed. It is shown, that due to higher pressure of the explosive products, the efficiency of hydroacoustic generation and reflection pressure are higher than from nuclear explosions. Similar effect leads to much smaller craters from above ground (surface) nuclear explosions than from chemical. Explosion energy partition between air and water as a function of height above water is investigated. It is shown that hydroacoustic energy drops steeply with the height increase. Ratio of hydroacoustic and air energies, however, may increase when the former propagates in a wave guide.
3. Results of hydroacoustic, infrasound, seismic, and radionuclides methods measurements from above water and coastal (on the top of a tower) explosions are presented. Only the latter three methods provide reliable measurements. Hydroacoustic methods recorded only seismic waves refracted into water. It is associated with specific features of nuclear explosions in shallow closed basins, where a larger portion of energy is transmitted into air and ground, and hydroacoustic energy portion is low and its transmission into the ocean is prevented by relief of the bottom. In such conditions multiple (complex) techniques using all methods are useful.

4. Results of hydroacoustic signals measurements from coastal underground nuclear explosions of megaton class in near-field zone (the Matochkin Shar strait and Barents Sea) and far-field zone (SP-22 station) at a distance of 3000 km are presented. Hydrophones recorded refracted into water seismic waves from the explosions. Hydroacoustic and infrasound waves were not recorded.
5. Hydroacoustic noise in Arctic basin is investigated in a frequency band to 50 Hz by literature sources and by measurements at SP-22. The noise level decreases with frequency beneath ice as well as in the open ocean. At maximum frequencies and large depths in the open ocean the noise may be as low as 0.002 dyne/cm^2 , and beneath drifting ice at depths of 100 to 500 m - below 0.01 dyne/cm^2 . When recording at SP-22 in the frequency band from 1.2 to 1.6 Hz at a depth of 470 m during a passive drift the noise was 1.4 to 1.7 dyne/cm^2 . During an active drift the noise was increased o 50 to 350 dyne/cm^2 . Thus, hydroacoustic stations at drifting ice are not recommended for the IMS.

4. Monitoring underwater and above water nuclear explosions.

It is experimentally proved that any explosion with yield larger than about 1 kt can be detected and identified wherever it is conducted on the Earth (hard surface, oceans or atmosphere). Depending on its height (depth) H and yield M the following classification of the explosions under investigation is used [4]: underwater or underground - $H < 0.3 \cdot M^{1/3}$; above water and above ground - $0.3 \cdot M^{1/3} < H < 3.5 \cdot M^{1/3}$, where H is measured in meters and M - in tons.

The Comprehensive Test Ban Treaty, which bans nuclear testing in any medium, foresees creation of a global monitoring system for detection and identification nuclear explosions. It is supposed that the system will include 170 seismic, 80 radionuclides, 60 infrasound and 11 hydroacoustic stations placed over the world. It is planned to collect all information from the stations in the International Data Centre in Vienna.

The hydroacoustic methods are of large importance for the detection and identification underwater and above water explosions in the ocean, especially, low-yield explosions, since hydroacoustic methods allow to detect signal at much larger distances than other monitoring methods. Due to limited number of hydroacoustic stations improvement of their capabilities is an actual task. Useful is a combination of various methods which provides additional capabilities for improved location, energy and height (depth) estimates, and increased reliability for separation of natural explosion-like sources (earthquakes, meteorite impacts, volcano eruptions, etc.).

4.1. Specific features of identification underwater and above water explosions by seismic and infrasound observations.

Hydroacoustic methods combined with different methods, at first, seismic and infrasound which are successfully used for detection nuclear explosions, are the most reliable for detection and identification not too deep explosions in the ocean.

An elaborated seismic network allowed detection and identification most of underwater and above water nuclear explosions. Some results of seismic methods delectability range are given in Table 4.1 [36].

Table 4.1

Delectability ranges for longitudinal P, shear S and surface L seismic waves from underwater and above water nuclear explosion [36].

Explosion type depth H (m)	Yield, kt	Delectability range (in thous. km) for waves		
		P	S	L
Underwater	5	10-11	2-3	3
H<150	20	11	2-3	3-4
Underwater	4	11	4-5	4
H>150	30	11-12	10	12
Above water	20	0.7-1	1	2
	15000	10-12	11	12

Fig. 2.2 presents a characteristic seismic recording from an underwater explosion at the NZTS (23.10.1961) obtained at 120 km from the epicentre by broad-band equipment with pass band from 0.2 to 30 sec. Such seismic recordings are typical for underwater explosions in shallow basins at relatively small ranges (<1000 km). There are seen distinct arrivals of longitudinal (P), shear (S) and surface (L) waves in the form of short wavetrains with periods from 0.8 to 2.5 sec associated with reflections on interfaces in the crust. They are modulated by short-period oscillations decreasing with distance and usually recorded at distances below 200 to 300 km.

Fig.4.1a,b,c,d presents seismic recordings from underwater nuclear explosions obtained at Soviet seismic stations ranged from 2,000 to 10,000 km.

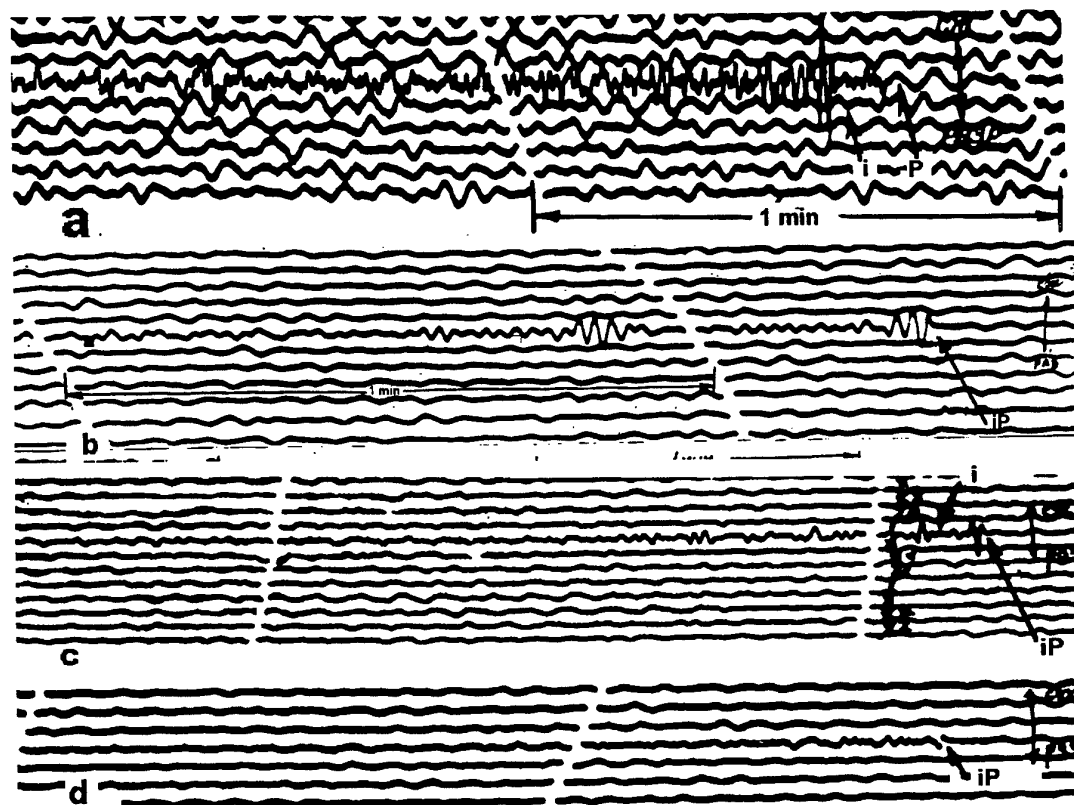


Fig. 4.1 a,b,c,d. Examples of seismic recordings from underwater nuclear explosions obtained at Soviet stations ranged from 2,000 to 10,000 km.
 (a) - explosion at NZTS on 23.10.1961. Seismic station of IDG RAS "Mikhnevo" near Moscow. (b) - explosion "Wahoo" on 16.05.1958. Seismic station at the Far East 5150 km far from the explosion [2]. (c) - explosion "Swordfish" on 11.05.1962. Seismic station "Vsevolodo-Blagodatsk". North Urals. (d) - explosion "Swordfish" 11.05.1962. Seismic station "Borovoye", Kazakhstan.

Characteristics of seismic waves generated by deep and shallow water explosions are different. Seismic waves generated by shallow explosions are similar by spectral content to those from underground explosions. Deep water explosions generate longitudinal and shear waves of longer periods than underground ones, and also intensive surface waves. Seismic energy from underwater explosions is an order of magnitude larger than that of underground explosions. This effect favours long range detection of underwater explosions.

Soviet explosions of about 5 kt yield have been recorded in the USA at stations Pasadena and Woody at ranges of 8,000 to 9,000 km. American explosions have been recorded in the USSR at range as large as 10,000 km. It is worth noting that onsets of seismic waves from shallow explosions are not distinct at some stations.

Recordings from the Soviet above water explosion on 27.10.1961 are similar to those from the underwater explosions in the same region.

American underwater explosion "Swordfish" 11.05.1962 has been recorded at 27 Soviet stations ranging from 6,500 to 10,500 km. By using data from Soviet stations and American station Pasadena coordinates and origin time for this explosion have determined : 30.3 N, 124.4 W, 20:02:34 (± 1 sec). This explosion had been conducted close to the Wigwam explosion of 30 kt, 600 m , 14:05:55.

Swordfish's yield by Soviet seismic station has been estimated as 7 kt. On the recordings from this explosion, in 6 sec after the first compression arrival the second arrival is observed (phase i). The second arrival from Wigwam is observed in 30 sec, from Wahoo (5 to 10 kt at 150 m) - in 29 sec. It is supposed that phase i is associated with the gas bubble pulsation for deep explosions and with the cavity collapse for shallow explosions. A short time delay for Swordfish may be explained by shallow depth of the explosion.

Detection and identification of low yield explosions are of very high complexity for the monitoring nuclear underwater explosions. Seismic waves from these explosions are sometimes very similar to those from shallow earthquakes, industrial or casual chemical explosions. In dubious cases, the IMS should include water and air sampling and following radiochemical analysis.

Depending on explosion type seismic waves periods may vary from several tenths of second to minute. For underground and underwater explosions short period oscillations are characteristic. Atmospheric explosions are of the longest periods. Above water and above ground explosions are in between.

Longitudinal waves are of principal importance in seismic methods for detection and identification of all explosion types except, may be, low-yield (below 20 kt) atmospheric explosions, where the waves can be recorded not far than 1000 km in many cases. Location by longitudinal waves is 2 to 4 km accurate and origin time is determined with accuracy below 1 sec. Yield is determined from amplitudes.

Distinct P wave arrivals, compression as a rule, are recorded from underwater and underground explosions. In all cases, P waves consist of a short

wavetrain with one or two-three oscillations with a period almost independent on yield and epicentral range, but dependent on explosion type.

Shallow underwater explosions at the NZTS generated P wave periods of 0.2 to 1.0 sec observed at ranges from 100 to 1,000 km. American underwater nuclear explosions conducted within deep Pacific regions generated P waves with periods of 1.0 to 1.5 sec for depths 50 to 150 m and 2.5 to 3 sec for depth of 600 m as observed at distances from 4,000 to 12,000 km.

Characteristic body wave periods for various nuclear explosion types and earthquakes are presented in Table 4.2.

P wave periods at small ranges are longer for earthquakes than for underground and underwater explosions. In general, however, as seen from the table, periods of seismic waves do not separate nuclear explosions and earthquakes, especially at far ranges. More reliable criterion is some characteristic wavetrains associated with only nuclear explosions but not with earthquakes.

A specific feature for underwater explosions is a sharp impulse, marked as i on Fig. 2.2, merged with rarefaction phase. The impulse is of a peak shape below

Table 4.2

Mean P and S wave periods from nuclear explosions and earthquakes [36].

Source type	Region	Yield range, kt	Depth, height, m	Range th. Km	Periods, sec	
					P	S
Underwater explosions	Pacific, Novaya Zemlya	5-30	150-600	5-12	2.5-3	-
		5-20	50-150	4-12	1-1.5	-
		3-10	12-50	0.1-0.2	0.2-1	0.7-
		3-10	12-50	1-5	0.5-1.2	1.2 -
Above water explosions	Pacific	10-15 th.	-	4.5-11	4.5-5.5	7-12
Underground explosions	USA	1-200	300-700	3-12	0.7-2	1.2- 4.0
Air explosions	Pacific	11-27 th.	-	8-10	8-10	8-15
Earthquakes	Various	-	0-10	3-11	3-5	10-16

100 km range and is transformed into a wavetrain with 0.2 to 0.6 sec period beyond 300 km. The impulse amplitude is of 1.5 to 2 times larger than that of the first P wave arrival at ranges from 100 to 300 km. The first arrival/impulse time delay is constant at all ranges and depends of explosion depth, yield and, may be, basin depth. The time delay is of 4 to 7 sec for shallow water explosions near coasts.

For underwater explosions at depth of 150 to 600 m conducted by USA within deep Pacific regions an intensive seismic arrival is observed in 10 to 30 sec after the first P wave arrival. This intensive arrival is associated with gas bubble pulsations.

Among other specific features separating seismic recordings of underwater and underground explosions from other types and earthquakes the most informative are: difference in longitudinal, shear and surface waves relative intensity; differences in frequency spectra (especially for longitudinal waves); different character of various wavetrains envelopes.

These differences themselves or in combination with other seismic waves specific characteristics, and also in combination with hydroacoustic and infrasound control methods, provide high enough identification probability for underwater and abovewater nuclear explosions.

Deep underwater explosions do not generate air waves of large enough intensity. For shallow and above water explosions infrasound control methods are effective. These explosions generate a wide spectra of acoustic energy. For low-yield explosions acoustic energy concentrates at high frequency. Such disturbances can be generated by natural and industrial processes. Since attenuation grows with frequency, sound frequencies attenuates in the atmosphere and infrasound in the range from 0.1 to 10 Hz propagates effectively at large distances. Thus, infrasound method is of principal importance for the IMS. Infrasound equipment works better in regions with low near-surface winds and at planes covers by vegetation. Fig. 3.1 presents a recording from an explosion at the coast of the bay of Chernaya, 07.09.1957 in 11:00:01 MSK, obtained by a microbarograph at Gamburtsevo station at 4430 km, Far East. The signal arrival time 15:04:10 MSK.

4.2. Hydroacoustic monitoring underwater and above water nuclear explosions.

According to the Comprehensive test ban treaty 11 hydroacoustic stations (HS) will be deployed. The stations will be placed in the southern oceans for monitoring underwater and above water nuclear explosions.

Nuclear explosions in the oceans, even low yield ones, generate hydroacoustic waves detectable at distances beyond 10,000 km if propagating in SOFAR. At tropic and intermediate latitudes the channel is at depth from 800 to 1500 m. HS may be spaced by 5,000 km and provide signal recording at frequencies from 1 to 50 Hz where 80 to 90 per cent of energy is concentrated. In order to maximise signal level the stations should be situated at the axis of the channel, since sound energy dissipation increases with deviation from the axis. HS locations should take into account bottom relief, since underwater mountains and islands can prevent sound propagation.

Natural explosion-like events, such as volcano, meteorite impact, etc. can generate acoustic disturbances similar to those from nuclear explosions. Identification of these sources may demand hydroacoustic data comparison with obtained by different methods. For shallow basin underwater explosions hydroacoustic energy is very low, but it favours detection and identification by other methods. Thus, for deep enough explosions, detectability by seismic methods is larger than for underground explosions of the same yield [38]. Infrasound intensity grows with decreasing depth of underwater explosions. Ejection of radioactive ground and water can be identified by radioactive sampling.

Geneva expert group [38] has recommended in 1958 to use hydroacoustic equipment only in the oceans. Several hydrophones should be placed on each point in SOFAR and connected by wires with island-based recording stations. Recording should be carried out in several frequency bands from 1 to several tens Hz. A network of control stations should include 10 ships and 60 stations on small and large islands. In this case, spacing between stations would be of 2,000 to 3,500 km, and spacing between stations in seismic regions - about 1,000 km.

According to the expert group proposal (CD/NTB/WP.283 from 20.12.1995) HS subsystem shown on Fig. 4.2 includes stationary cable HS and island-based seismic stations. 11 HS create 4 practically independent networks including 4 stations (2 HS and 2 seismic stations) in the Pacific, 3 HS in the Indian Ocean, 2 station (1 HS and 1 seismic) in the Southern Atlantic and 2 seismic stations in the Northern Atlantic [39].

Hydroacoustic signals from underwater and above water nuclear explosions consist of time separated seismic and hydroacoustic components with velocity of 5 km/sec and 1.5 km/sec, respectively. Seismic waves arrive to sensor vertically and hydroacoustic waves - along sound waveguide. Hydroacoustic component from underwater explosions has frequencies of 10 to 50 Hz, and seismic component - from 5 to 20 Hz. Amplitude ratio between hydroacoustic and seismic components is of 10 to 100. This ratio is much lower for earthquakes, with seismic component being even larger in some cases. Hydroacoustic signal from underwater nuclear explosions is of the largest amplitude to thousand Pa within the open ocean. In the spectrum of the signal first mode oscillations are observed which associated with gas bubble pulsations. The oscillations frequency is from 0.1 to 1-2 Hz depending of yield and depth. Hydroacoustic signal from above water explosions is characterised by a high frequency precursor induced by light impulse effect on the water free surface. The precursor duration can reach a

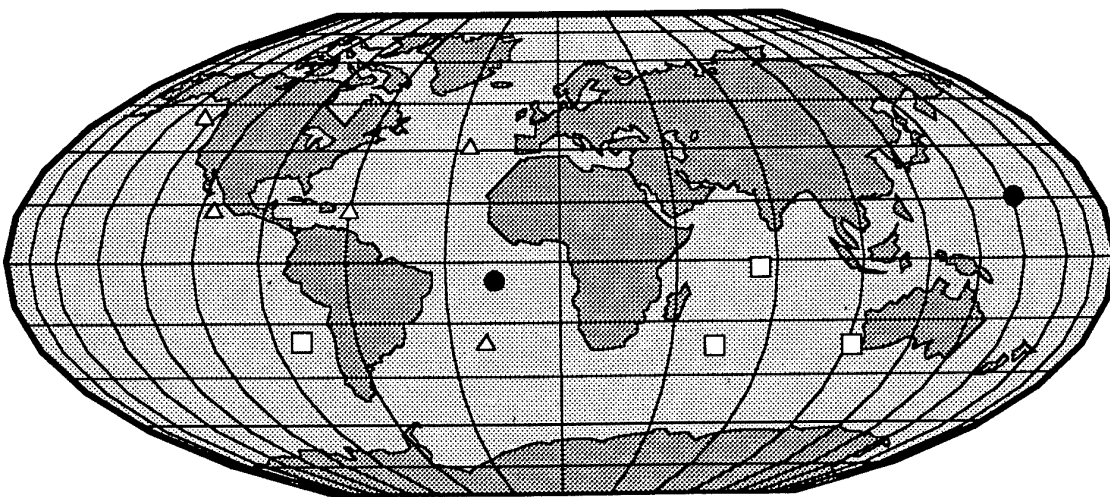


Fig. 4.2 Hydroacoustic monitoring subsystem and zones under control.

- - existing stationary cable HS (MILS).
- - designed stationary cable HS.
- Δ - island seismic stations.

second depending on the explosion height. Seismic signals from above water explosions are usually very low.

Taking into account these specific features and analysis of signal's shape and structure permits reliable identification nuclear explosions. Only powerful chemical explosions are an exception. For separation these events water sampling and radiochemical analysis are useful.

For navigation control and at the Russian sea boarder HS are used, which represent an analog of the designed system. Fig. 4.3a shows a scheme of an autonomous immersing station attached by an anchor to the sea bottom. The station consists of a container with equipment and power supply, a set of sensors connected by cables to the container, immersing RF buoy connected by an elastic cable to the container, and an anchor. There are some versions of the equipment: 1 - deployment depth to 1800 m with a receiving aerial to 80 m deep (a combined receiver is used as the receiving aerial); 2 - deployment depth to 2500 m with a receiving aerial 1000 m deep. Fig. 4.3b displays a scheme of a stationary near-coast station. This station consists of underwater sensor (hydroacoustic aerial or hydrophones) and cable connection part and coastal data acquisition and processing part.

The international expert group (CD.NTB/WP.283) proposed, according to national security reasons, do not use hydroacoustic aerial [39]. Thus, for directly

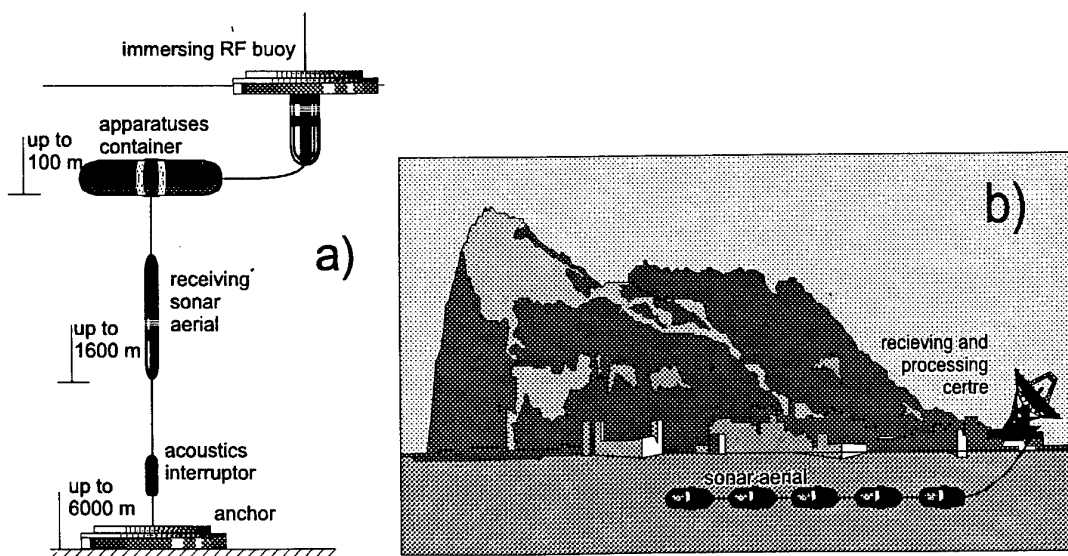


Fig. 4.3a,b Schemes for hydroacoustic stations. Autonomous immersing hydroacoustic buoy - (a). Stationary hydroacoustic station - (b).

determination of a wavefield only an isolated 3-C receiver or a small aperture array of non-directed hydrophones spaced by several kilometres can be used.

4.3. Conclusions.

Results of hydroacoustic, infrasound, seismic and radionuclides measurements are analysed. The latter three methods provide reliable results for the NZTS nuclear explosions recorded at large distances. Hydroacoustic equipment recorded only seismic waves refracted into water. This relates to specific features of nuclear explosions in shallow closed basins, where a larger portion of energy is transmitted into air and ground. Hydroacoustic energy of such explosions is low and its transmission into the ocean is prevented by bottom relief. Combined methods are preferable for such events.

1. Characteristic features of detection and identification underwater and above water nuclear explosions by seismic and infrasound measurements at ranges from 120 to 10,000 km over the Russian territory are studied. A characteristic feature of the underwater recordings is a distinct intensive rarefaction impulse "i" following after the first P wave arrival. Time delay between these phases is range independent and is determined by pulsation period of gas bubble for deep explosions or gas ejection from gas bubble for shallow explosions.
2. Problems associated with control and identification of underwater and above water explosions by hydroacoustic methods, equipment selection for the international monitoring system in conditions of SOFAR are considered. It is recommended to use stationary immersing and coastal hydroacoustic stations for recording seismic and hydroacoustic signals. Data on the bottom relief are necessary for understanding detectability range for low yield explosions, since islands and underwater mountains can prevent effective propagation in the SOFAR.

5. General conclusions.

This report presents, analyses and generalises experimental data available on processes during underwater, above water and coastal nuclear and chemical explosions conducted in Russia which can be used for the IMS hydroacoustic monitoring methods improvement. Hydroacoustic methods, which provide detection, yield estimation, location, and origin time determination as well as identification, are principal in the IMS for oceanic (underwater and above water) explosions and additional for underground explosions. In the proposed IMS configuration, 11 hydroacoustic stations are recommended from total 322 various stations. Thus, in order to reach a designed efficiency of these stations operation in the frame of the monitoring system it is helpful to use all experimental data (including presented in the report) and their analysis.

1. Data from nuclear explosions at the Novaya Zemlya test site including 3 underwater and 3 above water explosions as well as coastal explosions: 1 surface, 4 underground, and 1 surface chemical explosion of 1000 ton. Conditions for the explosions are described as well as techniques and equipment used for study explosions effect associated with the problem under investigation.
2. Results of measurements from underwater and above water chemical explosions in various basins, including deep bomb blasts in the Sea of Okhotsk, 3 ton detonating cord blast in the Black Sea, 100 kg cast TNT charge blasts in artificial basins with a sandy bottom, model small charge explosions in deep and shallow basins with various bottoms are presented. Bottom, free surface and basin depth effects on parameters and spectral content of hydroacoustic waves in near-field zone were investigated.
3. Nuclear and chemical explosion energy concentration effects are studied in water, air, ground and on long-range energy propagation. Optimal conditions correspond to TNT explosions, but for nuclear explosions and chemical explosions in cavities hydroacoustic energy drops sharply. Large cavities favour hiding nuclear tests, but these explosions are hard to conduct.
4. Specific features of hydroacoustic signal propagation in inhomogeneous liquid are considered on an example of a 3 ton detonating cord blast in a

basin with positive sound velocity gradient near the bottom, where a sharp amplitude increase was observed due to focusing effect. Shadow zones, however, are also possible. Optimal conditions for long range hydroacoustic signal propagation are created in the SOFAR, which is situated in the southern and intermediate parts of the world ocean. At frequencies below 100 Hz, which are characteristic for explosion-generated signals, attenuation in the SOFAR is negligible, and recording is possible to ranges as large as 10,000 km.

5. Above water explosion generated pattern is studied. Explosion height effect is studied in water and air. It is shown, that due to higher pressure of the explosive products from chemical explosion, the reflection overpressure and efficiency of hydroacoustic energy generation much more greater in comparison with nuclear explosion. Similar effect leads to much smaller craters from above ground nuclear explosions than from TNT ones.
6. Results of hydroacoustic noise measurements are presented for the Sea of Okhotsk, North Pole-22 station in the Arctic Ocean. The results are compared with those obtained from literature. The noise level drops with frequency increase and at 50 Hz may reach 0.1 to 0.01 dyne/cm² for deep and quiet regions. Floating objects (submarines, ships, ice-floe), however, generate much higher noise than natural one. Hydroacoustic signals from active ice-floe motion with cracking may reach 200 dyne/cm² what is similar to a signal from underground nuclear explosion at 3,000 km. Thus, these objects are not recommended for monitoring.
7. Results of observations of underwater, above water and coastal explosions by hydroacoustic, infrasound, seismic and radionuclides methods are presented. For the explosions at the NZTS only the latter three methods gave reliable results, and hydroacoustic equipment recorded only seismic waves refracted into water. This is due to specific features of nuclear explosions in shallow closed basins where hydroacoustic energy generation is low. Combined methods are helpful in this situation.
8. Problems associated with control and identification of underwater and above water explosions by hydroacoustic methods, equipment selection for the

international monitoring system in conditions of SOFAR are considered. It is recommended to use stationary immersing and coastal hydroacoustic stations for recording seismic and hydroacoustic signals. Data on the bottom relief are necessary for understanding delectability range for low yield explosions, since islands and underwater mountains can prevent effective propagation in the SOFAR.

References.

1. Soviet Nuclear Weapons. Thomas B. Cochran, William M. Arkin, Robert S. North and Jeffrey I. Sands. Natural Resources Defense Council, Inc. 1989. Harper & Row, Publishers, New York.
2. Same (in Russian). Moscow, 1992.
3. Nuclear archipelago. Ed. B.I.Ogorodnikov. M. IzdAT, 1995, 256 pp. (in Russian)
4. Nuclear explosions in the USSR. Northern test site. V. 1., Ed. V.N.Mikhailov. M., 1992, 194 pp. (in Russian).
5. Matushenko, A.M., G.A. Kaurov, G.A. Krasilov, K.V. Kharitonov. Nuclear test site unclassified. Novaya Zemlya. Proceedings Marine Arctic complex expedition. Ed. P.V.Boyarskii. M., 1994. V.3, N4, pp. 54-57. (in Russian).
6. Emel'yanenkov, A.F. Secret records of nuclear archipelago. Novaya Zemlya. Proceedings Marine Arctic complex expedition. Ed. P.V.Boyarskii. M., 1994. V.1, pp. 97-106. (in Russian).
7. Nuclear archipelago. Ed. B.I.Ogorodnikov. M. IzdAT, 1995, 256 pp. (in Russian)
8. Vetlitsky, P. Test site creation. Marine collection. 1994, N1, pp. 63-67. (in Russian).
9. Adushkin V.V., Khristoforov B.D. About the control of the underwater and above water nuclear explosions by hydroacoustic methods. Proceedings of the 17 th annual seismic research symposium on monitoring comprehensive test ban treaty. 12-15 september 1996. p. 960-967.
10. Koul, P. Underwater explosions. IIL. 1950. (in Russian)
11. Arons A.B. Underwater explosion shock wave parameters at large distances from the charge:-J.A.S.A. 1954,26, N 3.
12. Khristoforov, B.D. Shock wave and gas bubble parameters from underwater explosions of various density of PETN and lead azide. PMTF. 1961. N4, pp. 118-127. (in Russian)
13. Khristoforov, B.D. Underwater explosion in a air-filled cavity. PMTF. 1962. N6, pp. 128-132. (in Russian)

14. Khristoforov, B.D. On similarity of shock waves from spherical charge blasts in water and air. PMTF. 1963. N2, pp. 142-147. (in Russian)
15. Nuclear weapon action. Military publications DoD USSR. M. 1960. (in Russian)
16. Khristoforov, B.D. Water shock wave interaction with the free surface. PMTF. 1961. N1, pp. 30-37. (in Russian)
17. Korobeinikov, V.P., B.D.Khristoforov. Underwater explosion. summary of science and technology. Hydromechanics. V.9. M. 1976. Pp. 54-119. (in Russian)
18. Grib, A.A., A.G.Ryabinin, S.A.Khristianovitch. Reflection of a plane shock wave on the free surface. JAMM. 1956. V.20, N4, pp. 532-544. (in Russian)
19. Kozatchenko, L.S. and B.D.Kristoforov. Shock wave parameters in water near the bottom. FGV. 1971. V.7, N1, pp.127-135. (in Russian)
20. Kozatchenko, L.S. and B.D.Khristoforov. shock waves in shallow basins. PMTF. 1970. N4, pp. 165-171. (in Russian)
21. Dolbilkina, N.A. and N.A.Patrikevitch. On variation of the first pulsation parameters from a standard underwater explosions in deep sea. Seismic sounding of earthquake source regions. IPE AN USSR. M. 1976. (in Russian)
22. Khristianovitch, S.A. Shock wave at long range from explosion. JAMM. 1956. V.20, N5. (in Russian)
23. Brehovskikh. Waves in layered media. 1968. V.20, N4, pp.532-544. (in Russian)
24. Lugovtsev, B.A. Long range shock wave propagation in a constant depth basin. PMTF. 1962. N3, pp. 31-40. (in Russian)
25. Kozatchenko, L.S. and B.D.Khristoforov. Surface effects from underwater explosions. FGV. 1972. V.8, N3, pp. 433-438. (in Russian).
26. Kostyuchenko, V.N. and N.N.Symonov. Experimental study of air shock wave from underwater explosion within shallow basin. PMTF. 1960. N1, pp. 135-137. (in Russian)
27. Underwater and above water explosions. M. Mir. 1974. 415 pp. (in Russian)

28. Adushkin, V.V., Burtchik V.N. *et al.* Hydroacoustic waves from nuclear and chemical explosions. In. Dynamic processes in inner and outer Earth's shells. IDG RAN. M. 1995. Pp. 272-281. (in Russian)
29. Khristoforov, B.D. Shock wave parameters in air from PETN and lead azide explosions of various density. PMTF. 1961. N6, pp. 175-182. (in Russian)
30. Polyakova, L.I. and N.I.Ivanovskaya. Catalog of underground nuclear explosions conducted over the USSR territory from 1961 to 1989. IDG Report. 1990. (in Russian)
31. Novaya Zemlya. proceeding of Marine Arctic complex expedition. Ed. Boyarskii V.P. M. 1994. Vyp. 4, vol. 3, 240 p. (in Russian)
32. Infrasonic Observations of Large-Scale HE Events. R. W. Whitaker, J. Paul Mutschlecner and etc. 1990, 4 International Symposium on Long-Range Sound Propagation, NASA-CP-3101.
33. Adushkin, V.V. and A.I.Korotkov. Shock wave parameters near chemical explosion in air. PMTF. 1961. N5, pp.119-123. (in Russian)
34. Adushkin, V.V. and I.V.Nemtchinov. Approximate determination of gas parameters behind shock wave front by the front motion law. PMTF. 1963. V.4, pp. 58-67. (in Russian)
35. Yakovlev, Yu.S. Explosion hydrodynamics. Izd. sudostroitel'noi promyshlennosti. Leningrad. 1961. 314 pp.
36. Passechnik, I.P. Seismic wave characteristics from nuclear explosions and earthquakes. M. Nauka. 1970. 192 pp.
37. Glasston . The Effects of Nuclear Weapons. U.S.Atomic Energy Commission, Washington D.C., 1962.
38. Report of expert group on detection methods for violation a possible test ban treaty. News of science and technology. 1958.
39. (CD/NTB/WP.283 from 20.12.95)